UCRL-11598

University of California

Ernest O. Lawrence Radiation Laboratory

TWO-WEEK LOAN COPY

This is a Library Circulating Copy which may be borrowed for two weeks. For a personal retention copy, call Tech. Info. Division, Ext. 5545

FORMATION OF Be^7 IN He^3-INDUCED NUCLEAR REACTIONS

Berkeley, California

DISCLAIMER

This document was prepared as an account of work sponsored by the United States Government. While this document is believed to contain correct information, neither the United States Government nor any agency thereof, nor the Regents of the University of California, nor any of their employees, makes any warranty, express or implied, or assumes any legal responsibility for the accuracy, completeness, or usefulness of any information, apparatus, product, or process disclosed, or represents that its use would not infringe privately owned rights. Reference herein to any specific commercial product, process, or service by its trade name, trademark, manufacturer, or otherwise, does not necessarily constitute or imply its endorsement, recommendation, or favoring by the United States Government or any agency thereof, or the Regents of the University of California. The views and opinions of authors expressed herein do not necessarily state or reflect those of the United States Government or any agency thereof or the Regents of the University of California.

Research and Development

UCRL-11598

UNIVERSITY OF CALIFORNIA

Lawrence Radiation Laboratory
Berkeley, California

AEC Contract No. 7405-eng-48

FORMATION OF Be^7 IN He^3-INDUCED NUCLEAR REACTIONS

Arthur J. Pape

(Ph.D. Thesis)

...because the fastenings of the atoms are of various kinds while their matter is imperishable, compound objects remain intact until one of them encounters a force that proves strong enough to break up its particular constitution.

Lucretius[1]

FORMATION OF Be^7 IN He^3-INDUCED NUCLEAR REACTIONS

Contents

Abstract vi

I. Introduction 1

II. Experimental Method

A. Ion Beams 2

B. Experimental Apparatus

1. Bombardments at the Hilac 3

2. Bombardments at the 60-in. cyclotron 6

3. Bombardments at the 88-in. cyclotron 6

C. Foils 7

D. Chemistry 9

E. Counting 11

III. Experimental Results 15

IV. Analysis of Experimental Data

A. Analysis of the $C^{12}(He^3,Be^7)$ Reaction at He^3 Bombarding Energy of Approximately 30 MeV

1. Fitting of the activity profile in the sandwiched thin-target experiment 64

2. Calculation of Be^7 angular distribution for the $C^{12}(He^3,Be^7)$ reaction 73

3. Calculation of fraction of Be^7 recoils forward and backward from 2.48 mg C per cm^2 target for the $C^{12}(He^3,Be^7)$ reaction 73

4. Calculation of fractions forward and backward for other targets of "intermediate thickness" for the $C^{12}(He^3,Be^7)$ reaction

a. Target of 120 micrograms C per cm^2 76

b. Target of 270 micrograms C per cm^2 78

5. Energy distribution of Be^7 from the $C^{12}(He^3,Be^7)$ reaction 80

B. Analysis of the $C^{12}(He^3,Be^7)$ Reaction at He^3 Bombarding Energy of 23.8 MeV 83

C. Analysis of the $C^{12}(He^3,Be^7)$ Reaction at He^3 Bombarding Energy of Approximately 15 MeV

1. Calculation of activity profile for target of 227 micrograms C per cm^2 and average He^3 bombarding energy of 15.2 MeV 85

2. Calculation of fractions forward and backward

a. Target of 227 micrograms C per cm^2 85

b. Target of 417 micrograms C per cm^2 87

c. Target of 2.48 milligrams C per cm^2 87

D. Analysis of the $C^{12}(He^3,Be^7)$ Reaction at an Average He^3 Bombarding Energy of 10.3 MeV 87

E. Analysis of the $Al^{27}(He^3,Be^7)$ Reaction 88

V. Discussion

A. General 91

B. The $He^3 + C^{12} = [O^{15}]^* = Be^7 + Be^8$ Mechanism 92

C. The $He^3 + C^{12} = [O^{15}]^* = \alpha_1 + [C^{11}]^* \hookrightarrow \alpha_2 + Be^7$ Mechanism 95

D. The $He^3 + C^{12} = He^4 + [C^{11}]^* \hookrightarrow \alpha + Be^7$ Mechanism 96

E. The $He^3 + C^{12} = Be^7 + Be^8$ Direct Interaction Mechanism 97

F. Separation of the Compound Nucleus Type Processes in the $C^{12}(He^3,Be^7)$ Reaction at $E^{lab}_{He^3} = 31.2$ MeV . . 105

1. The $O^{15} = Be^7 + Be^8$ break-up 105

2. The $O^{15} = \alpha_1 + \alpha_2 + Be^7$ mechanism 107

G. The $Al^{27}(He^3,Be^7)$ Results 108

VI. Summary and Conclusions 109

Acknowledgments 111

Appendix I 112

Appendix II 117

Appendix III 121
Appendix IV 128
Appendix V 130
Appendix VI 132
Appendix VII 134
Appendix VIII 136
Appendix IX 137
References 140

FORMATION OF Be^7 IN He^3-INDUCED NUCLEAR REACTIONS

Arthur J. Pape

Lawrence Radiation Laboratory and Department of Chemistry
University of California
Berkeley, California

August 4, 1964

ABSTRACT

This work was begun to determine the importance of the direct interaction mechanism ${}_2He^3 + {}_2He^4(\text{cluster}) = {}_4Be^7$ for the "alpha-cluster" nucleus C^{12} and for the Al^{27} nucleus.

The results of the investigation indicate that of a $C^{12}(He^3,Be^7)$ cross section of 57 mb at a He^3 bombarding energy of 31.2 MeV, the direct interaction process has a cross section of approximately one millibarn. The remainder of the Be^7 is formed by compound nucleus type processes of which the $C^{12}(He^3;\alpha_1\alpha_2)Be^7$ mechanism is the most important. Recoil data at lower He^3 bombarding energies were fitted assuming only compound nucleus processes.

The results of the $Al^{27}(He^3,Be^7)$ thick-target recoil experiments indicate that at He^3 bombarding energies up to 30 MeV, Be^7 evaporation accounts for approximately 90 percent of the Be^7 production cross section. The other 10 percent is attributed to direct interaction processes. The magnitudes of the direct interaction cross sections for (He^3,Be^7) and (He^4,Be^7) reactions on aluminum are consistent with the idea that alpha clustering is favored over He^3 clustering in the nuclear surface.

I. INTRODUCTION

In view of successes of the cluster model,[2] it was decided to test the idea that the He^3 beam will act as a probe to study surface alpha-clustering in nuclei via the ${}_2He^3 + {}_2He^4(\text{cluster}) = {}_4Be^7$ reaction. Because this idea necessarily leads to mechanism studies of the (He^3,Be^7) reaction, the "alpha-cluster" carbon nucleus with its large (He^3,Be^7) cross section (110 mb at the peak of the excitation function) and the aluminum nucleus were chosen for more detailed experiments.

Three other reasons that carbon was singled out are that the foils and films can be fabricated relatively easily (for instance, as opposed to a nitrogen target). Also carbon will withstand the large ion currents necessary to perform these experiments, and the carbon results, because of the relatively high Be^7 production cross section, are not sensitive to small amounts of light element impurities such as oxygen and nitrogen whose (He^3,Be^7) cross sections are estimated to be high.

A complicating feature in the study of the $C^{12}(He^3,Be^7)$ reaction is that at most He^3 bombarding energies, several mechanisms for producing Be^7 are energetically possible. However, as the (He^3,Be^7) or "alpha-pick-up" reactions studied in this work always appear to be more probable than (He^4,Be^7) or "He^3 pick-up" reactions, even though the excitation functions are not directly comparable, it was decided to learn if the large $C^{12}(He^3,Be^7)$ cross section (0.1 geometric) could be attributed wholly or in part to a direct alpha pick-up reaction.

Aluminum was chosen as a target because the $Al^{27}(He^3,Be^7)$ cross section is large enough to allow thick target recoil experiments to be performed, and the interpretation of the results is simplified since Be^7 is envisioned to occur only by evaporation and by direct interaction. The $Al^{27}(He^3,Be^7)$ results can then be compared with similar mechanism studies on the $Al^{27}(He^4,Be^7)$ system.[3]

Once the excitation functions for the (He^3,Be^7) and (He^4,Be^7) reactions had been obtained, further work on the reaction mechanism was performed using conventional counting methods in conjunction with

standard chemical separations (where applicable) to separate and identify the 53.6-day Be^7. Another possibility was to turn to direct counting at the accelerator of the reaction products using solid state dE/dx and E counters. Even at the present time, however, electronic identification of the Be^7 product would be very difficult because of the problem of fabricating extremely thin and uniform dE/dx counters. (An alternative is to use a gas dE/dx counter.) It was decided to remain with conventional counting and chemical separations.

The major problems encountered throughout this work were those associated with detection of low activities of Be^7. The 10% branching ratio of the 0.477 MeV gamma ray by which the Be^7 was detected by NaI scintillation spectroscopy, and the 53.6-day half-life gave low counting rates for bombardments of moderate length with the available He^3 beams. For this reason, mechanism studies of the types performed here are best limited to the light elements where the Be^7 production cross section is of the order of millibarns or higher.

II. EXPERIMENTAL METHOD

A. Ion Beams

The $He^3(+1)$ ion beams were obtained at the Hilac at an incident energy of 10.4±0.2 MeV/nucleon.[4] Stacked foil targets were placed in a Faraday cup. In order to facilitate foil cooling, the beam was usually wobbled randomly over the target surface. The ion current integrator was standardized with a calibrated Weston cell following all runs where absolute cross sections were determined. This integrator standardization was performed on one occasion both from the experimental cave area and then directly into the integrator. No significant difference was noted, so subsequent calibrations were made in the control room. Corrections applied to the observed integrated beam were usually a few percent.

Ion beams of 48-MeV $He^4(++)$ were obtained at the 60-in. cyclotron. Three runs were made at the 60-in., but due to the extremely

rushed schedule immediately before the machine was dismantled, time was not available for integrator calibration. All work performed at the 60-in. cyclotron was later repeated and extended in energy at the new 88-in. cyclotron.

External beams of $He^4(++)$ were also obtained at the 88-in. cyclotron. The integrator was again always calibrated in experiments in which cross sections were determined. Energies of the He^4 ions were taken at the quoted value, but are probably not accurate to more than ±2 percent.[5]

B. Experimental Apparatus

1. Bombardments at the Hilac

Five preliminary runs were performed. Stacks of foils were placed where they would intercept "rejected" beam, on the collimator and in the direct beam in the Faraday cup. In these cases, the amount of beam impinging on the target was calculated from the Na^{22} beta activity produced in an aluminum monitor foil and the known Na^{22} production cross section.[6]

The standard copper "tag" target assembly was used for other experiments in which a stack of foils was bombarded.

In order to determine the angular distribution of Be^7 produced in the $C^{12}(He^3,Be^7)$ reaction, two pieces of equipment were used inside a large chamber. This chamber is in essence a 7-inch inside diameter brass pipe, sectioned so that its length can extend up to several feet, if necessary.

The angular distribution apparatus shown in Fig. 1 allows the determination of angular distributions out to a laboratory angle of approximately 30 degrees. The apparatus shown in Fig. 2 will give the same type of data but at all laboratory angles.

A single run was made using an interesting angular distribution apparatus (described in detail in Ref. 7) in an attempt to obtain a

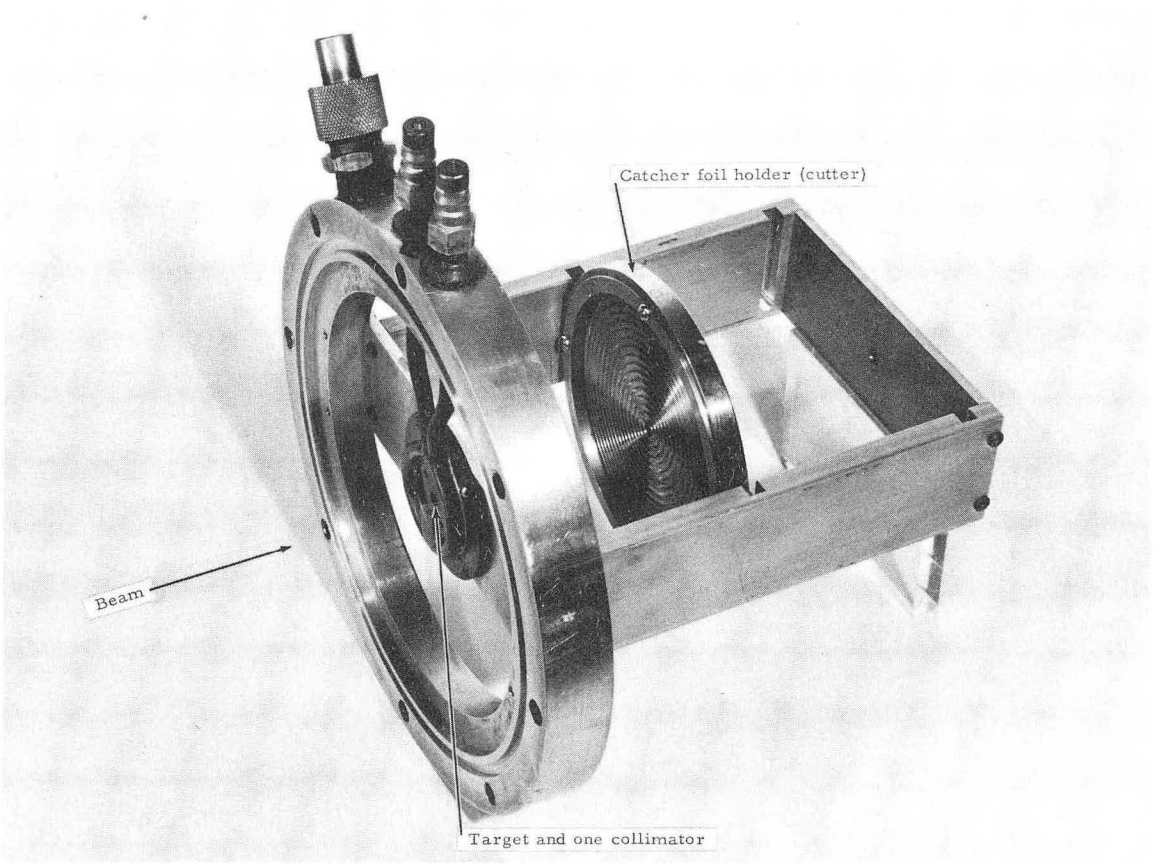

ZN-4395

Fig. 1. Cutter in its mount. When the cutter is placed in the position nearest the target as shown, recoils are collected out to a laboratory angle of approximately 30 degrees. When a catcher foil in the cutter is subjected to pressure, the numerous ridges in the cutter cut the foil into concentric annuli. In one experiment in this work, activity limitations dictated the angular resolution obtainable and the catchers were cut out manually into only a few rings.

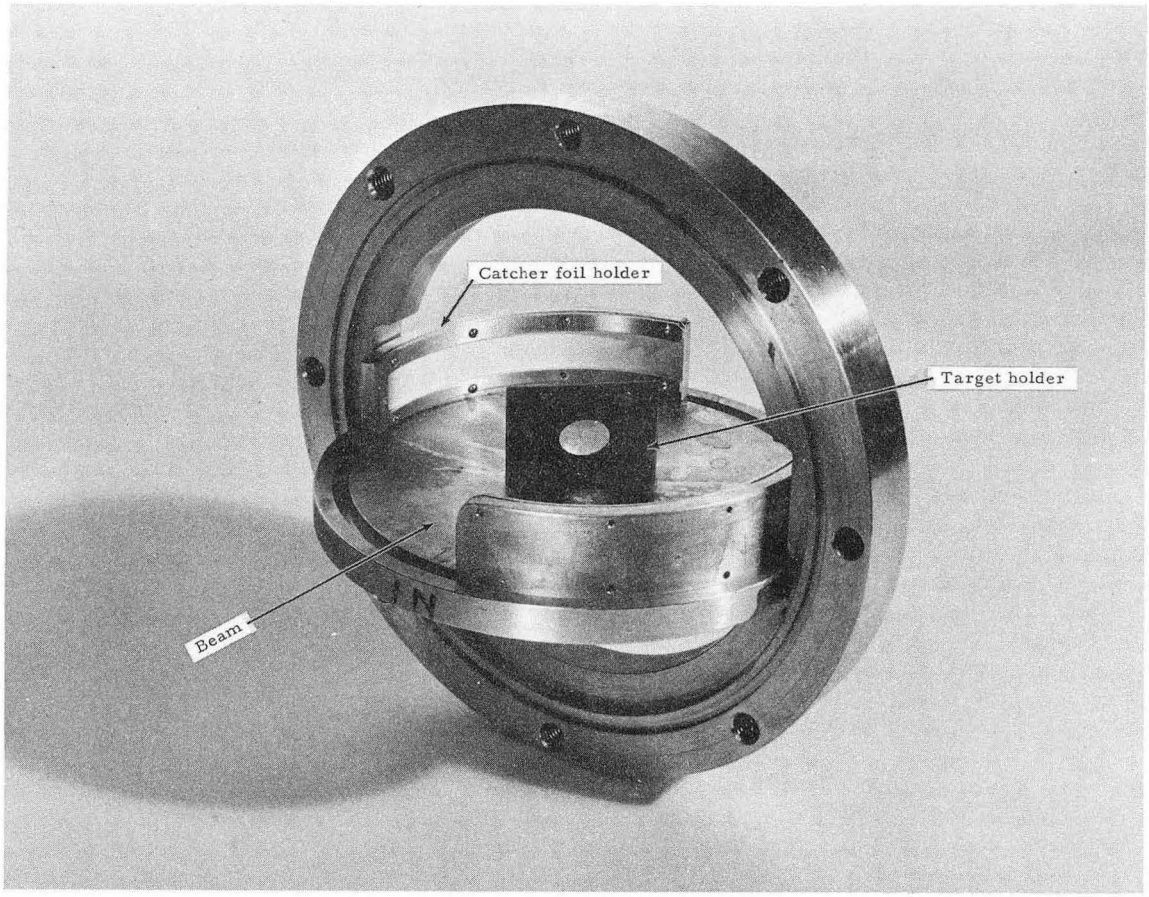

ZN-4394

Fig. 2. Angular distribution apparatus. This angular distribution apparatus is capable of determining the laboratory angular distribution of recoils at all angles.

double differential cross section—energy spectrum at each angle—for the $C^{12}(He^3,Be^7)$ reaction. The run produced an unobservable amount of Be^7 in the individual catcher foils despite an 8-hour bombardment with a 500 mμa beam. Therefore an apparatus having a much higher Be^7 collection efficiency had to be used for this type of experiment.

The apparatus used was the same as that shown in Fig. 1, with the holder loaded with a stack of thin aluminum catcher foils. All of the Be^7 produced from a small angle (corresponding to the beam hole) out to 30 deg. (laboratory) will be collected. In this run the catcher foils collected sufficient Be^7 activity to yield a positive result.

2. Bombardments at the 60-in. cyclotron

The three bombardments performed at this accelerator were all on stacked foils mounted inside the standard water-cooled Faraday cup holder.

3. Bombardments at the 88-in. cyclotron

Three bombardments on stacked foils were made at the 88-in. cyclotron. The standard Hilac tag assembly was used as the target holder following some adaptation.

C. Foils

Most of the experiments on (He^3,Be^7) and (He^4,Be^7) reactions with various targets were dictated by the immediate availability of the target foils. Representative samples of metals used as targets were always analyzed spectroscopically before an experiment and were always found to be of extremely high purity. Foils were cut with a 1.0005-in. diam. punch and were visually checked for perforations.

An unknown factor is the small amounts of light difficult-to-analyze-for elements such as oxygen and nitrogen whose Be^7 production cross section in helium-ion bombardments is estimated to be relatively large. A study of the thicknesses of oxide layers on various metals by the methods of optical polarization[8] indicate that Be^7 produced from surface oxygen contamination is not a serious problem for aluminum. For metals whose (He^3,Be^7) and (He^4,Be^7) cross sections are several orders of magnitude smaller than the Be^7 production cross section from oxygen, dissolved or surface oxygen introduces an uncertainty into the cross section determinations. Respect for this uncertainty is a major reason why this work deals primarily with light target elements where contaminants pose a less serious problem.

For carbon targets, foils of polyethylene and of mylar were tried. The long bombardments, even at very low beam currents, always caused target charring (or else very low Be^7 activity). Aluminum spacers interspersed throughout the stack of plastic foils to facilitate cooling did not solve the low activity problem. Since more than a slight amount of heat damage causes inconsistent experimental results, we turned to using pure carbon targets. Naturally occurring carbon is 98.89 percent[9] C^{12} and the presence of effects due to C^{13} is ignored.

The pure carbon foils used in excitation function determinations and in some recoil experiments were approximately 2.5 mg C per cm^2 made of carbonized filter paper. Briefly, these were prepared by carbonizing one inch filter paper circles between graphite bricks. (This causes a slight amount of shrinkage.) To render the carbon discs "oxygen-free" they were outgassed at over 1000°C in a graphite crucible heated by

electron bombardment. The discs were then cooled to below 200 degrees before being exposed to the atmosphere. After such treatment, the discs remain "oxygen-free".[10]

For certain experiments, pure carbon films were prepared ranging in thinness down to approximately 100 micrograms per cm^2. The method, devised after some experimentation, consists of pouring an ethanol diluted suspension of "dag"[11] onto a mirror and allowing it to dry. The preparation "dag" is a commercially available suspension of colloidal graphite in organic solvents. Commercially available "Aquadag"[11] could also have been used. The uniformity of the films thus prepared is easily checked by noting the rates at which the various portions of the layered suspension dry, and by observing light reflected off the mirror through the film.

The next step is to let distilled water seep between the carbon film and the mirror. The film is then transferred onto a large surface of water where the film is lifted off the water surface with thin teflon plastic and dried under a heat lamp. The problem comes in separating large sections of carbon film from the teflon, but this can be done if extreme care is exercised. Teflon was chosen as the material most unlikely to adhere to anything, but other materials such as cellophane or a graphite-film-covered mirror were successfully used to free the carbon film from the water surface.

These carbon films were always outgassed between small graphite blocks in a metal evaporator at elevated temperatures for several hours before being used in a run. That this procedure produced a relatively oxygen-free film was shown by an $O^{16}(He^3,F^{18})$ activation analysis experiment.[12] Foils remained relatively oxygen-free even after storage in the atmosphere for long periods. The amount of oxygen was determined to be approximately one hundredth of a percent by weight in one carbon film.

The possibility of measuring (He^3,Be^7) excitation functions and doing recoil studies with nitrogen and oxygen targets has been investigated but not pursued. With these two elements, one problem is the preparation of self-supporting heat-resistant targets. It is probably

feasible to press thin (approximately 3 mil) wafers of Al_2O_3 and AlN at very high pressures.[13] Data obtained in this work would allow the $Al^{27}(He^3,Be^7)$ activation to be subtracted out. Thin films of Al_2O_3 can be made by electrolysis, but thin films of nitrogen-containing compounds are difficult to prepare. Wafers of TaN could probably be pressed.

D. Chemistry

An effort was made to determine the relatively low Be^7 activities by counting the foils directly. However, it was finally concluded that it was necessary to perform chemistry to separate Be^7 from the Na^{22} and other radioactivities produced in aluminum and other metal target foils. Stable beryllium carrier, and other "holdback" carriers were used. It was assumed that there was complete radiochemical exchange between the Be^9 carrier and the trace amounts of Be^7 that were formed in the bombardment.

A number of precipitation procedures for Be(++) were tried, but quite often the spectral analyses which were performed frequently during the chemistry indicated that the precipitate had the incorrect ratio of Be to other materials or that undesired elements were present. For this reason it was decided to work with the straightforward precipitation of $Be(OH)_2$ from solution, in spite of the fact that the final product BeO is extremely toxic and somewhat hygroscopic. Chemical yields were determined gravimetrically.

Because the chemical behavior of aluminum and beryllium are very similar, the separation of beryllium from aluminum foils posed a problem. The separation was finally effected by repeated precipitation of $Be(OH)_2$ in the presence of disodium ethylene-dinitrilo-tetra-acetate (EDTA). EDTA complexes aluminum and most metal ions strongly but beryllium only weakly.[14] Separation of beryllium from other metal foils followed fairly standard chemical procedures and extensive use of EDTA. The $Be(OH)_2$ precipitates were spectroscopically free of the matrix (foil) element and all hold-back carriers. One chemical procedure, the separation of Be from Al, is included in Appendix VIII. The composition of

random samples was spectroscopically checked occasionally during all of this work and was always found to be pure. The final BeO product was also radiochemically pure. (See next section.)

The $Be(OH)_2$, after being re-precipitated and washed eight times per sample after the separation chemistry was performed, was filtered on Whatman 42 paper. (Whatman 40 allowed some precipitate to pass.) After filtration, the $Be(OH)_2$ was transferred to a platinum crucible and ignited. (BeO will fuse with porcelain.) The weight of the ignited filter paper was determined to be negligible. Although BeO is hygroscopic, it becomes much less so if it is ignited at 1000°C for several hours.

After ignition at 1000°C the BeO was crushed, slurried with ethanol and transferred uniformly to the surface of a 1.8-cm diam. filter paper circle which was mounted in a filter chimney apparatus. The filter disc had previously been treated with ethanol, dried, and weighed. Ordinary filter paper was used for the disc, but some Millipore filters[15] were also obtained for this purpose. These are attractive filters for some uses because a large fraction of their area is composed of uniform and extremely fine pores. Unfortunately, however, these filters swell in ethanol.

After the BeO on its filter disc was dried for several hours under an infrared heat lamp, it was weighed and finally scotch-taped to a standard aluminum counting plate. All weighings on the filter disc before application of the BeO, and on the filter disc plus BeO were performed quickly after removal from the heat lamp and repeated until two successive weighings agreed to within 0.1 mg. All transfers to the balance of the filter disc plus BeO were made in a dessicator to minimize uptake of moisture by the BeO. Typically the filter disc alone weighed approximately 45 mg (accurately known) and an (accurately known) amount of Be(++) carrier corresponding to approximately 25 mg BeO was added to each sample analyzed. Most chemical yields were in the vicinity of 80 percent.

For each sample analysis new glassware was used to avoid Be^7 contamination from one sample to another. In the cases of platinum crucibles and filter chimneys where it is obviously not practical to use new equipment for each analysis, the materials were cleaned twice with scouring powder before their reuse.

Chemical separation of Be^7 produced in bombardments of plastic and carbon foils was neither feasible nor necessary. After allowing shorter-lived isotopes to decay for a few days, the only spectrum present when these foils were counted was due to Be^7.

For recoil experiments, chemical separation of Be^7 from catcher foils was necessary in some cases. Separation of Be^7 was necessary when the catcher foil directly intercepted the helium ion beams.

E. Counting

The single 0.477-MeV gamma ray following electron capture in Be^7 was detected with an unbeveled 3 × 3-in. NaI(Tl) crystal used in conjunction with a pulse height analyzer. The analyzer used was a 100-channel Penco, which was later replaced by a 100-400-channel RIDL. The entire system of amplifiers and analyzer was calibrated both in energy and in efficiency for the energy region of interest. The system was linear in energy over a wide energy range. Since in many cases low activity samples were counted, long counts of approximately a half day were usually taken in order to build up good counting statistics. For all counts, both long and short, the detection system was checked for drift before and after each count by means of a Na^{22} source. Unless the 0.511 MeV annihilation peak appeared in the same channel both before and after the count, the count was rejected and the sample was recounted. During certain periods, the recounting took up a sizable fraction of the analyzer time.

The analyzer was adjusted for all counts so that the 0.511 MeV peak was centered in channel 30 (Be^7 in channel 28) and the Ne^{22} 1.28 MeV peak, formed in Na^{22} decay, in channel 78. This was done so that

the samples could be checked readily for presence of Na^{22} which is a common contaminant and which will make a contribution to the 0.477 MeV Be^7 peak by means of positron annihilation. No Na^{22} peaks were seen in any of the samples where Be^7 peaks were determined. The scintillation spectra taken in the gamma cave were always identical with background except for the Be^7 activities. As further checks on the radiochemical purity of the plastic, carbon, and BeO samples, some of these were beta counted in a gas flow proportional counter. Any appreciable beta contamination would appear, but no beta activity was apparent above background. The half-life of the Be^7 peak was checked for two random samples and was found to decay with approximately the proper 53.6 day period. The radiochemical purity of the samples is emphasized because when Be^7 peak areas are finally determined, it is assumed that no positron contribution above background is present.

In one experiment in which many catcher foils had to be counted each for a long period, the RIDL was set up to count three NaI(Tl) crystals simultaneously in successive 100-channel intervals.

Almost all Be^7-containing samples were counted on the first shelf below the crystal. In one case this distance was 1.59 cm, and in another cave used, 1.00 cm. Those samples not counted in these geometries were all from the experiment where three catcher foils were counted simultaneously, in which instance the catcher foils were taped directly to the plastic crystal coverings.

It is possible that the background to Be^7 activity ratio in a scintillation crystal could be reduced by reducing the size of the crystal. This also has the effect of lowering the area of the Be^7 photopeak because more 0.477 MeV gammas can escape the crystal. Counting of low activity samples in a high-geometry well-type scintillation crystal was tried. This idea will work but it was not pursued because the available crystals were being used in other work and also because they were not completely uncontaminated. Other methods of Be^7 detection, namely by means of Auger electrons or X-rays, were investigated. Although these methods could provide higher specific activities than is obtained

for the 0.477 MeV gamma-ray, it was concluded that absolute count rate determinations by either of these two methods would introduce major difficulties.

The method for calculating the total Be^7 activity from its 0.477 MeV peak area for preliminary cross section purposes consisted of using values of crystal efficiencies and peak-to-total ratios of Heath.[16] However, as the NaI(Tl) crystal has a covering of 1/16 in. packed aluminum oxide which serves as a light reflector, 0.040-in. neoprene sponge rubber, and a 0.019-in. aluminum container,[17] the true conversion factor for obtaining the total activity of Be^7 from its peak area had to be determined experimentally as follows.

Thin plastic VYNS[18] films were layered on water. Each film was transferred to an aluminum disc with a 3/4-in. hole in its center. The uniformity of the VYNS can be inferred from the diffraction pattern produced in the film by visible light. The thickness can be estimated from the apparent color of the film.[19] After the films were prepared, a "weightless" film of gold metal was evaporated onto the VYNS to render it conducting. A small amount of $Na^{22}Cl$ in HCl was then micropipetted onto the film and gently dried. Such a salt solution, even when very dilute, tends to form crusts around the edge of the droplet as it dries and hence certain areas of the beta emitting source are not completely weightless. Such a phenomena occurred in several samples and no good method was found to avert this.

The VYNS film with its Na^{22} source was then counted in a 4π beta counter. The geometry of the counter was assumed to be 4π and a small correction for positron absorption[20] in the VYNS film was made. The 1.28-MeV γ-ray which is formed in the Na^{22} decay is emitted in coincidence with the positron, as far as the 4π counter is concerned, so no correction had to be made for gammas. One can then calculate the absolute positron activity of the Na^{22} source.

The next step is to mount the Na^{22} disc onto a counting plate, cover it with sufficient thickness of absorber (577 mg Cu per cm^2 was used) to completely stop and annihilate the positrons, and count this

gamma source in the same geometry in which the Be^7 samples were counted. Taking into account the fact that two gammas are produced per positron annihilated, making a small correction for gamma ray absorption in the copper cover and a small correction for the difference of crystal efficiency for detection of 0.511-MeV and 0.477-MeV gammas, one can calculate the factor which converts a Be^7 gamma count rate to the total Be^7 gammas emitted by the sample.

A Cs^{137} source calibrated in a manner very similar to that just described for the Na^{22} source is available in this laboratory.[21] Results for the factor converting the Be^7 count rate to total Be^7 gammas emitted by the sample were the same for both the Cs^{137} and the Na^{22} sources.

None of the Be^7 activities counted were point sources, but instead the activity extended more or less uniformly over circular areas of diameters up to 1.8 cm. No efficiency correction was made for the finite extent of the Be^7 sources, but this was at least partly compensated for by the fact that the sources used in the crystal calibration were also not point sources.

In five early runs, the total beam current incident upon the stack of foils was determined from the beta activity (Na^{22}) produced with known cross section in a thin (sandwiched) monitor foil. The counting efficiencies of the beta counters in the different shelf geometries were obtained from absolute 4π beta counting of a Na^{22} source and then counting the same source in a standard mounting below the proportional counter. Small corrections were made for the beta-absorption in the monitor foil[20] and in the approximately one mg per cm^2 Videne-TC[22] plastic sample cover.

The proportional counters were always operated in the middle of a plateau having typically a slope of one percent per 100 volts over a high voltage range of 900 volts. Before and after all counts, a Cl^{36} source was used to give a standard beta count rate and thus show that the counter characteristics had not changed during a sample count.

It must be noted that the beam current determination by this method is probably not very accurate because the diameter of the monitor

foils (approximately one inch) is comparable to the window diameter of the proportional counter. Hence efficiencies determined for the standard Na^{22} source will be different from that of a given monitor foil because of a difference in the area of the emitting surface.

Because Be^7 has a half-life long compared to even the longest bombardments, decay during bombardment was small. Initial activities of Be^7 were calculated to the midpoint of the bombardment. The decay factors necessary to perform this calculation were taken from a "Time, Half-Life" nomogram.[23]

III. EXPERIMENTAL RESULTS

The cross sections presented in this section were calculated using a half-life of 53.6 days[24] and a branching ratio of 0.1032[25] for the 0.477-MeV gamma ray which follows electron capture in Be^7.

In the excitation function experiments, no correction was made for recoil migration of the Be^7 product. Because the stacked foil method was used (with its assumption that any products recoiling downstream and out of a given target foil are compensated for by recoils entering the given foil from upstream) it is assumed that this correction is small. An exception occurs for the first one or two foils in a stack. Their observed activity was always low.

In several runs where duplicate experiments were performed, the effect of target heating on excitation functions and on recoils from targets was checked by varying the beam current. This will vary the amount of target heating and presumably affect diffusion of Be^7 product, if diffusion is of any major importance. No effect due to varying beam intensities during a run was ever noticed.

It has been noted that the presence of air in a gas target leads to an anomalously large production of Be^7.[26] Since in all runs, the total pressure in the beam pipe was on the order of 20 microns, atmospheric contamination was not present; no correction was made for it. (The role of light element impurities in low Be^7 cross section materials

such as Ni and Au is another matter and introduces errors into these experiments.)

The role of Rutherford scattering in experiments similar to the type performed in this work has been studied by Hower.[27] From his work it is concluded that wide-angle scattering should not be a source of anxiety, at least for the more energetic recoils. For Be^7 recoils of 3 MeV and lower where the Be^7 is not fully ionized, it is difficult to evaluate the role of the scattering, and it may be large.

Since most of the runs in this work were lengthy, most of the experiments were not repeated under identical conditions. Instead, an effort was made to vary target thicknesses, collimations, beam intensities, and catcher foil materials from run to run for similar experiments. When duplicate runs were performed, as in the $C^{12}(He^3,Be^7)$ and the $Al^{27}(He^3,Be^7)$ excitation function measurements, results derived from the individual runs were virtually identical.

No checks were made specifically to determine the uniformity of the foils used as targets and as catchers. However, several commercial foils have been checked and variations in superficial densities were small.[28]

Range-energy curves for He^3 in various materials were taken from several sources.[29,30,31] Range-energy relationships for He^4 were calculated from those of He^3 by the relationship $R_{He^4} = R_{He^3}(4/3)$ for He^4 and He^3 ions of the same (non-relativistic) velocity. It is not known how accurate most of the range-energy curves are. Experimental data for Be^9 (hence Be^7) and other ions in various stopping materials are scarce, so the calculated range-energy curves were accepted at face value. The range-energy curves are discussed in Appendix VI and calculated ranges are compared with experimental.

The method used in calculating the errors follows the treatment presented by Evans.[32] For the most part the error bars deal with random errors inherent in such processes as weighings, variations in foil thicknesses, or measurements of distances. Any systematic error, such as crystal calibration, will remain constant throughout the data.

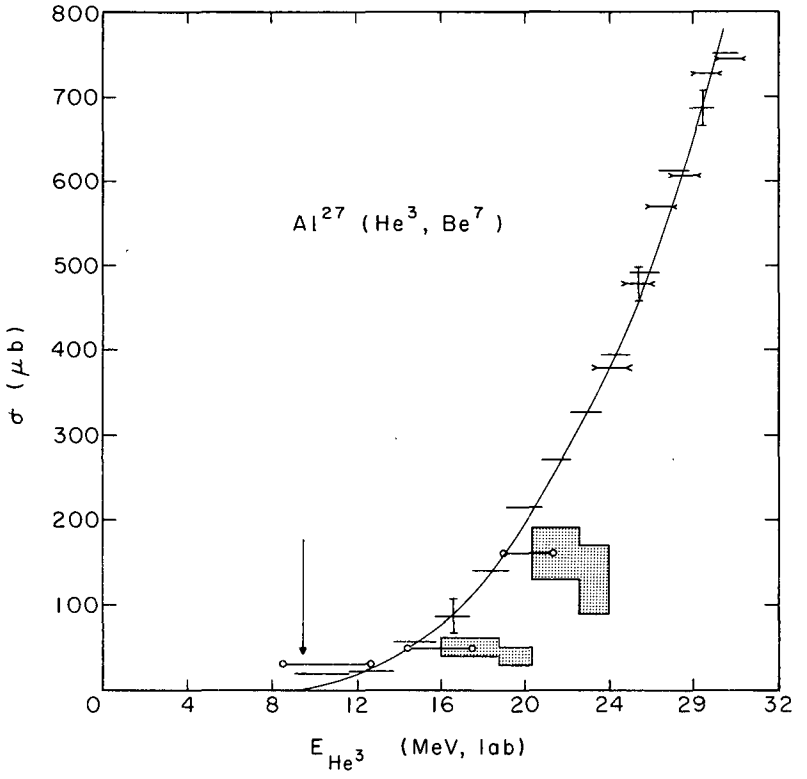

MU-34496

Fig. 3. Excitation function for the $Al^{27}(He^3,Be^7)$ reaction. The range-energy relationship was taken from Rich and Madey.[29] The horizontal bars representing the data denote ΔE_{He^3} in a given target foil. Data are compiled from three runs.
Cross section data of Cochrane and Knight[33] for the same reaction together with a reconstructed ΔE_{He^3} and their estimated uncertainties are indicated by the shaded boxes. Their data has been adjusted for the Be^7 branching ratio and half-life used in this work.
In estimating the errors the formula $\sigma^2 = \frac{1}{n-1} \sum_1^n (X_i - \bar{X})^2$ was used. The values used for $\bar{X}$ were those on the curve drawn through the experimental points and σ was determined in the two regions where the error bars are drawn. Error bars in Figs. 3, 4, 6, 11, and 12 were determined in this manner.
The threshold for the $Al^{27}(He^3,Be^7)Na^{23}$ reaction is 9.47 MeV.

Several thick-target recoil experiments were performed in an effort to elucidate the mechanisms of the $Al^{27}(He^3,Be^7)$ reaction. In these experiments aluminum targets were sandwiched between thick catcher foils. The fraction of the total Be^7 produced which recoiled forward out of the target is denoted by F. Likewise, the fraction of Be^7 recoiling backward is B, and the fraction remaining in the target is T. Low Be^7 activation in the catcher foils was assumed to be the same as that in the blank foils immediately next to the catchers in the stack. The data are presented in Table I.

Uncertainties are estimated by assuming a ±10 percent variation in the observed Be^7 count rates of the active foils.

Table I. Recoil data on $Al^{27}(He^3,Be^7)$ reaction.

$\langle E_{He^3} \rangle$	He^3 energy across target	Al thickness	Catcher foil	F	B	T
24.6 MeV	25.2 - 24.0 MeV	7.34 mg/cm^2	Ag	0.28±0.04	0.048±0.007	0.67±0.09
24.6	25.2 - 24.0	7.42	Ag	0.27±0.04	0.043±0.006	0.69±0.10
26.6	28.2 - 25.1	22.95	Ni	0.086±0.012	- [a]	0.91±0.12
26.9	28.4 - 25.4	23.02	Ni	0.088±0.012	- [a]	0.91±0.12
29.6	30.1 - 29.2	7.30	Ag	0.33± 0.04	0.049±0.007	0.62±0.08
30.7	31.2 - 30.2	7.30	-	0.36[b]		
30.7	31.2 - 30.2	8.40	-	0.30[b]		

[a] The Be^7 activity was too small to detect accurately.

[b] These F-values were obtained from the runs where the excitation function was determined. The first target foil of the stack is not fed with Be^7 recoils from behind, and its observed activity is less than the value obtained by extrapolation of the activities of the other downstream foils. The difference between the extrapolated activity and the measured activity for the first foil in the stack is then a measure of F.

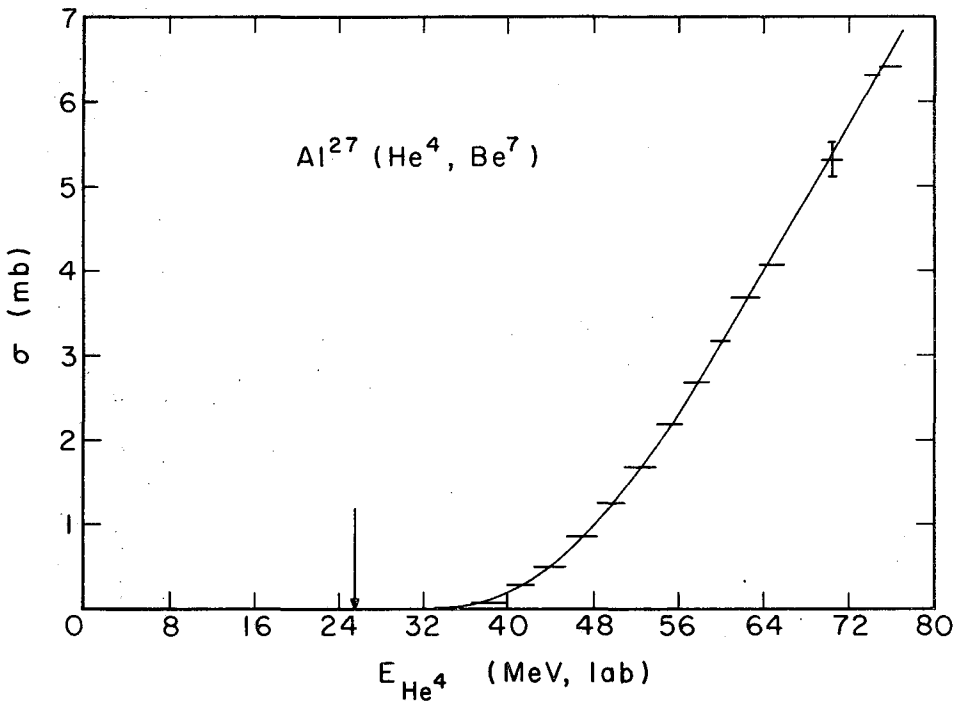

MU-34497

Fig. 4. Excitation function for the $Al^{27}(He^4,Be^7)$ reaction. Threshold for the $Al^{27}(He^4,Be^7)Na^{24}$ reaction is 25.5 MeV.

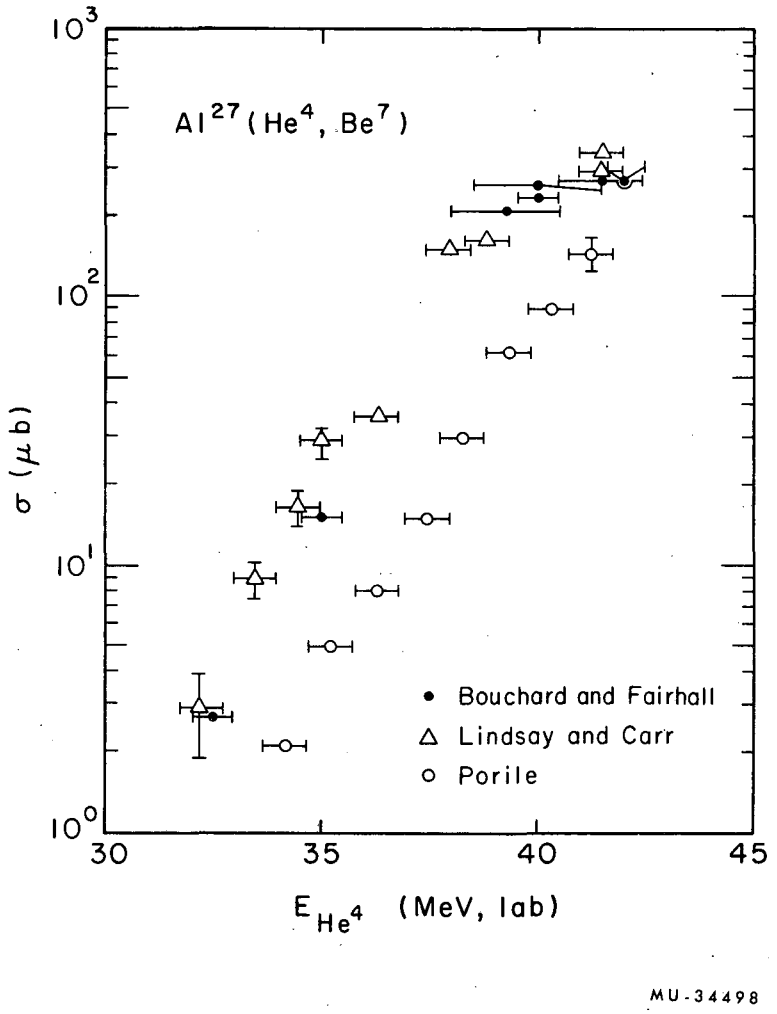

Fig. 5. Excitation function data of other investigators[3,34,35] for the reaction $Al^{27}(He^4,Be^7)$. Their results are taken as they were published with no correction made for the Be^7 half-life or branching ratio used in this work.

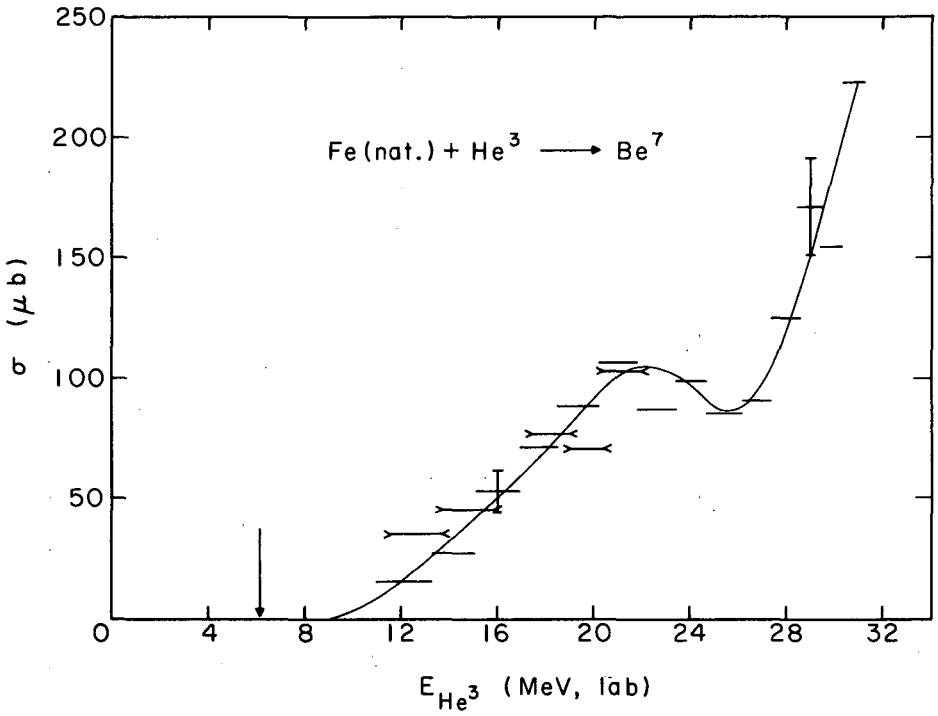

MU-34499

Fig. 6. Excitation function for the Fe(natural)(He^3,Be^7) reaction. The threshold for the Fe^{56}(He^3,Be^7)Cr^{52} reaction is 6.1 MeV. Data are compiled from two runs.

Since no range-energy curves for He^3 ions in Fe are available, several range-energy curves were calculated using the Bragg-Kleeman Rule[36] and available curves for He^3 in Cu and in Ni.[29,30,31] None of these schemes gave the proper range-energy relationship for it was known from heat damage in which foil the beam was stopped. The range-energy curve of He^3 in Ni was finally used to calculate the He^3 ion energy throughout the Fe stack. Although the electron density of Fe is approximately 12 percent lower than that of Ni, this range-energy curve for He^3 in Ni had the He^3 beam stopping in the correct foil.

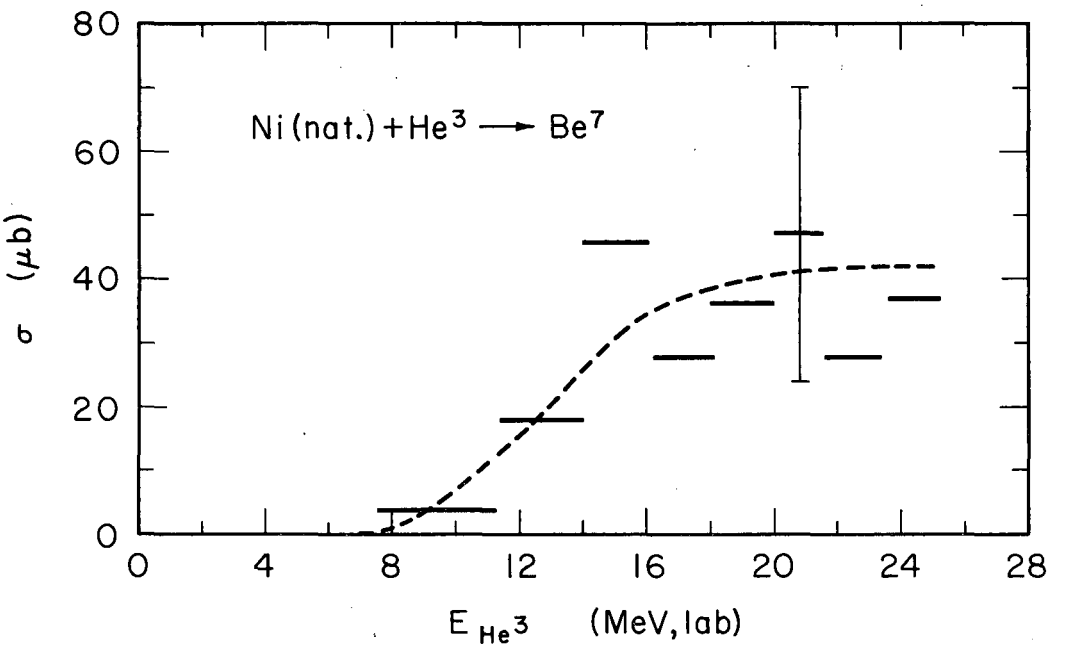

MU-34500

Fig. 7. Excitation function for the Ni(natural)(He^3,Be^7) reaction. The beam flux was determined by means of a monitor foil. The threshold for the $Ni^{58}(He^3,Be^7)Fe^{54}$ reaction is 5.1 MeV. Threshold for $Ni^{60}(He^3,Be^7)Fe^{56}$ is 4.9 MeV. Range-energy curve for He^3 in Ni was taken from Bromley and Almqvist.[30] The error bars indicated on this and the next figure are ±50 percent which reflect the facts that these were single runs where the integrated beam was determined by means of a monitor foil. The Be^7 production from impurities contained in the Ni and Cu foils may be large.

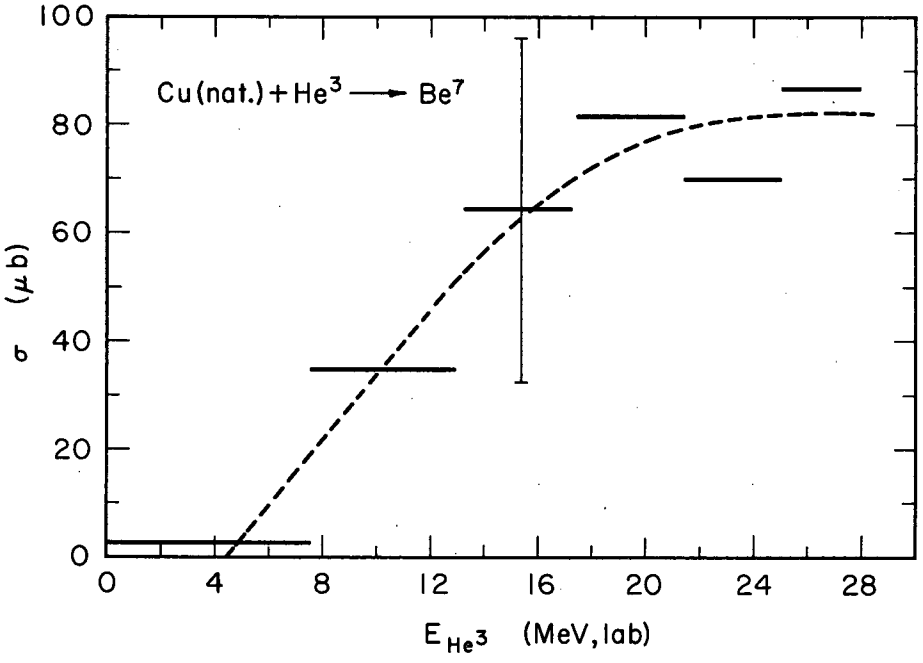

MU-34501

Fig. 8. Excitation function for the Cu(natural)(He^3,Be^7) reaction. The stack of foils was run on the collimator during another experiment. The beam flux was monitored by means of the Na^{22} activity induced in a thin aluminum (sandwiched) monitor foil. The range-energy relationship for He^3 in Cu was taken from Rich and Madey.[29] The threshold for the $Cu^{63}(He^3,Be^7)Co^{59}$ reaction is 4.4 MeV. The threshold for $Cu^{65}(He^3,Be^7)Co^{61}$ is 5.4 MeV.

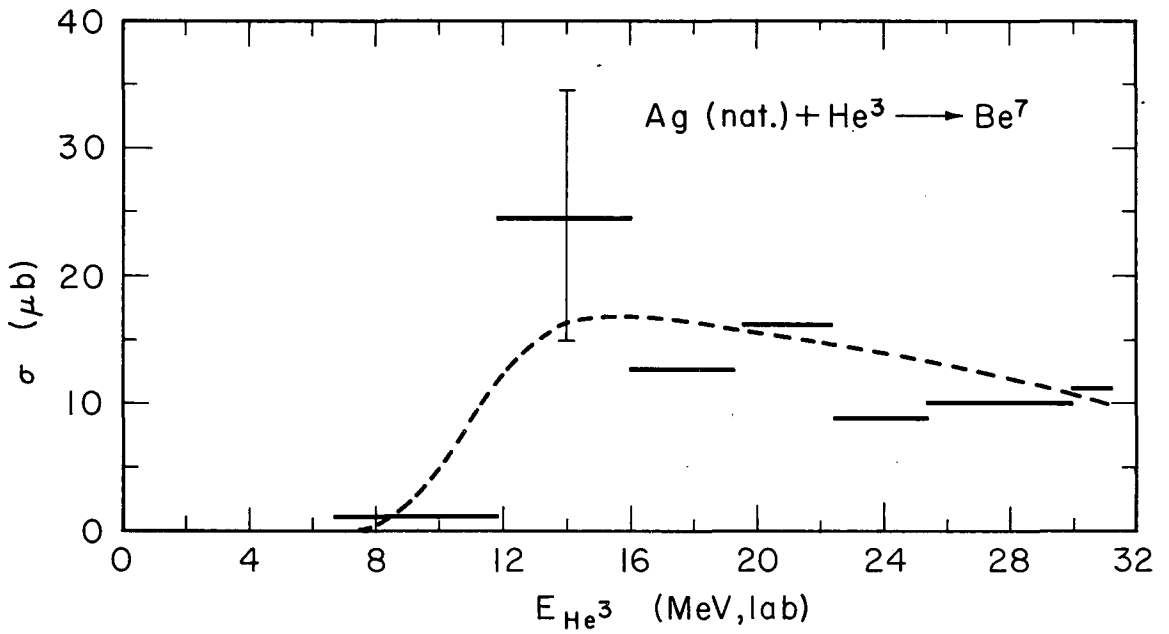

MU-34502

Fig. 9. Excitation function of the Ag(natural)(He^3,Be^7) reaction. The range-energy curve for He^3 in Ag was taken from Bromley and Almqvist.[30]

The threshold for the $Ag^{109}(He^3,Be^7)Rh^{105}$ reaction is 1.4 MeV. The threshold for $Ag^{107}(He^3,Be^7)Rh^{103}$ is 0.70 MeV. The Coulomb barrier for He^3 onto Ag is 14.6 MeV.

The ±50 percent uncertainty indicated on the data reflects the fact that this is data from a single experiment and that the role of light element impurities in Be^7 production is probably significant.

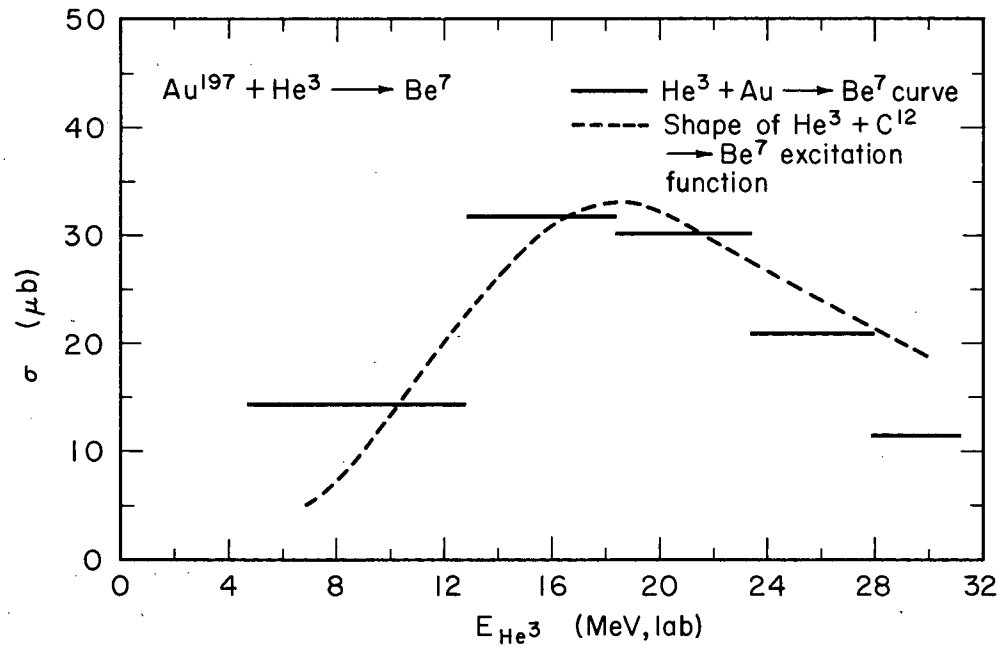

MU-34503

Fig. 10. Results of an $Au^{197}(He^3,Be^7)$ experiment. Since gold foils contain sufficient carbon impurity to account for the observed production of Be^7,[37] it is probable that the $Au^{197}(He^3,Be^7)$ cross section is very low. The dashed curve shows the shape of the $C^{12}(He^3,Be^7)$ excitation function for comparison with the observed Be^7 cross section as determined from Au foils. The Q-value for the reaction $Au^{197}(He^3,Be^7)$ is +3.1 MeV. However, the Coulomb barrier for He^3 onto Au is 26.9 MeV.
The range-energy curve for He^3 in Au were taken from Bromley and Almqvist.[30] The horizontal energy uncertainty denotes beam degradation in the respective target foils.

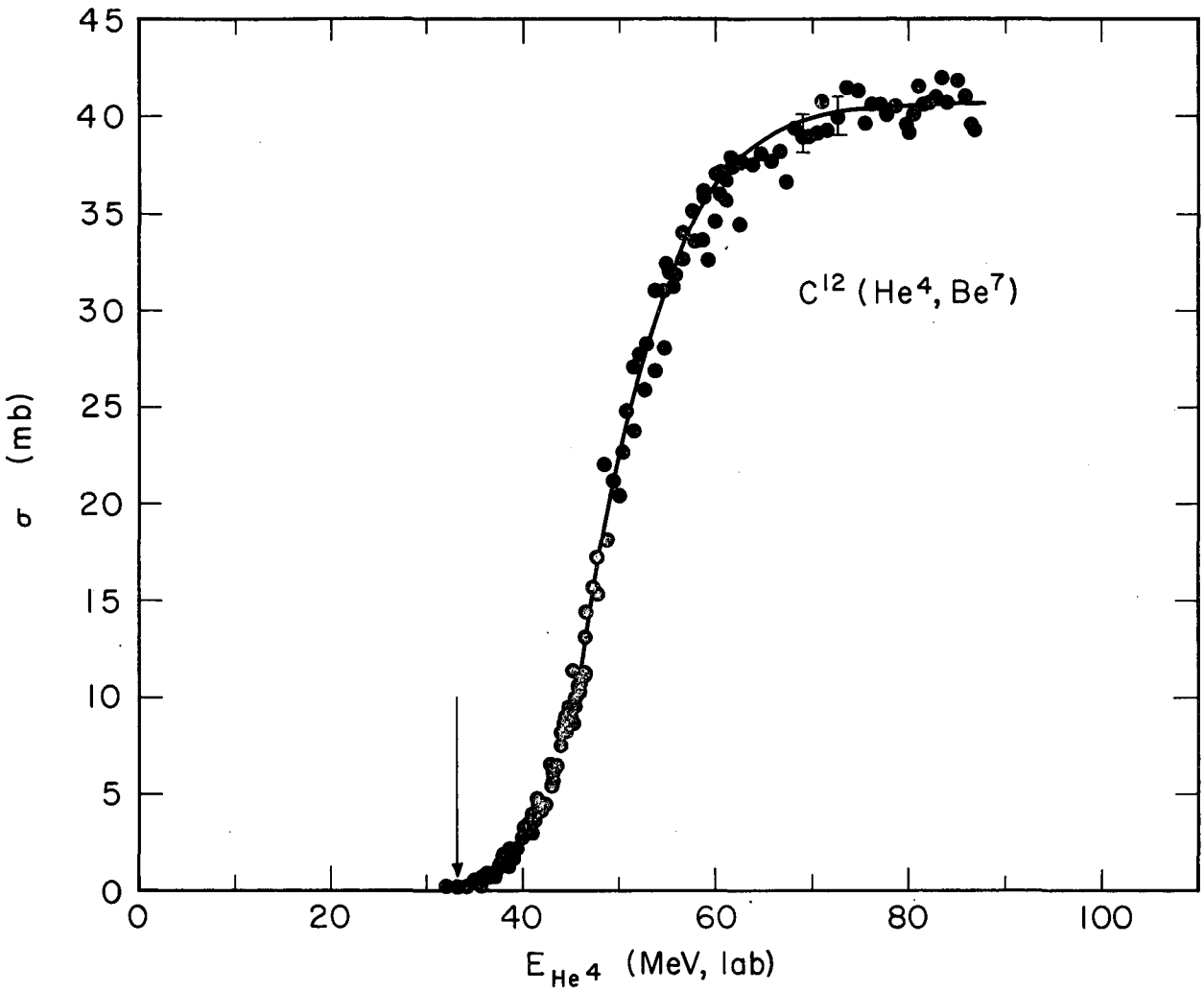

MUB-3184

Fig. 11. Excitation function for the $C^{12}(He^4,Be^7)$ reaction. The range-energy curve for alphas in carbon was calculated from the range-energy curve for He^3 in carbon as presented in Rich and Madey.[29] Data are compiled from four runs.
The threshold for the $C^{12}(He^4,Be^7)Be^9$ reaction is 32.9 MeV.

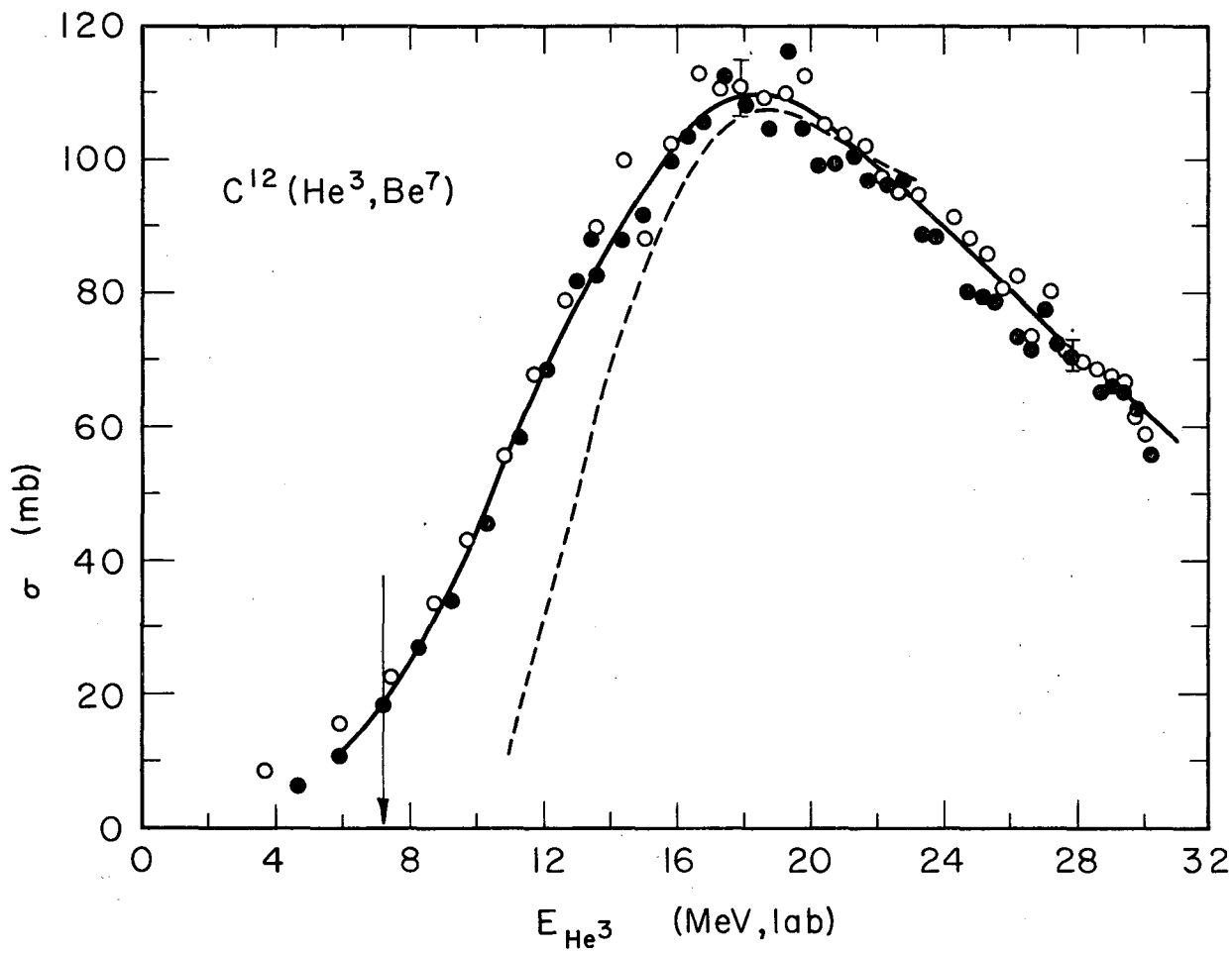

MUB-3174

Fig. 12. Excitation function for the $C^{12}(He^3,Be^7)$ reaction. The range-energy curve for He^3 in carbon was taken from Rich and Madey [29] Data are compiled from two runs.
The dashed curve is the same excitation function as determined by Cochran and Knight[33] using thin machined graphite discs as targets. Their data has been adjusted for the Be^7 half-life and branching ratio used in this work.
The threshold for the $C^{12}(He^3,Be^7)Be^8$ reaction is 7.2 MeV. The threshold for the $C^{12}(He^3,2\alpha)Be^7$ reaction is also 7.2 MeV.

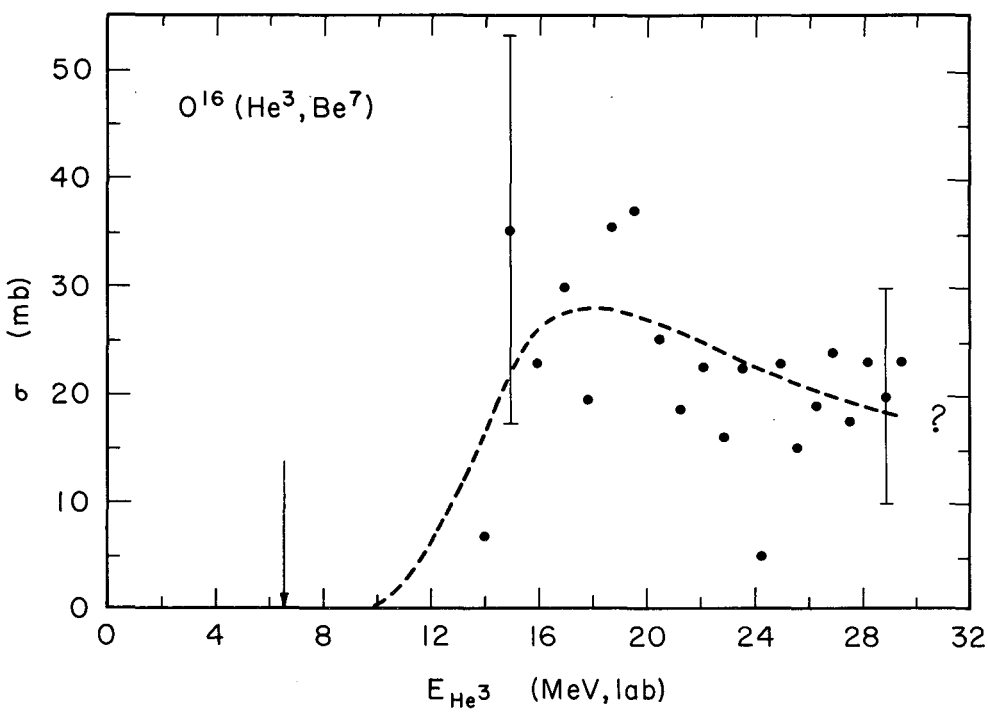

MU-34504

Fig. 13. Data on the $O^{16}(He^3,Be^7)$ reaction. The targets were mylar (33.3 percent oxygen, 62.5 percent carbon, and 4.2 percent hydrogen) and a large fraction of the Be^7 production in the target foils was due to the carbon. The Be^7 activity due to the carbon was subtracted using cross sections from Fig. 12, but the difficulty in accurately obtaining a small difference between the large Be^7 count rates per mylar foil and the large $C^{12}(He^3,Be^7)$ correction are reflected in the scatter of the points given in this figure.
The range-energy curve for He^3 in mylar was taken from Demildt.[31]
The threshold for the $O^{16}(He^3,Be^7)C^{12}$ reaction is 6.6 MeV.

In the following $C^{12}(He^3,Be^7)$ recoil experiment (Table II, Fig. 14) a 2.48 mg C per cm^2 target was sandwiched between many silver catcher foils. The He^3 energy varied from 30.2 to 30.0 MeV across the carbon target.

It was necessary to perform Be^7 radiochemical separations from the silver foils. Many up- and downstream foils on either side of those listed in Table II and Fig. 14 were analyzed in order to be certain that the Be^7 activity is represented by the data presented here. A small Be^7 activation of approximately 0.3 counts per minute in each Ag catcher foil has been subtracted.

Since a large amount of recoil positron activity appeared in the carbon target and thus precluded an accurate Be^7 activity determination, the activity of Be^7 remaining in the target was calculated.

The uncertainties were obtained by estimating a ±5 percent variation in the observed count rates of the target and each catcher.

The data for this run are presented in Table II and in Fig. 14. The beam strikes the stack first at 3-Ag and proceeds downstream.

In this experiment

$$F = 0.49 \pm 0.02$$
$$B = 0.011 \pm 0.001$$
$$T = 0.50 \pm 0.03$$

Table II. Data from $C^{12}(He^3,Be^7)$ sandwiched target recoil experiment. The target thickness was 2.48 mg C per cm^2 and $\langle E_{He^3} \rangle$ = 30.1 MeV.

Foil	Foil thickness	Be^7 activity
4-Ag	2.61 mg/cm^2	0 cpm
5-Ag	2.68	121.7
6-C	2.48	5450 (calculated)
7-Ag	2.53	1828
8-Ag	2.55	1274
9-Ag	2.51	831
10-Ag	2.64	551
11-Ag	2.66	357
12-Ag	2.72	247
13-Ag	2.51	142
14-Ag	2.66	52.5
15-Ag	2.51	0

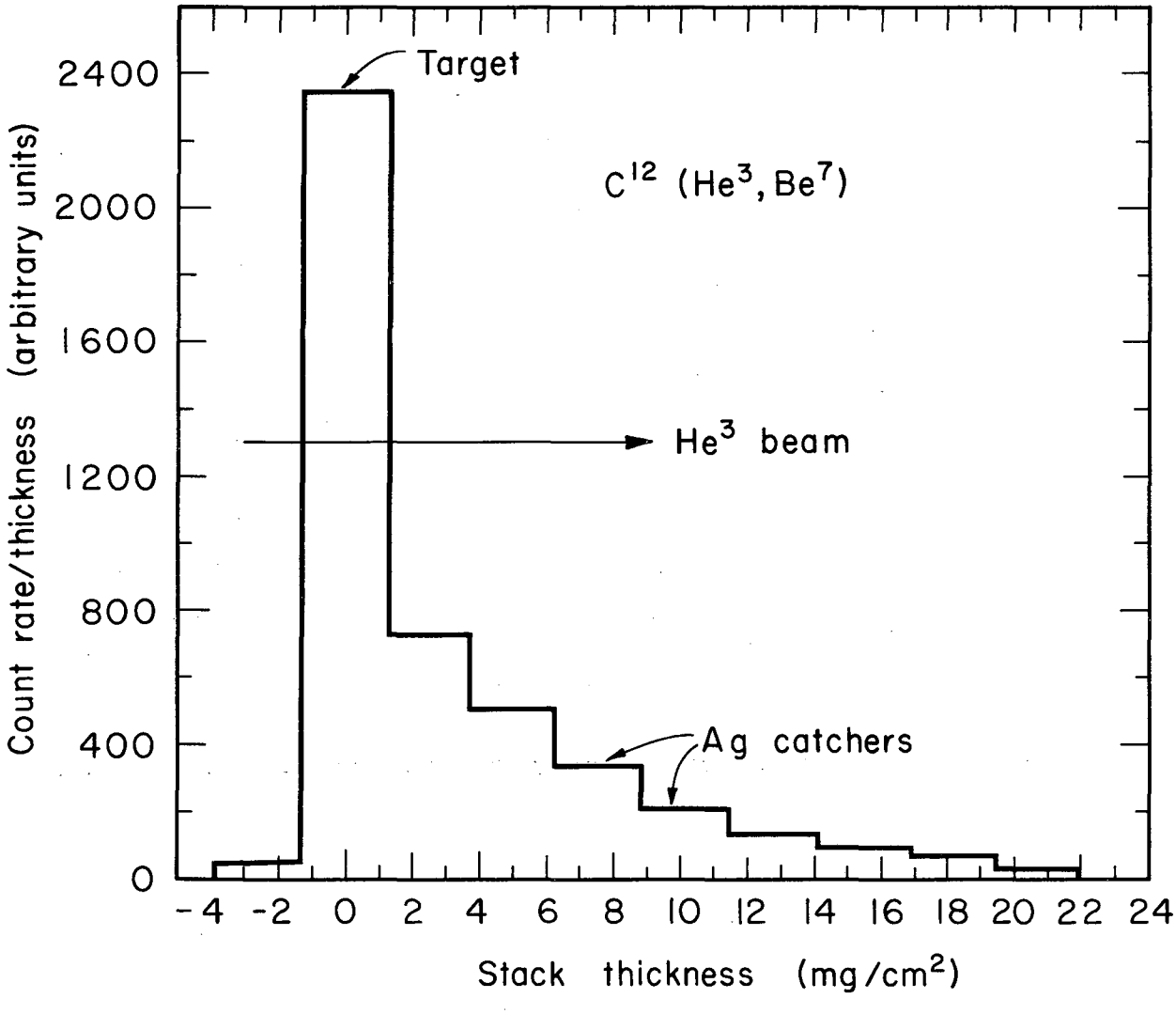

MUB-3179

Fig. 14. Activity profile for Be^7 produced in a stacked foil experiment. The 2.48 mg C per cm^2 target was sandwiched between many silver catcher foils. The average He^3 ion energy in the target was 30.1 MeV

The following $C^{12}(He^3,Be^7)$ recoil experiment was similar to the last one. Here the He^3 was degraded in energy from 24.0 to 23.5 MeV upon passing through the 2.42 mg C per cm^2 target. Nickel foils were used as catchers and the Be^7 was radiochemically separated from them.

Uncertainties were estimated to be ±5 percent in all of the active foils.

In this experiment

$$F = 0.33 \pm 0.02$$
$$B = 0.0072 \pm 0.0004$$
$$T = 0.66 \pm 0.04.$$

The data are presented in Table III and shown in Fig. 15.

Table III. Data from $C^{12}(He^3,Be^7)$ sandwiched target recoil experiment. The target thickness was 2.42 mg C per cm^2. The average bombarding energy in the carbon target was 23.8 MeV.

Foil	Foil thickness	Be^7 activity
9-Ni	2.28 mg/cm^2	0 cpm
10-Ni	2.44	111
11-C	2.42	10,177 observed 10,435 calculated
12-Ni	2.37	2502
13-Ni	2.24	1394
14-Ni	2.42	805
15-Ni	2.31	281
16-Ni	2.42	31.8
17-Ni	2.40	0

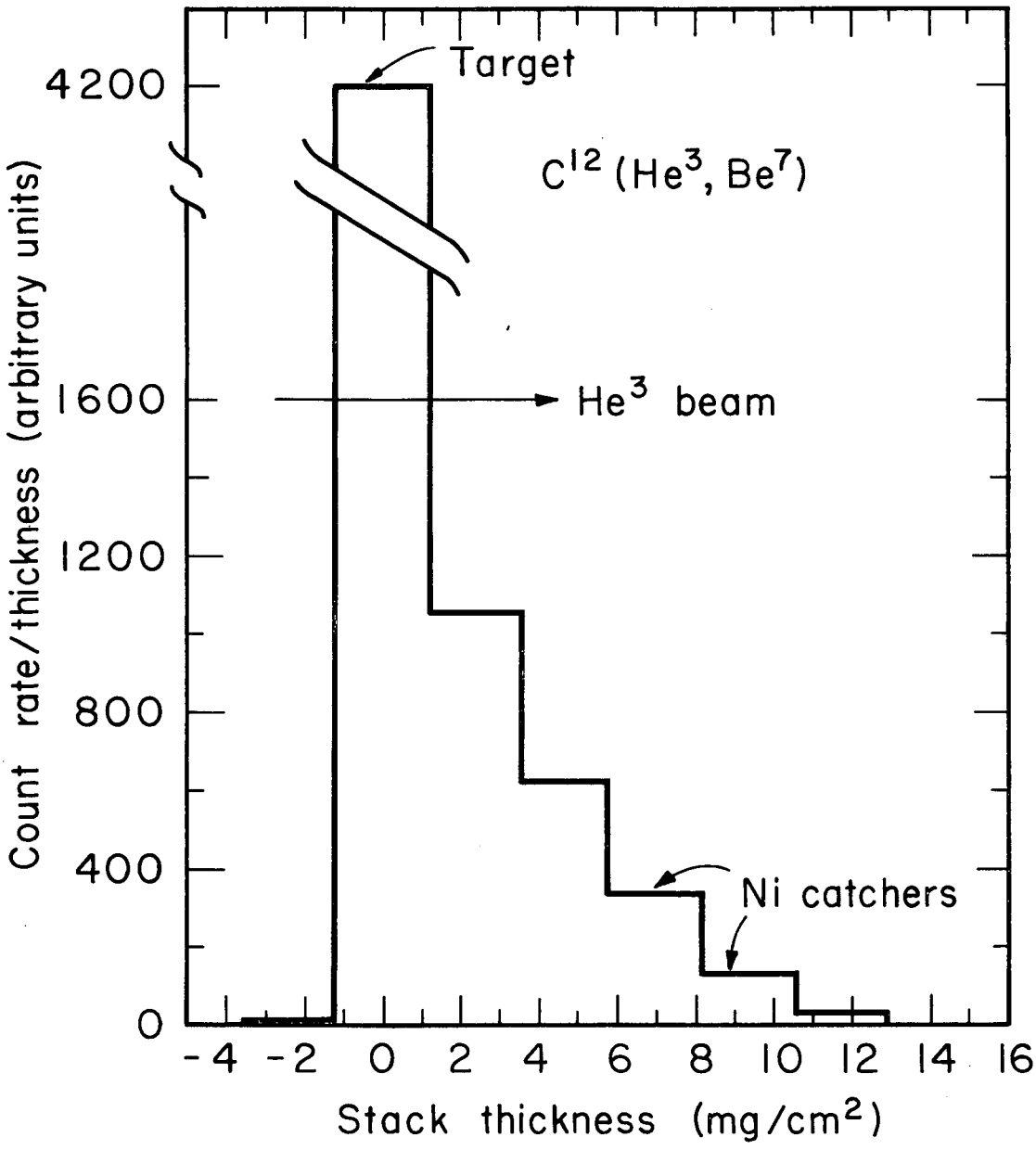

MUB-3180

Fig. 15. Activity profile for Be^7 produced in a stacked foil experiment. The 2.42 mg C per cm^2 target was sandwiched between many nickel catcher foils. The average He^3 ion energy in the target was 23.8 MeV.

The following $C^{12}(He^3,Be^7)$ recoil experiment was similar to the last one. Here the He^3 was degraded in energy from 14.9 to 14.2 MeV upon passing through the 2.48 mg C per cm^2 target. Silver foils were used as catchers and the Be^7 was radiochemically separated from them.

Uncertainties are estimated to be ±5 percent in the observed activity of each catcher foil. The activity remaining in the target is taken to be ±10 percent of the value calculated because of the rapidly decreasing excitation function in this region and because of the inaccurately known beam energy after degradation to approximately half energy.

In this experiment

$$F = 0.21 \pm 0.02$$
$$B = 0.0014 \pm 0.0001$$
$$T = 0.79 \pm 0.10$$

The data are presented in Table IV and shown in Fig. 16.

Table IV. Data from $C^{12}(He^3,Be^7)$ sandwiched target recoil experiment. The target thickness was 2.48 mg C per cm^2. The average bombarding energy in the carbon target was 14.6 MeV.

Foil	Foil thickness	Be^6 activity
31-Ag	2.72 mg/cm^2	0 cpm
32-Ag	2.62	22.4
33-C	2.48	12,856 (calculated)
34-Ag	2.37	2471
35-Ag	2.64	774
36-Ag	2.58	87
37-Ag	2.74	0

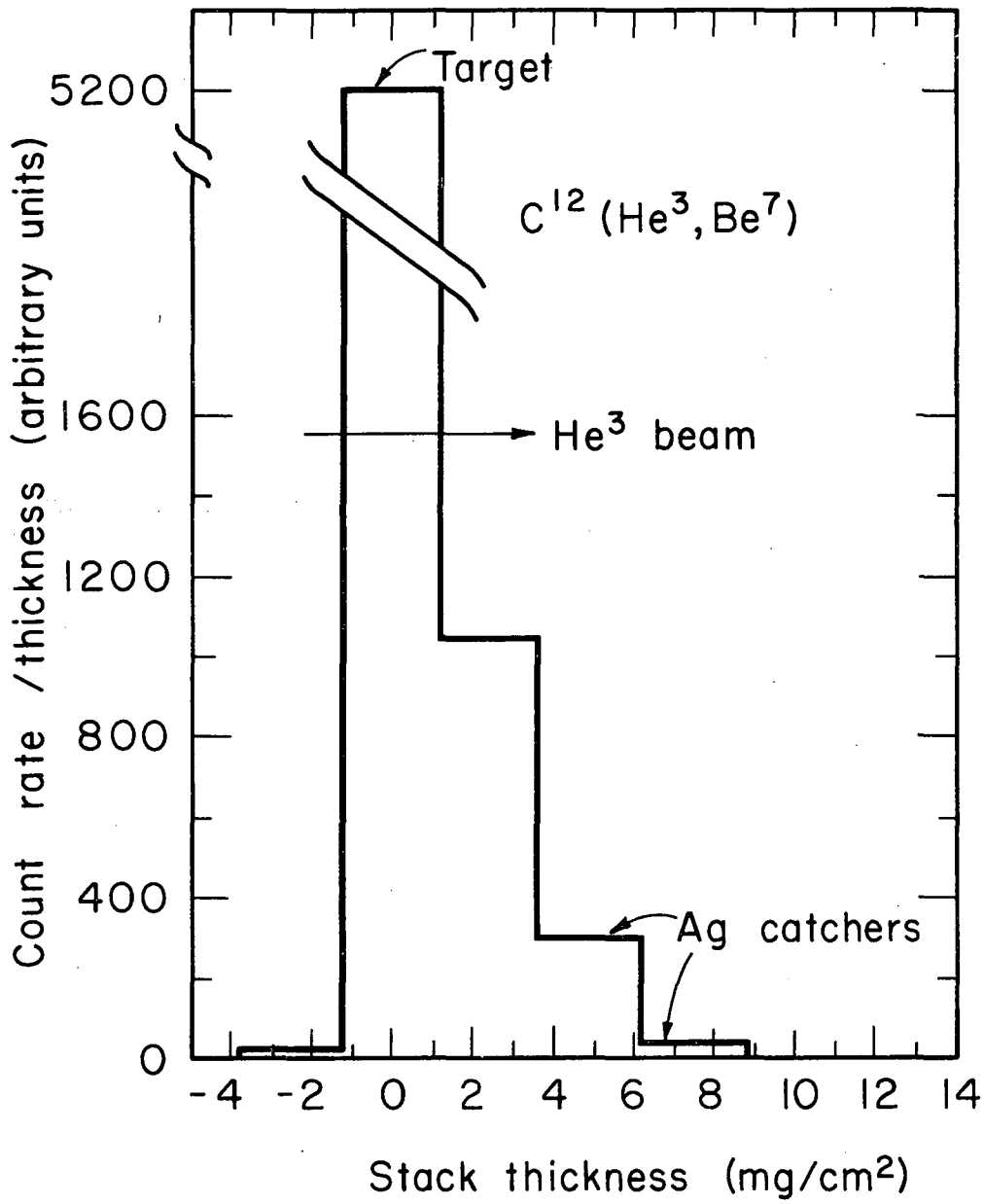

MUB-3182

Fig. 16. Activity profile for Be^7 produced in a stacked foil experiment. The 2.48 mg C per cm^2 target was sandwiched between many silver catcher foils. The average He^3 ion energy in the target was 14.6 MeV.

The following $C^{12}(He^3,Be^7)$ recoil experiment was similar to the last one. Here the He^3 beam was degraded in energy from 10.8 to 9.8 MeV in passing through the 2.46 mg C per cm^2 target foil. Nickel foils were used as catchers and the Be^7 was radiochemically separated from them.

The uncertainties in the activities of the two most active foils is estimated to be ±5 percent for each. The uncertainty in the value of B is estimated by assuming that the backward count rate is 2 ±.2 counts per minute.

In this experiment

$$F = 0.078 \pm 0.005$$
$$B = 0.004 \pm 0.004$$
$$T = 0.92 \pm 0.06.$$

The data are presented in Table V and shown in Fig. 17.

Table V. Data from $C^{12}(He^3,Be^7)$ sandwiched target recoil experiment. The target thickness was 2.46 mg C per cm^2. The average bombarding energy in the carbon target was 10.3 MeV.

Foil	Foil thickness	Be^7 activity
33-Ni	2.35 mg/cm^2	0
34-C	2.46	420 (observed)
35-Ni	2.29	35.3
36-Ni	2.40	0

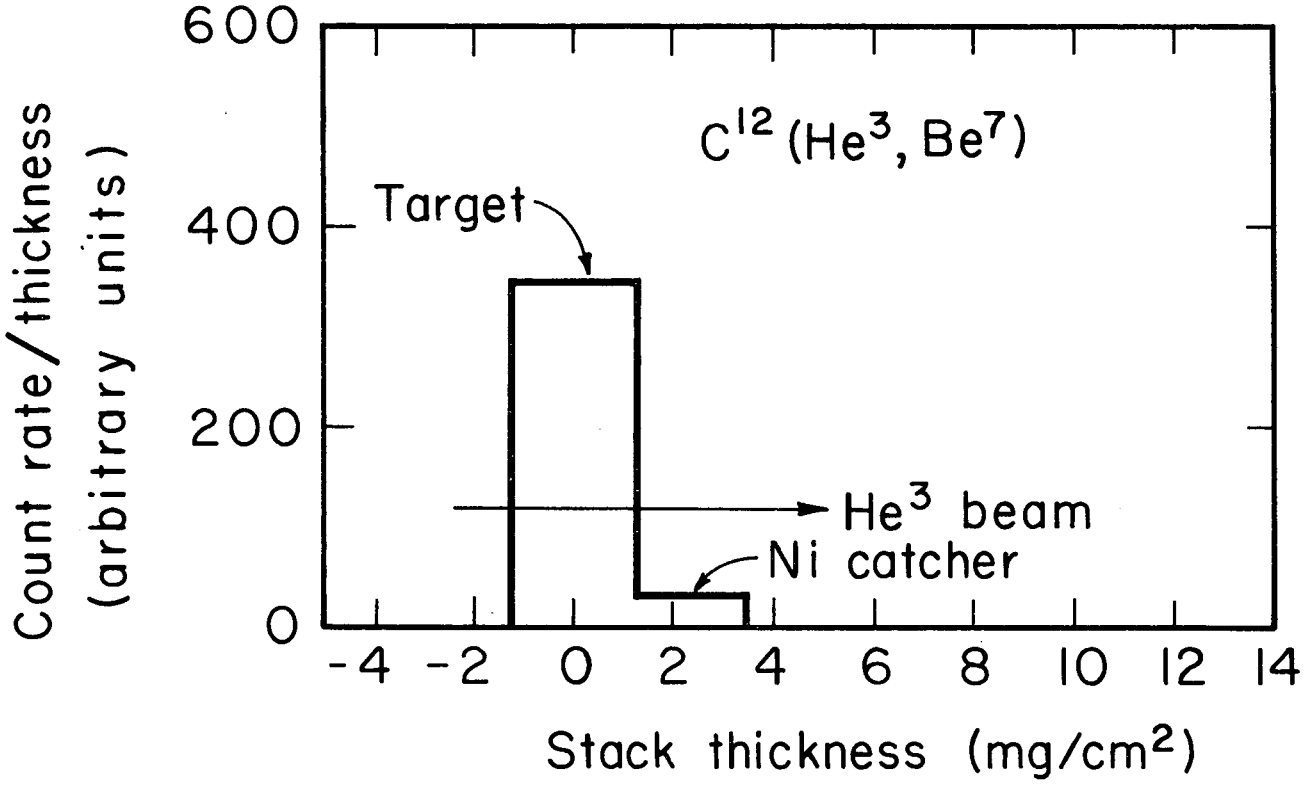

MUB-3181

Fig. 17. Activity profile for Be^7 produced in a stacked foil experiment. The 2.46 mg C per cm^2 target was sandwiched between many nickel catcher foils. The average He^3 ion energy in the target was approximately 10.3 MeV.

The following $C^{12}(He^3,Be^7)$ recoil experiment is similar to the last one. However, here the target is a thin carbon film of 120 micrograms per cm^2. The catcher foils are nickel. For plotting purposes, the carbon film has been converted to an equivalent thickness of nickel by the factor 1.73, the ratio of the stopping power of carbon to that of nickel.

The Be^7 activity in the target film is subject to large uncertainty because of the high recoil positron activity it contained from neighboring nickel foils. Be^7 was radiochemically separated from the catcher foils.

Deviations in the activities of the catcher foils were taken to be ±5 percent for each. The uncertainty in the count rate of the target was estimated to be ±50 percent.

The data are presented in Table VI and shown in Fig. 18. In this experiment

$$F = 0.85 \pm 0.03$$
$$B = 0.11 \pm 0.01$$
$$T = 0.044 \pm 0.022.$$

Table VI. Data from $C^{12}(He^3,Be^7)$ sandwiched target recoil experiment. The target thickness was 120 micrograms per cm^2. The bombarding energy at the target was 30.4 MeV.

Foil	Foil thickness	Be^7 activity
2-Ni	2.63 mg/cm^2	0
3-Ni	2.46	22.8
4-Ni	0.53	37.6
5-C	0.120	25
6-Ni	0.60	64.6
7-Ni	2.21	185
8-Ni	2.28	99.5
9-Ni	2.25	55.9
10-Ni	2.18	34.1
11-Ni	2.25	20.8
12-Ni	2.24	14.1
13-Ni	2.28	10.9
14-Ni	2.28	0

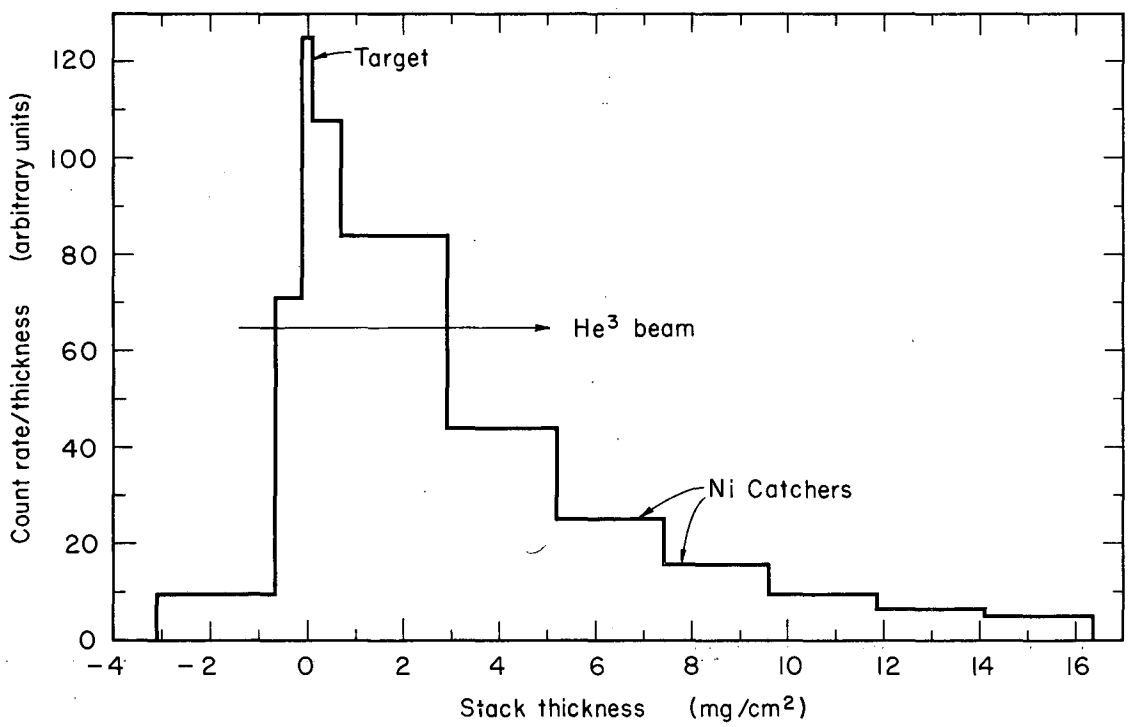

Fig. 18. Activity profile for Be^7 produced in a stacked foil experiment. The 120 microgram C per cm^2 target was sandwiched between many nickel catcher foils. The He^3 ion energy at the target was 30.4 MeV.

This run is also similar to the preceding ones. This $C^{12}(He^3,Be^7)$ sandwiched target recoil experiment utilized a carbon target of 227 micrograms per cm^2. For plotting purposes, this is converted to an equivalent nickel thickness. Be^7 was radiochemically separated from the nickel catcher foils, but since no separation was feasible for the Be^7 in the carbon target, its activity is subject to a large uncertainty.

The variation in the count rate of the catchers is taken to be ±5 percent and that in the target, ±50 percent.

The data from this run are presented in Table VII and in Fig. 19. In this experiment

$$F = 0.81 \pm 0.08$$
$$B = 0.019 \pm 0.002$$
$$T = 0.17 \pm 0.10.$$

Table VII. Data from $C^{12}(He^3,Be^7)$ sandwiched target recoil experiment. The target thickness was 227 micrograms C per cm^2. The average bombarding energy at the target foil was 15.2 MeV.

Foil	Foil thickness	Be^7 activity
24-Ni	2.35 mg/cm^2	0 cpm
25-Ni	0.56	22.8
26-C	0.227	200
27-Ni	0.60	209.9
28-Ni	2.28	594
29-Ni	2.35	128
30-Ni	2.28	0

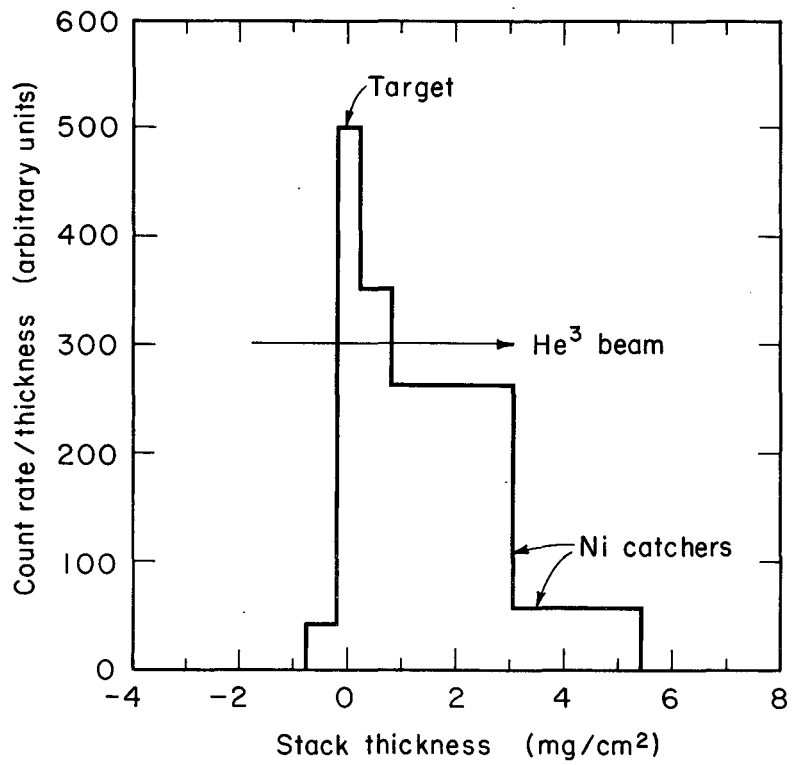

Fig. 19. Activity profile of Be^7 produced in a stacked foil experiment. The 227 microgram C per cm^2 target was sandwiched between many nickel catcher foils. The average He^3 ion energy in the target was 15.2 MeV.

In one $C^{12}(He^3,Be^7)$ recoil experiment, thin carbon films were bombarded in a stack of gold catcher foils. After a sufficiently long waiting period, there remained no activity (specifically β^+) which would interfere with the determination of the Be^7 peak, and the gold catchers could be counted directly.

A ±10 percent variation was taken for the count rates in targets and catchers.

The results are presented in Table VIII.

Table VIII. Recoil data for $C^{12}(He^3,Be^7)$ reaction.

Target thickness	$\langle E_{He^3} \rangle$	F	B	T
270 micrograms/cm^2	30.4 MeV	0.76±0.03	0.078±0.006	0.16±0.02
417	15.0	0.72±0.04	0.008±0.001	0.27±0.03

In this experiment (Fig. 20) the differential cross section (the angular distribution of Be^7 from the $C^{12}(He^3,Be^7)$ reaction integrated over energy) is obtained as a function of laboratory angle from 0 to 31 deg.

The 2-mil silver catcher foil was mounted on a holder which also served as a cutter to cut the catcher foil into seventeen concentric rings. (See Fig. 1.) The 920 microgram C per cm^2 target was placed perpendicular to the beam axis. Beam energy was 31.2 MeV and the collimation was one-eighth inch. All linear measurements of dimensions were performed four times and the average was taken to calculate angles. The very low observed count rate per ring was divided by $\Delta\cos\theta_{lab}$ to obtain a quantity proportional to $(d\sigma/d\Omega)_{lab}$, the Be^7 cross section per unit solid angle, at each laboratory angle. Count rates were corrected for chemical yields and for decay after bombardment. Because the beam passed through the catcher foil, a 0.6 cpm Be^7 activation correction was calculated for the catcher that subtended the laboratory angle 0.00 to 2.04 deg. No Be^7 activation corrections were made for the other catcher rings.

Attempts were made to obtain angular distributions in similar experiments using degraded He^3 beams. Degrader foils were placed, in turn, behind the first collimator, the second collimator, and finally immediately ahead of the target. However, the beam flux was attenuated considerably after degradation. It is probable that after some beam development the Hilac could accelerate half-energy He^3 ions with sufficient intensity to perform this experiment successfully.[38]

In Fig. 20 a horizontal bar represents the angle subtended by a given catcher foil annulus.

The following experiment (Fig. 21) yielded the angular distribution of all Be^7 from the $C^{12}(He^3,Be^7)$ reaction from 8.20 to 171.40 deg. in the laboratory. Two-mil silver foil was loaded into the angular distribution apparatus shown in Fig. 2. After the run, the catcher foils were cut up into sections to obtain the angular distribution. Radiochemical separation of Be^7 was performed on all the individual foil

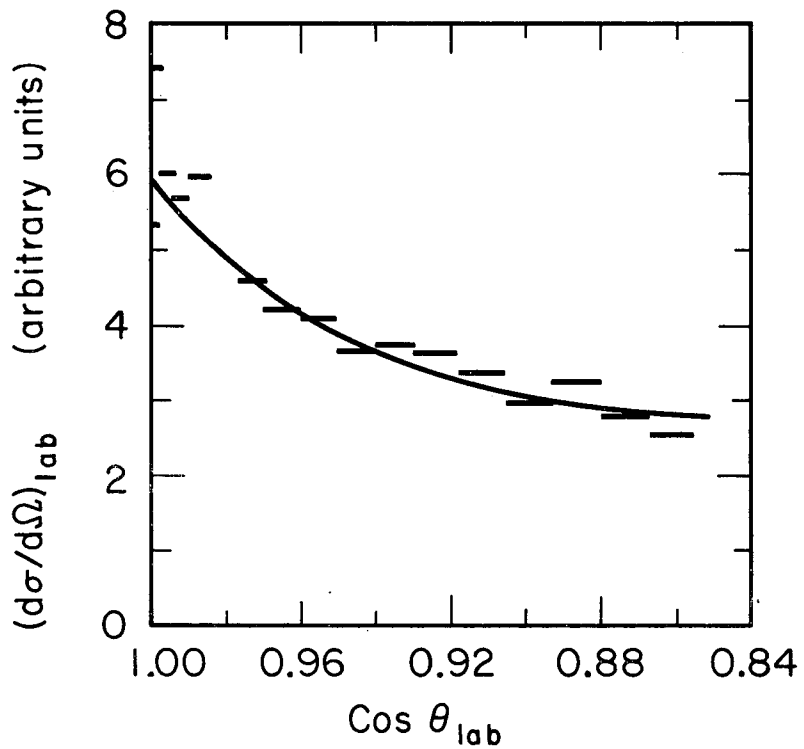

MU-34507

Fig. 20. Angular distribution of Be^7 from the $C^{12}(He^3,Be^7)$ reaction out to $31^o5.4'$ in the laboratory. The He^3 bombarding energy was 31.2 MeV.

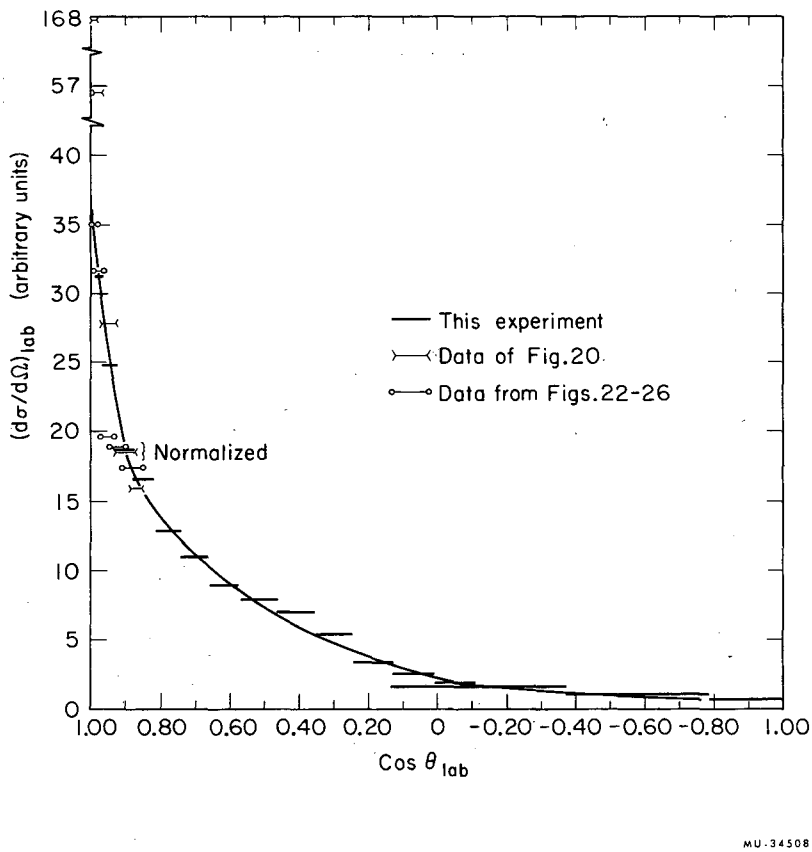

Fig. 21. Angular distribution of Be^7 from the $C^{12}(He^3,Be^7)$ reaction from $8^\circ 12'$ to $171^\circ 24'$ in the laboratory. The He^3 bombarding energy was 31.2 MeV.

sections. The results are corrected for chemical yield and decay after bombardment. The target thickness was 780 micrograms C per cm^2 and was oriented at 45 deg. to the beam axis. The energy of the He^3 was 31.2 MeV. The beam was directed through a 1/8-in. collimation system. The horizontal bars represent the angle subtended by the respective catcher foil segments.

In the following experiment (Figs. 22-26) a target of 264 micrograms C per cm^2 was placed perpendicular to the 31.2 MeV He^3 beam. Collimation was one-eighth inch. A stack of approximately quarter-mil aluminum foils was placed on the holder shown in Fig. 1. The aluminum catcher foils were cut from the center and most uniform portion of the aluminum sheets. A 1/4-in. beam hole was punched in the catcher foil stack. After the run the beam hole was enlarged slightly and the remainder of the catcher area was cut into five concentric annuli. The stacked foils constituting each of these rings were then counted to determine their Be^7 content. No radiochemical separation of Be^7 was performed, and activation in all the catcher foils was negligible after a period of waiting.

The range-energy curve for Be^7 in aluminum was calculated from the published[39] range-energy curve for Be^9 ions in aluminum and the factor 7/9 for ions of the same velocity.

This experiment yielded a double differential cross section for Be^7 produced in the $C^{12}(He^3,Be^7)$ reaction. Figures 22 to 26 show the data.

The raw data presented in Figs. 22-26 were transformed into the O^{15} center-of-mass system by a transformation determined by the He^3 energy and the masses of the He^3 and C^{12}. The results of this transformation are shown in Figs. 27-30. These figures show the angular distribution for the different Be^7 center-of-mass energy groups.

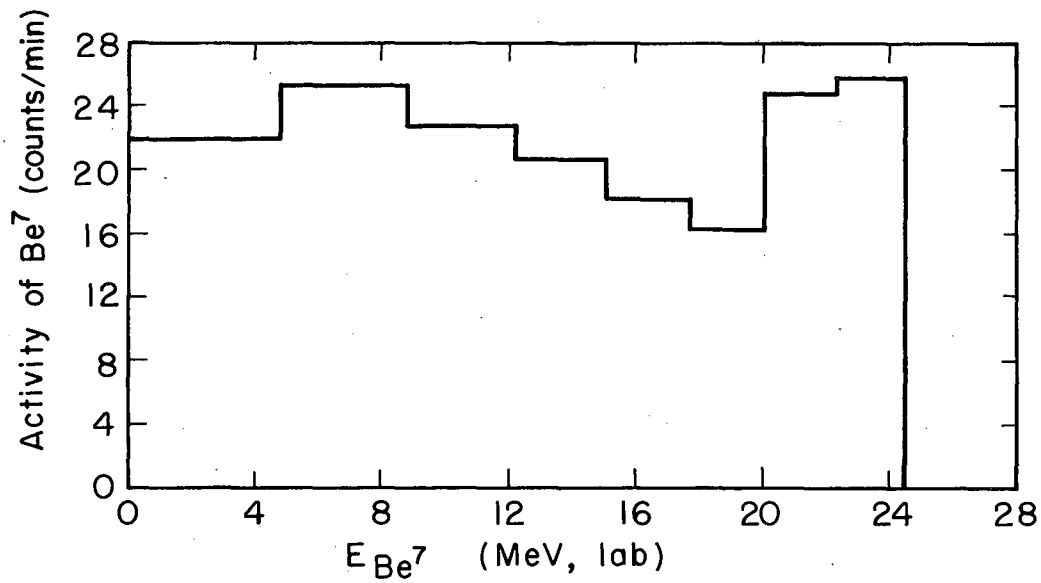

MU-34509

Fig. 22. Laboratory energy distribution of Be^7 produced in the $C^{12}(He^3,Be^7)$ reaction at a He^3 bombarding energy of 31.2 MeV. The laboratory angle subtended by this series of catcher foils ranges from $3^\circ 05'$ to $8^\circ 11'$.

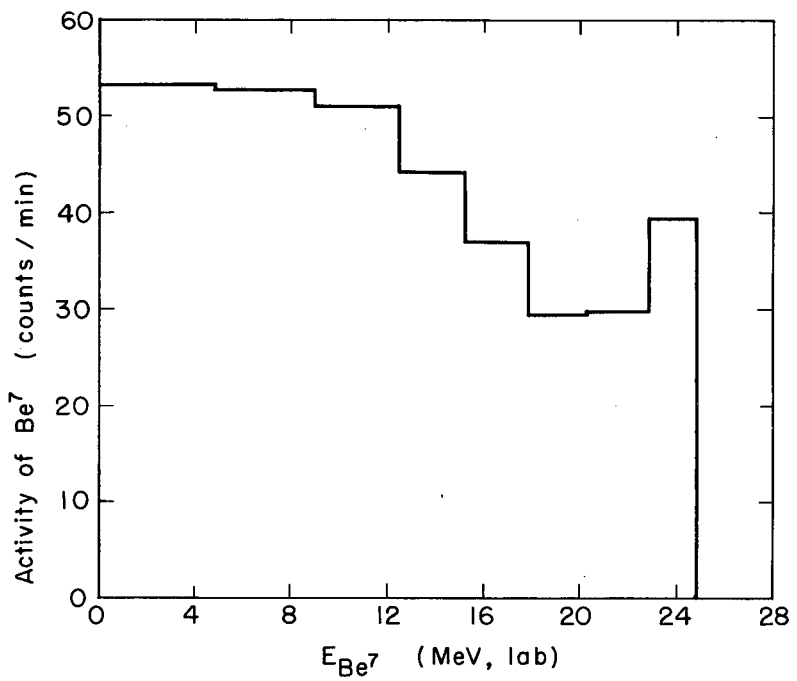

Fig. 23. Laboratory energy distribution for Be^7 produced in the $C^{12}(He^3,Be^7)$ reaction at a He^3 bombarding energy of 31.2 MeV. The laboratory angle subtended by this series of catcher foils ranges from $8^\circ 11'$ to $14^\circ 10'$.

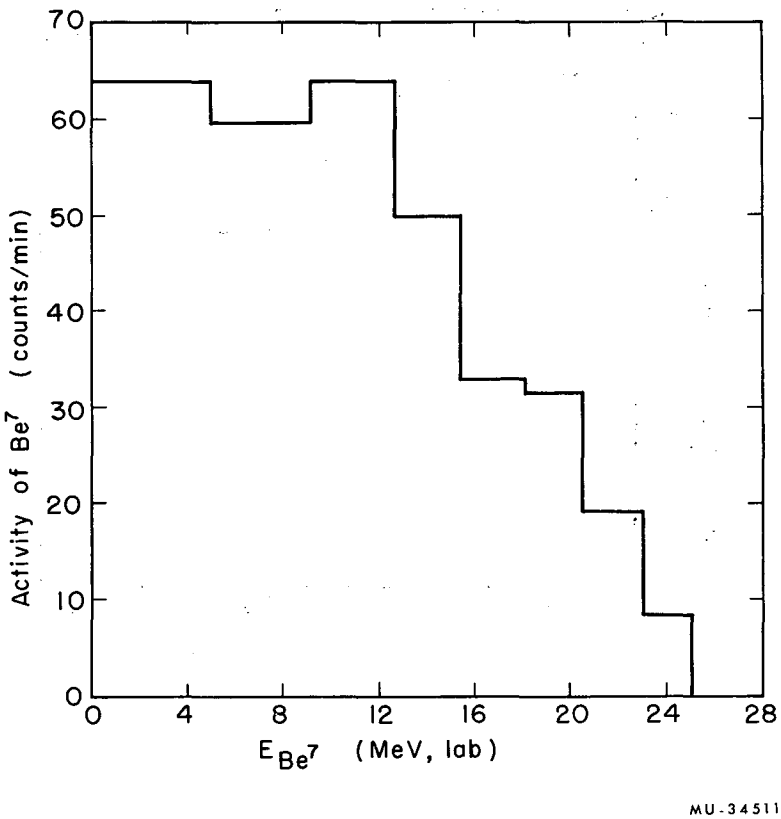

Fig. 24. Laboratory energy distribution of Be^7 produced in the $C^{12}(He^3,Be^7)$ reaction at a He^3 bombarding energy of 31.2 MeV. The laboratory angle subtended by this series of catcher foils ranges from $14^o10'$ to $19^o52'$.

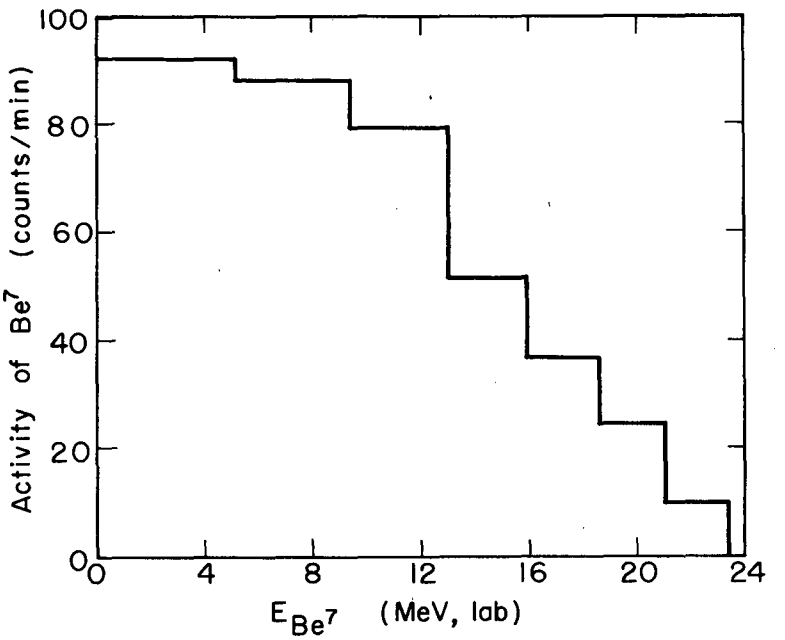

MU-34512

Fig. 25. Laboratory energy distribution for Be^7 produced in the $C^{12}(He^3,Be^7)$ reaction at a He^3 bombarding energy of 31.2 MeV. The laboratory angle subtended by this series of catcher foils ranges from $19^\circ 52'$ to $25^\circ 10'$.

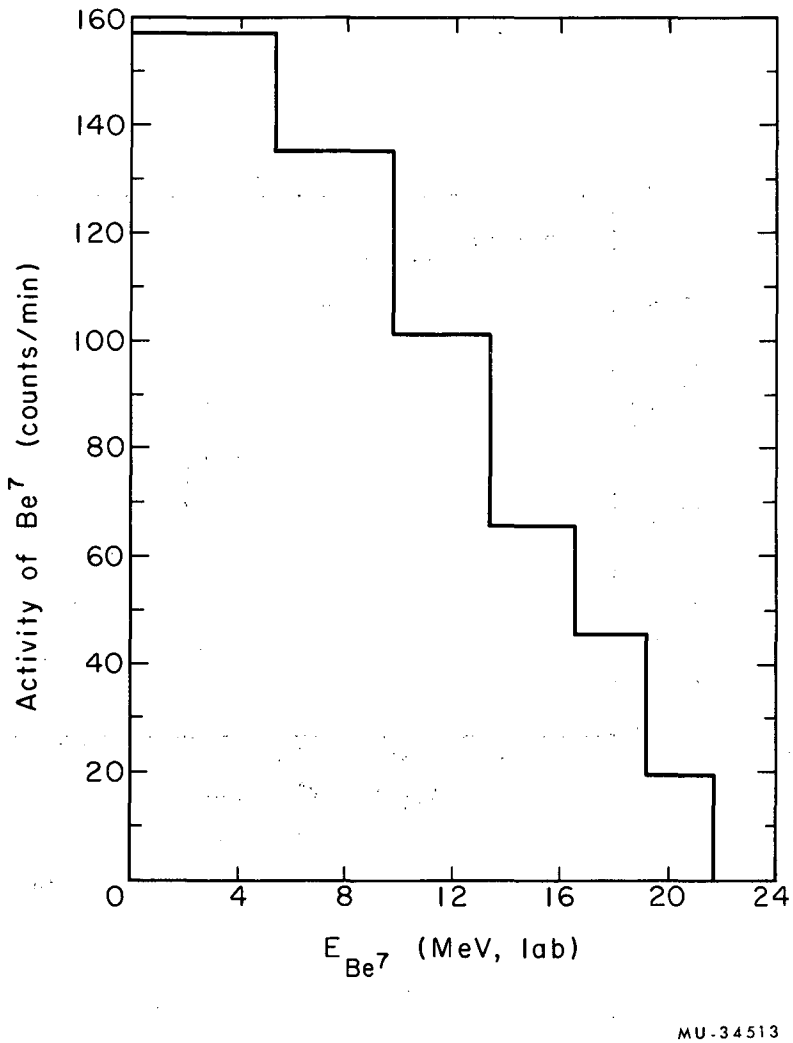

Fig. 26. Laboratory energy distribution of Be^7 produced in the $C^{12}(He^3,Be^7)$ reaction at a He^3 bombarding energy of 31.2 MeV. The laboratory angle subtended by this series of catcher foils ranges from $25^o10'$ to $31^o27'$.

An area in the following figures, that is $(d\sigma/d\Omega) \times \Delta\cos\theta$ is proportional to cross section. The area contained in the two peaks of Figs. 29 and 30 (which is attributed to direct interaction (DI); see Sec. V.-E) is approximately 2 percent of the total cross section for $C^{12}(He^3,Be^7)$ at He^3 energy of 31.2 MeV. From Fig.12 the total Be^7 formation cross section at 31.2 MeV is 57 millibarns. Hence σ_{DI} = one millibarn.

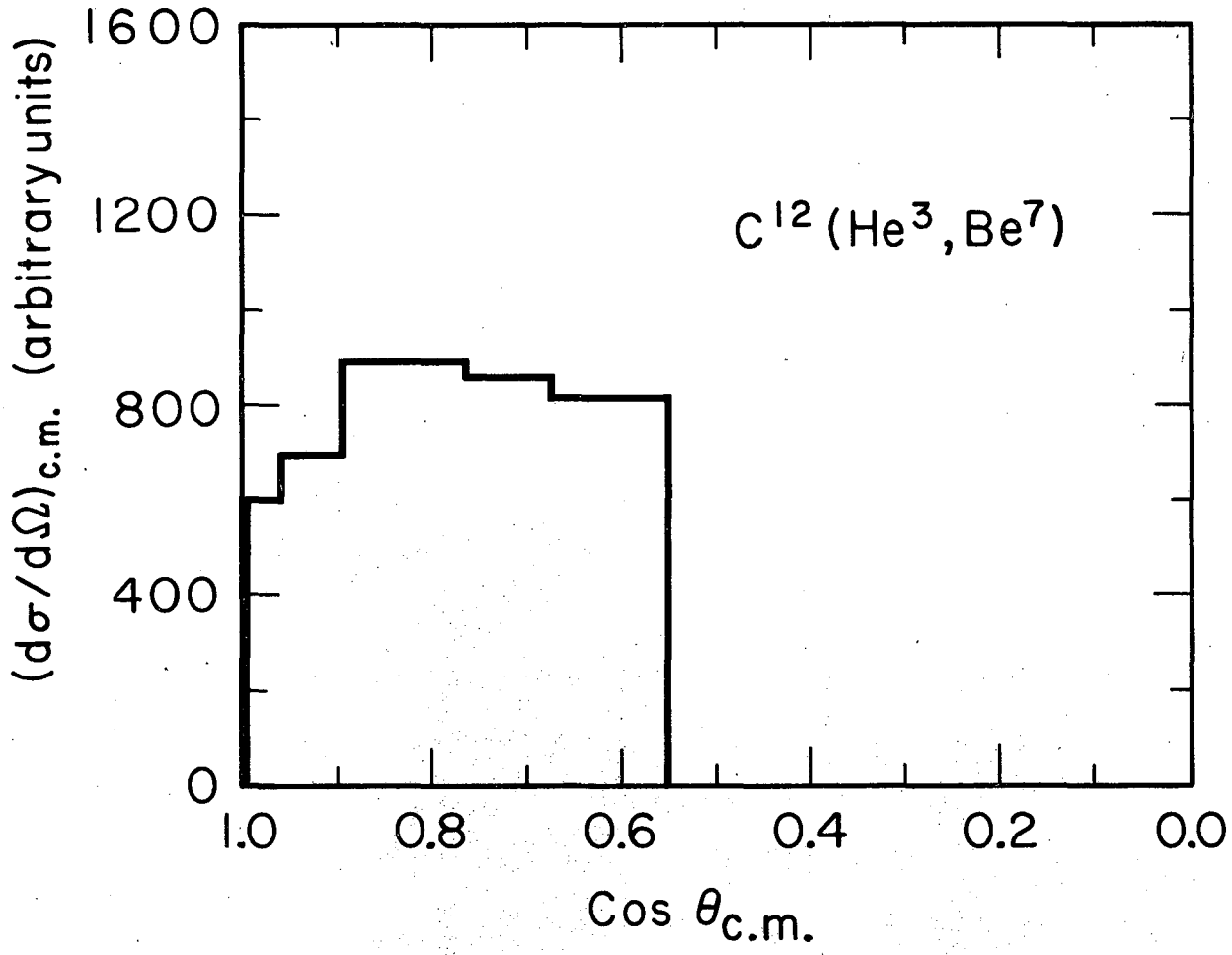

MUB-3172

Fig. 27. Angular distribution of Be^7 from the $C^{12}(He^3,Be^7)$ reaction in the O^{15} center-of-mass system. This figure represents the energy group, $3 \leqslant E^{CM}_{Be^7} \leqslant 5$ MeV. The center-of-mass cut-off angle is $56^{\circ}37'$.

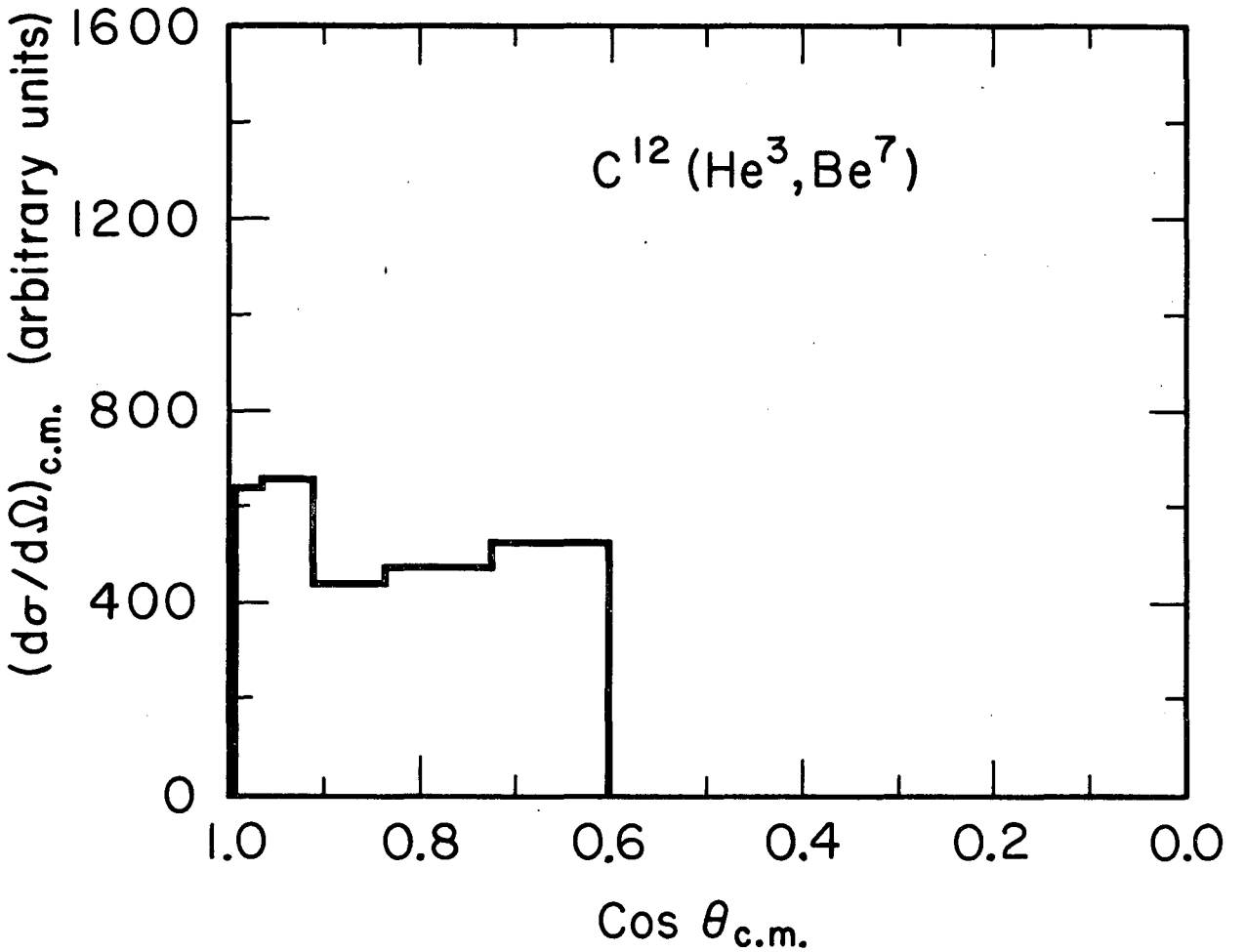

MUB-3175

Fig. 28. Angular distribution of Be^7 from the $C^{12}(He^3,Be^7)$ reaction in the O^{15} center-of-mass system. This figure represents the energy group, $5 \leqslant E^{CM}_{Be^7} \leqslant 7$ MeV. The center-of-mass cut-off is $52^\circ 58'$.

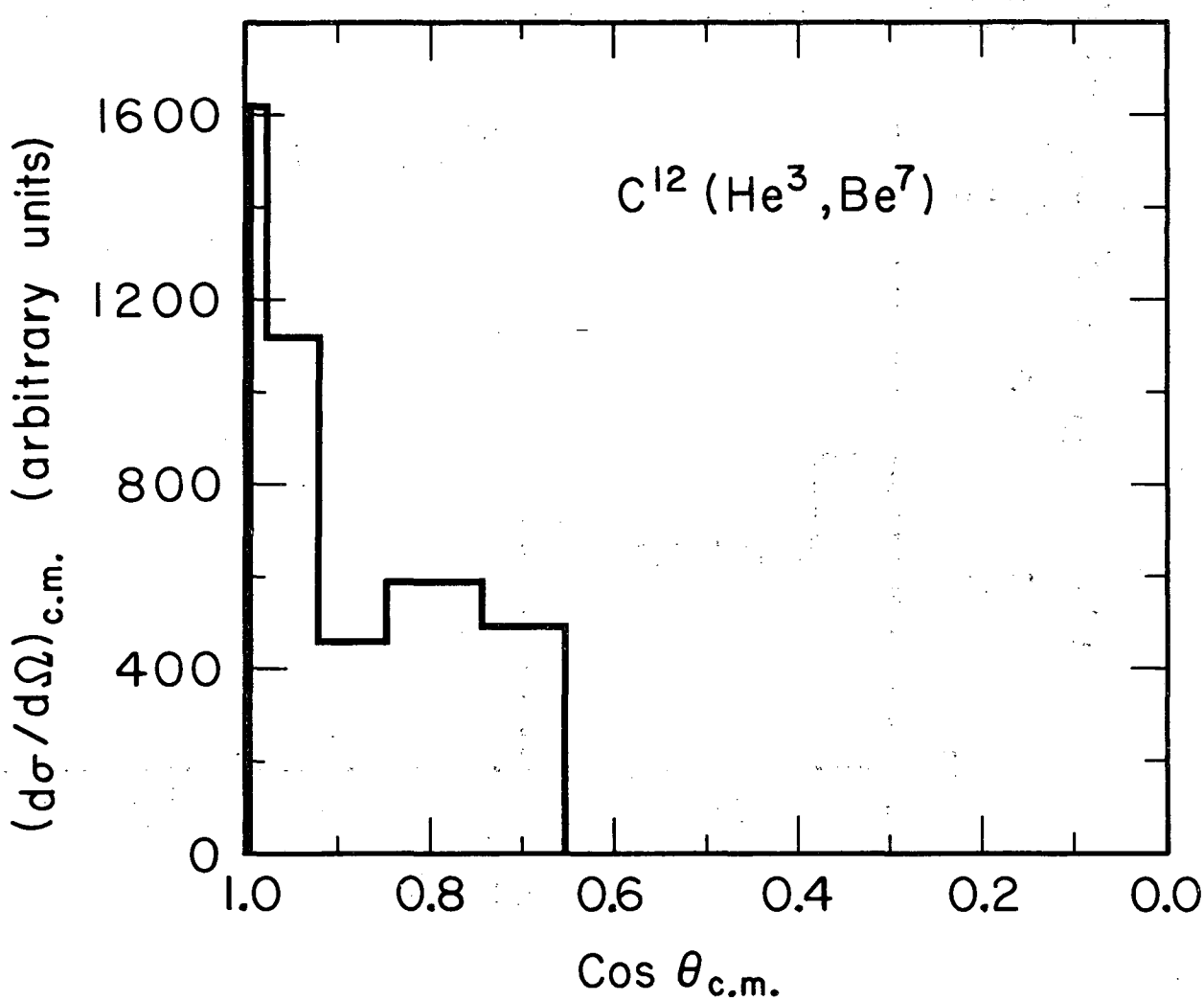

MUB-3176

Fig. 29. Angular distribution of Be^7 from the $C^{12}(He^3,Be^7)$ reaction in the O^{15} center-of-mass system. This figure represents the energy group, $7 \leqslant E^{CM}_{Be^7} \leqslant 9$ MeV. The center-of-mass cut-off angle is $49^\circ 25'$.

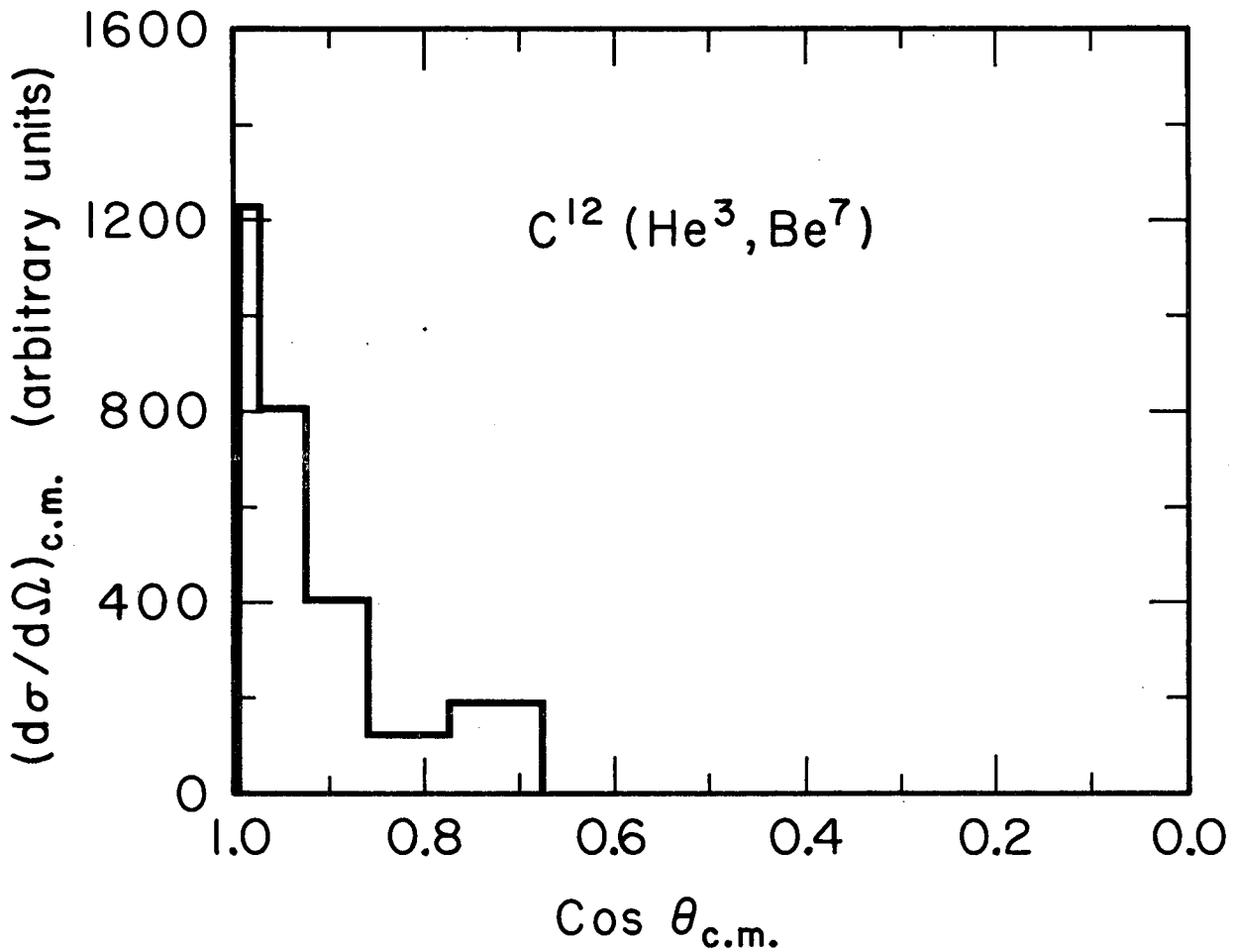

MUB-3177

Fig. 30. Angular distribution of Be^7 from the $C^{12}(He^3,Be^7)$ reaction in the O^{15} center-of-mass system. This figure represents the energy group, $E^{CM}_{Be^7} > 9$ MeV. The center-of-mass cut-off angle is $47^o40'$.

IV. ANALYSIS OF EXPERIMENTAL DATA

A. Analysis of the $C^{12}(He^3,Be^7)$ Reaction at He^3 Bombarding Energy of Approximately 30 MeV

1. Fitting of the activity profile in the sandwiched thin target experiment.

The nearly isotropic distributions (Figs. 27-30) contribute much more to the total Be^7 production cross section than does the higher energy Be^7 contained in the forward peaks (Figs. 29-30). The approach taken throughout this analysis is to fit all the data at all He^3 bombarding energies with compound-nucleus-type mechanisms. In the absence of more detailed information, these mechanisms are assumed to produce Be^7 isotropically in the center-of-mass (CM) system. It will be seen that all the data can be fit using this model. It is never necessary to invoke any sizable fraction of the direct interaction process ${}_2He^3 + {}_2He^4(\text{cluster}) = {}_4Be^7$ which presumably gives energetic Be^7 in the forward direction. (See Sec. V.-E.)

The key for the analysis is the double differential cross section data shown in Figs. 27-30 The two lower energy Be^7 groups in the O^{15} center-of-mass system (Figs. 27 and 28) are assumed to be isotropic, and the two higher energy groups (Figs. 29 and 30) are assumed to be composed of an isotropic contribution and an additional forward-peaked component. (See Table IX.)

The amount of the very lowest energy group, $E^{CM}_{Be^7} = 1\text{-}3$ MeV is difficult to obtain from the double differential cross section experiment because the velocity of the center-of-mass in the laboratory system is greater than the velocity of the Be^7 in the center-of-mass. The contribution of this energy group was estimated using the data of Fig. 18 (sandwiched thin target recoil experiment) by a procedure described in the following paragraphs.

The Be^7 activity in individual up- and downstream catcher foils can be calculated for thin target type experiments using a vector model, provided an assumption is made regarding the center-of-mass angular distribution of Be^7. Also the range-energy relationship for the Be^7 in the catcher foil material must be known.

Table IX. Relative amounts of the Be^7 center-of-mass energy groups as determined in the double differential cross section experiment.

$E^{CM}_{Be^7}$	$\langle E^{CM}_{Be^7} \rangle$ used in analysis	Isotropic contribution	Relative amounts of different groups
1-3 MeV	2 MeV	(See text)	10.0 parts
3-5	4	804[a]	5.1
5-7	6	516[b]	3.2
7-9	8	514[c]	3.2
> 9	10	159[d]	1.0

[a]Average of the ordinates shown in Fig. 27.

[b]Average of the ordinates shown in Fig. 28.

[c]Average of the three wide angle pieces of data shown in Fig. 29.

[d]Average of the two wide angle pieces of data shown in Fig. 30.

Figures 31-35 show the calculated laboratory activity profiles for an isotropic CM distribution for the energy groups $E^{CM}_{Be^7} = 2, 4, 6, 8$, and 10 MeV. The range-energy relationship used was $R_{Be^7} = k(vel)^2_{Be^7}$. The justification for this approximation is included in Appendix I, together with the derivation used to calculate the following activity profiles. Because the calculations aim to reproduce the experimental activity profile of Fig. 18, the nickel catcher foil thicknesses used in the calculated profiles are the same as those used in the actual experiment.

Forming a hybrid of the Figs. 31-35 using the relative weights of the different energy groups as indicated in Table IX, and assigning a relative weight of 10 for the 2 MeV CM Be^7 energy group, the experimental activity profile of Fig. 18 is reproduced in Fig. 36.

The small percentage of Be^7 appearing in the forward peaks of Figs. 29 and 30 is not included on Fig. 36. Inclusion of this forward peaking in the calculated activity profile would slightly raise the activities in the last two downstream catcher foils.

This treatment has assumed the relative amounts of the energy groups are known. It has also assumed CM isotropy, a zero thickness target, and the range-energy relationship $R_{Be^7} = k(vel)^2_{Be^7}$ over the entire energy range. These last three assumptions are not completely correct.

A similar calculation using calculated activity profiles for a $1/\sin\theta_{CM}$ angular distribution was tried in order to see how well the experimental activity profile would be reproduced. The calculated $1/\sin\theta_{CM}$ profiles are peaked forward and backward in the laboratory. Adding up the profiles weighted according to Table IX gives a calculated profile which is also too strongly peaked forward and backward when compared to experimental.

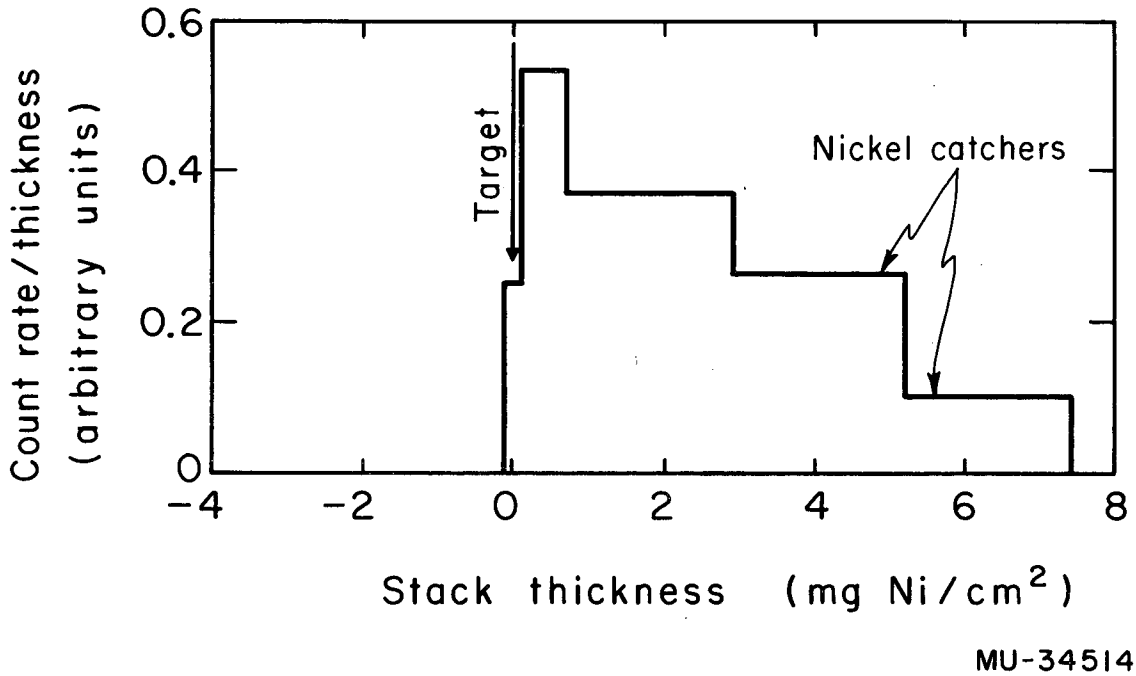

Fig. 31. Calculated activity profile for Be^7 from $C^{12}(He^3,Be^7)$ reaction. $E^{lab}_{He^3} = 31$ MeV and $E^{CM}_{Be^7} = 2$ MeV. The maximum Be^7 laboratory energy is 9.8 MeV.

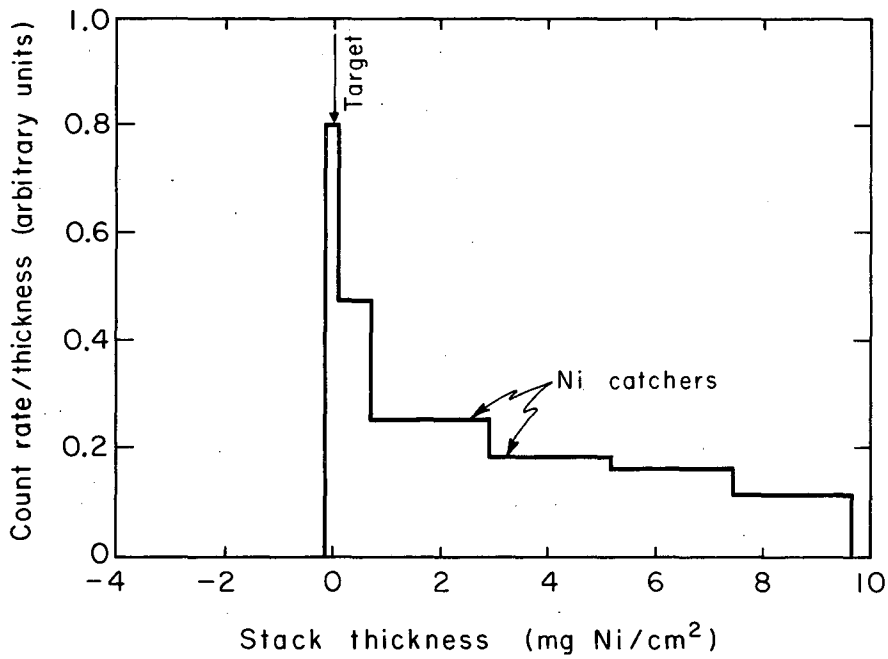

MU-34515

Fig. 32. Calculated activity profile for Be^7 from $C^{12}(He^3,Be^7)$ reaction. $E^{lab}_{He^3} = 31$ MeV and $E^{CM}_{Be^7} = 4$ MeV. The maximum Be^7 laboratory energy is 13.7 MeV.

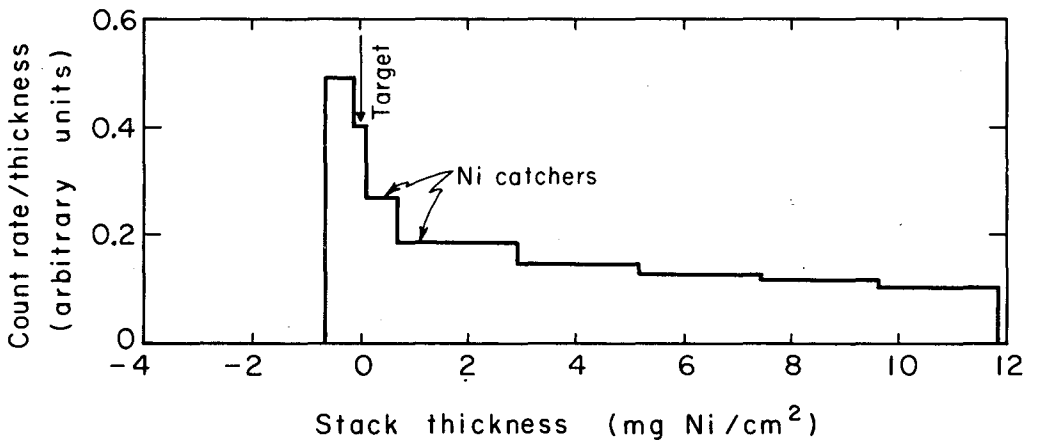

MU-34516

Fig. 33. Calculated activity profile for Be^7 from $C^{12}(He^3,Be^7)$ reaction. $E^{lab}_{He^3} = 31$ MeV and $E^{CM}_{Be^7} = 6$ MeV. The maximum Be^7 laboratory energy is 17.1 MeV.

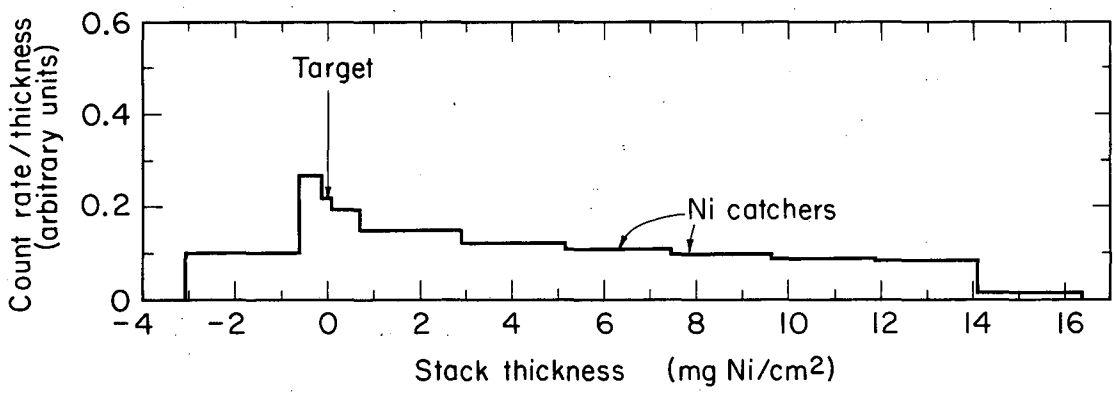

MU-34517

Fig. 34. Calculated activity profile for Be^7 from $C^{12}(He^3,Be^7)$ reaction. $E^{lab}_{He^3} = 31$ MeV and $E^{CM}_{Be^7} = 8$ MeV. The maximum Be^7 laboratory energy is 20.2 MeV.

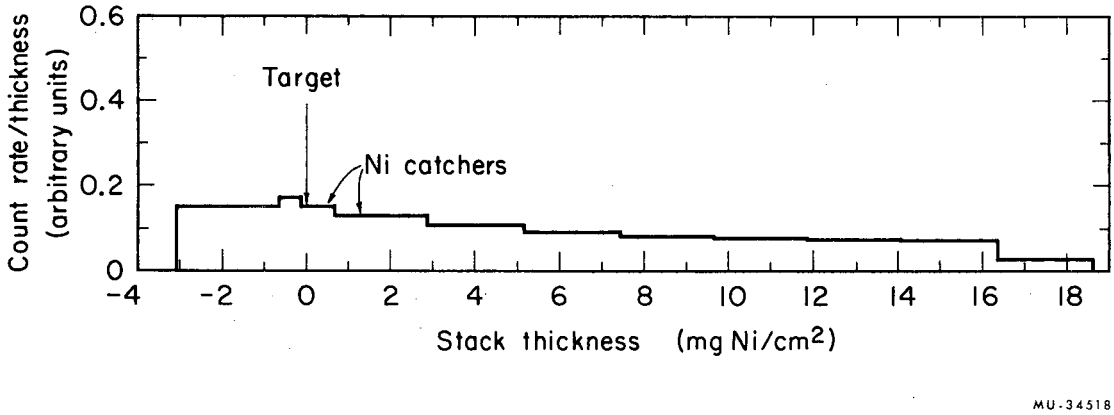

Fig. 35. Calculated activity profile for Be^7 from $C^{12}(He^3,Be^7)$ reaction. $E^{lab}_{He^3}$ = 31 MeV and $E^{CM}_{Be^7}$ = 10 MeV. The maximum Be^7 laboratory energy is 23.6 MeV.

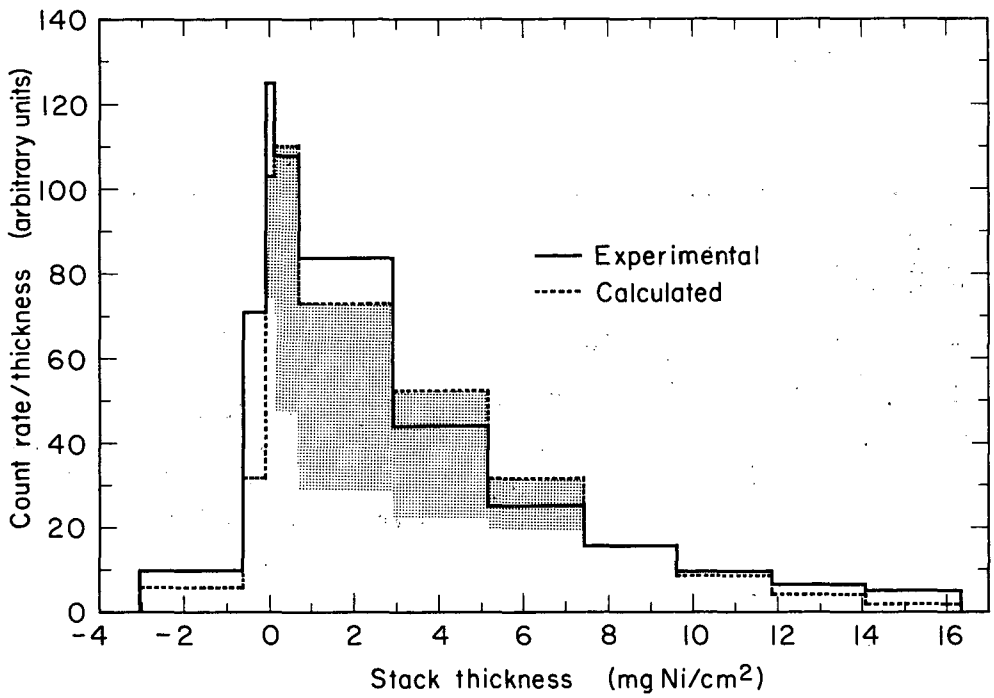

Fig. 36. Comparison of the calculated Be^7 activity profile with experimental data for the $C^{12}(He^3,Be^7)$ reaction at a bombarding energy of 31 MeV. The shaded area represents the contribution from 10 parts of the 2 MeV energy group. Other Be^7 CM energy groups are weighted according to Table IX.

2. Calculation of Be^7 angular distribution for the $C^{12}(He^3,Be^7)$ Reaction (for $E^{lab}_{He^3} = 31.2$ MeV).

For a given CM energy and angular distribution, the laboratory distribution of Be^7 can be calculated using simple equations[40] or by using tables computed expressly for this purpose.[41]

In the calculated curve (shown as the dashed curve in Fig. 37) the relative weights given to the Be^7 CM energy groups are those of Table IX. Center-of-mass isotropy was assumed. The small fraction of the activity appearing in the forward peaks of the 8 and 10 MeV groups (Figs. 29 and 30) is not superimposed. Their effect is to raise the calculated distribution at small laboratory angles out to approximately 17 deg. ($\cos\theta_L = 0.96$).

The reason for the prominent shoulder at $\cos\theta_L = 0.6$ is that the 2 MeV group is weighted so highly. It is probable that if the relative weights of more energy groups were known, the calculated curve could be smoothed out considerably.

3. Calculation of fraction of Be^7 recoils forward and backward from 2.48 mg per cm^2 target for the $C^{12}(He^3,Be^7)$ reaction ($E^{lab}_{He^3} = 30.1$ MeV.

Details of the calculations are supplied in Appendix II.

For forward laboratory recoils, the 2.48 mg C per cm^2 target is of "intermediate thickness", meaning that the maximum forward range of Be^7 recoils in the laboratory is greater than the target thickness. For backward laboratory recoils, the target is "thick". Here a "thick" target is one whose thickness is greater than the range of the recoil. Table X shows the calculated values for F and B which are used to reproduce the data shown in Fig. 14 and Table II. The amounts of the CM energy groups have been weighted according to Table IX.

The results of the calculation and the comparison with the experimental data are as follows:

$F_{calc.} = 0.51$ $\qquad$ $B_{calc.} = 0.006$

$F_{obs.} = 0.49 \pm 0.02$ $\qquad$ $B_{obs.} = 0.011 \pm 0.001$

The fraction observed to remain in the target is 0.50 ± 0.03 and the calculated value is $1.00 - (0.51 + 0.01) = 0.48$.

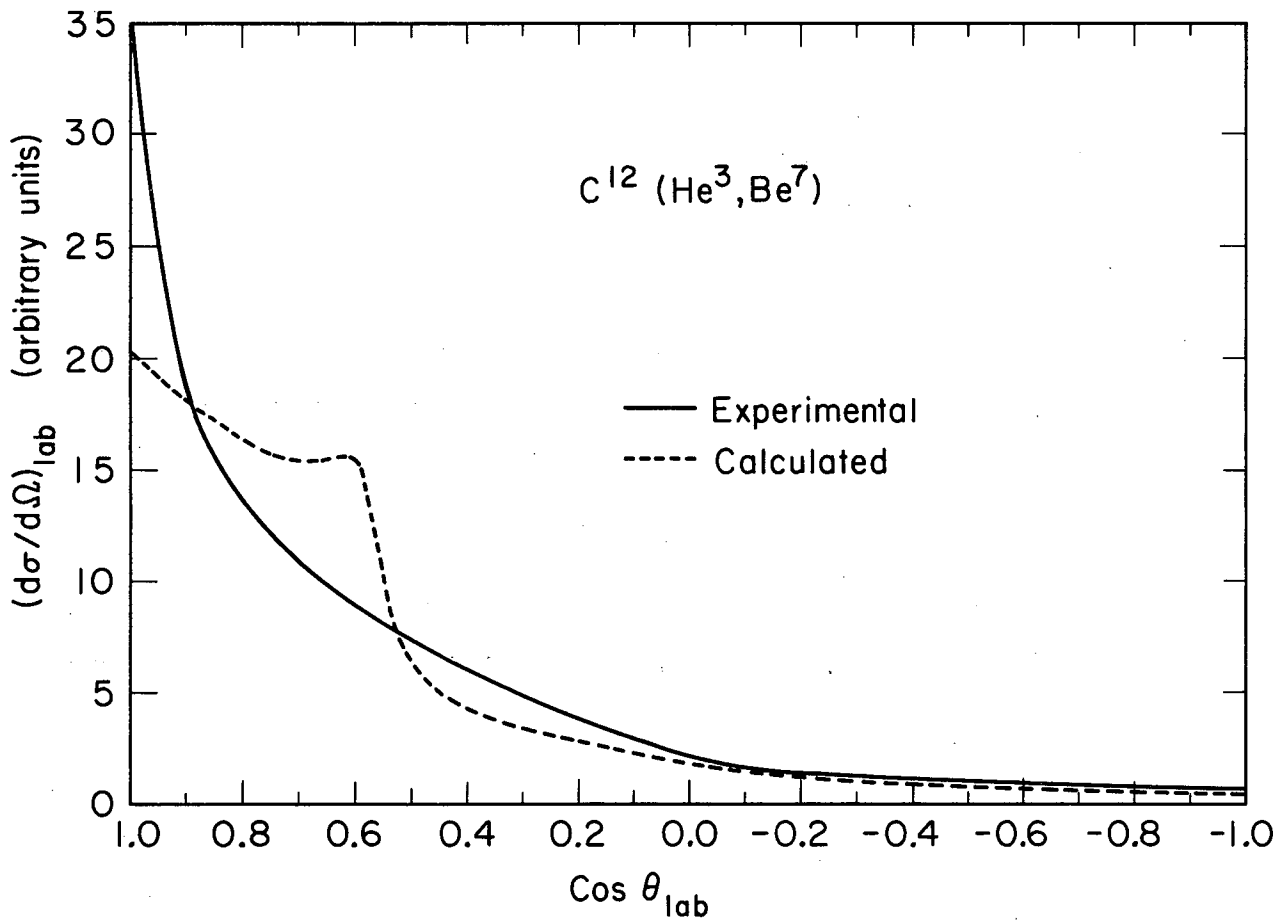

MUB-3183

Fig. 37. Comparison of the calculated angular distribution with the experimental curve for the reaction $C^{12}(He^3, Be^7)$. The bombarding energy was 31.2 MeV. The continuous curve is the experimental angular distribution. The dashed curve is calculated assuming isotropic CM components weighted according to values presented in Table IX. The calculated curve is normalized to 2 at a laboratory angle of 90 degrees.

Table X. Calculated values of F and B for various values of $E^{CM}_{Be^7}$. The He^3 bombarding energy is 30.1 MeV. Center-of-mass isotropy is assumed for the Be^7 product.

$E^{CM}_{Be^7}$	$F_{calc.}$	$B_{calc.}$
2 MeV	0.49[a]	0
4	0.51	0.00076
6	0.53	0.0073
8	0.56	0.020
10	0.59	0.041

[a]This value extrapolated from the other four values.

4. Calculation of fractions forward and backward for other targets of "intermediate thickness" for the $C^{12}(He^3,Be^7)$ reaction ($E^{lab}_{He^3}$=30.4 MeV)

a. Target of 120 micrograms C per cm^2. In the analysis using Figs. 31-35, the activity profiles of the various up- and downstream catcher foils were calculated assuming a zero thickness target. In Table XI, F, B, and T are calculated for a zero thickness target, and then for a target of "intermediate thickness" (120 micrograms/cm^2). Center-of-mass isotropy is assumed for the Be^7 product. The range of Be^7 is assumed to be proportional to energy.

Except as indicated by the notes a and b, the values given in Table XI were calculated using the equations of Winsberg.[42] All equations used were for "thin" (thickness = 0) targets or for targets of "intermediate thickness" except that used for the B value 0.0157. For this energy, the 120 microgram target is "thick" for backward laboratory recoils.

When the relative amounts of the energy groups are taken from Table IX, the results are as follows:

Infinitely Thin Target	Intermediate Thickness	Observed values
F = 0.92	F = 0.85	F = 0.85±0.03
B = 0.08	B = 0.059	B = 0.11±0.01

Table XI. Calculated values of F and B for various values of $E^{CM}_{Be^7}$. The He^3 bombarding energy is 30.4 MeV.

$E^{CM}_{Be^7}$	Infinitely thin target		Intermediate thickness target	
	F	B	F	B
2 MeV	1	0	0.900[a]	0
4	0.926	0.074	0.845[b]	0.0157
6	0.848	0.152	0.824	0.125
8	0.800	0.200	0.781	0.180
10	0.768	0.232	0.758	0.220

[a] By extrapolation of the other four points.

[b] Calculated with equations in Appendix II.

b. Target of 270 micrograms C per cm^2. The calculations of F and B in the last section indicate that it is a rather poor approximation to assume a target of 120 micrograms/cm^2 is infinitely thin. Better calculated values of F and B are obtained if the small target thickness is taken into account.

Table XII gives the calculated values of F and B for a target thickness of 270 micrograms C per cm^2. The calculations are the same as those outlined in the last section (Sec. 4a). Data are given in Table VIII.

When the CM energy groups are weighted according to Table IX, the results of the calculation and the comparison with experiment are as follows:

$F_{calc.} = 0.86$ $\qquad$ $B_{calc.} = 0.044$

$F_{obs.} = 0.76 \pm 0.03$ $\qquad$ $B_{obs.} = 0.078 \pm 0.006$

Table XII. Calculated values of F and B for various values of $E^{CM}_{Be^7}$. The He^3 bombarding energy is 30.4 MeV.

$E^{CM}_{Be^7}$	F	B
2 MeV	0.930[a]	0
4	0.858[b]	0.0071[c]
6	0.803	0.0672[c]
8	0.768	0.157
10	0.744	0.205

[a]Value obtained by extrapolation of the other four points.

[b]Calculated with equations in Appendix II.

[c]Thick target calculation.

5. Energy distribution of Be^7 from the $C^{12}(He^3,Be^7)$ reaction ($E^{lab}_{He^3}$ = 31.2 MeV)

The CM energy distribution of the Be^7 is plotted in Fig. 38. Figure 39 shows a similar plot where the abscissa has been converted into a decay energy.

The uncertainties on the experimental points are taken to be two times the standard deviation. The square of the standard deviation is

$$\sigma^2 \simeq \frac{1}{n-1} \sum_{1}^{n} (X_i - \overline{X})^2$$

and

$$\overline{X} = \frac{1}{n} \sum_{1}^{n} X_i .$$

The values of X_i are taken to be the weighted ordinates of the isotropic parts of Figs. 27-30.

The values of 2σ as a measure of the uncertainty reflect the facts that the experimental curve is drawn from a histogram and that some averaging had to be done in transforming the double differential cross section from the laboratory to the center-of-mass reference system.

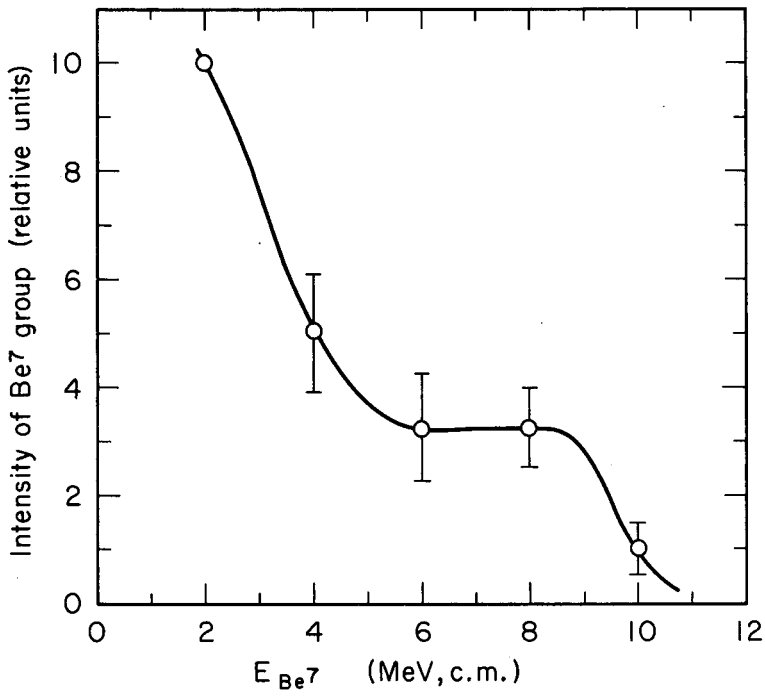

Fig. 38. Experimental energy distribution of Be^7 from the $C^{12}(He^3,Be^7)$ reaction. The He^3 bombarding energy was 31 MeV.

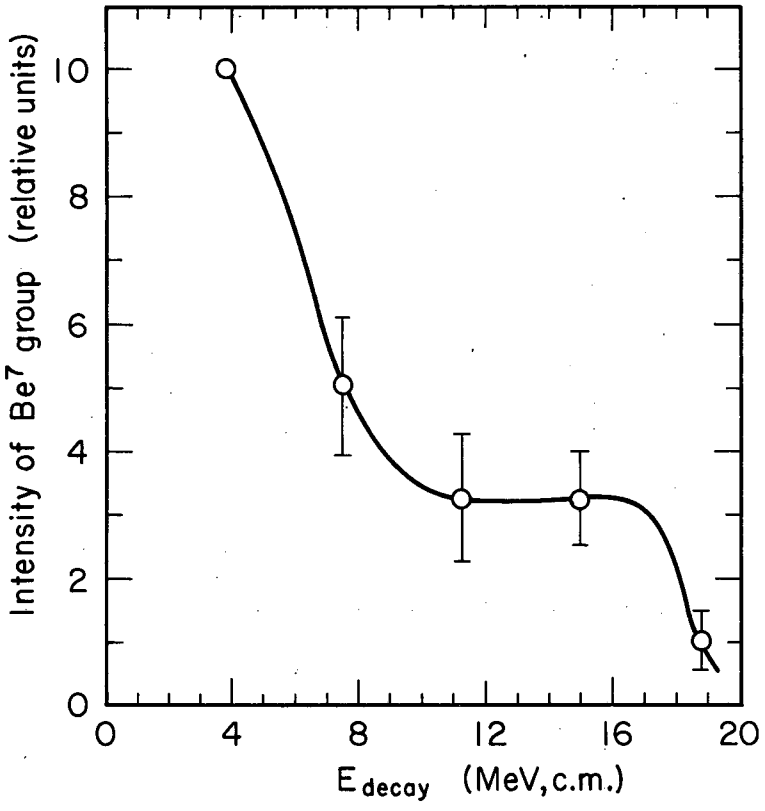

MU-34521

Fig. 39. This figure is the same as Fig. 38, except that the $E^{CM}_{Be^7}$ abscissa has been converted to E^{CM}_{Decay}.

B. Analysis of the $C^{12}(He^3,Be^7)$ Reaction at He^3 Bombarding Energy of 23.8 MeV

Experiments performed with He^3 beams degraded in energy were less detailed than those run at the maximum He^3 energy of 31.2 MeV because of the difficulty in obtaining intense, well-collimated, degraded beams.

The experimental data for the following analysis are given in Table III and in Fig. 15, which give forward and backward recoils from a sandwiched 2.42 mg C per cm^2 target. Values for F and B were calculated for the target using the energy groups $E^{CM}_{Be^7}$ = 2, 3.7, 5.4, and 7.1 MeV. (The maximum $E^{CM}_{Be^7}$ possible is 7.1 MeV.) The CM energy groups were weighted by assuming an energy distribution similar to that shown in Fig. 38.

For F calculations, the target is of "intermediate thickness" while for B calculations it is "thick". The range of Be^7 is again assumed to be proportional to energy. Calculated values of F and B for different $E^{CM}_{Be^7}$ are presented in Table XIII.

Note that the values of F and B are not very sensitive to $E^{CM}_{Be^7}$ and hence not very sensitive to the relative amounts of the different energy groups taken for the calculation. The calculated values of F and B, and the comparison with the experimental values are as follows:

$$F_{calc.} = 0.47 \qquad B_{calc.} = 0.003$$

$$F_{obs.} = 0.33 \pm 0.02 \qquad B_{obs.} = 0.0072 \pm 0.0004$$

The calculated fraction remaining in the target is 1-(0.47 + 0) = 0.53. The observed fraction is 0.66 ± 0.04.

Table XIII. Calculated values of F and B for various values of $E^{CM}_{Be^7}$. The He^3 bombarding energy is 23.8 MeV.

$E^{CM}_{Be^7}$	F	B
2 MeV	0.46[a]	0
3.7	0.47	0.002
5.4	0.49	0.010
7.1	0.52	0.024

[a]Extrapolated from the other three points.

C. Analysis of the $C^{12}(He^3,Be^7)$ Reaction at He^3 Bombarding Energy of Approximately 15 MeV

1. Calculation of activity profile for target of 227 micrograms C per cm^2 and average He^3 bombarding energy of 15.2 MeV

The data for this experiment are given in Table VII and in Fig. 19.

It was found by trial and error that a single CM Be^7 energy group of $E^{CM}_{Be^7} = 1.52$ MeV will reproduce the data. As usual, CM isotropy of Be^7 and $R_{Be^7} = k(vel)^2_{Be^7}$ is assumed. For purposes of this calculation, the target is assumed to be infinitely thin and the treatment outlined in Appendix I is used. The calculated activity profile shown in Fig. 40 is normalized to the experimental Be^7 activity.

The relationship $R_{Be^7} = k(vel)^2_{Be^7}$ is approximate here because k is not a constant, but is varying at the rather low laboratory Be^7 energies encountered in this experiment. (See Fig. 45, Appendix I.) If the variation of k is taken into account using $R_{Be^7} = k(vel)^2_{Be^7}$ + Constant or $R_{Be^7} = [k + C_1(C_2-E_{Be^7})^2]\ (vel)^2_{Be^7}$, where the constants are evaluated from the range-energy curve, the experimental activity profile can also be fitted satisfactorily.

2. Calculation of fractions forward and backward

a. Target of 227 micrograms C per cm^2 ($\langle E^{lab}_{He^3} \rangle$ = 15.2 MeV). The data are given in Table VII and in Fig. 19.

To calculate F, the equation in Appendix II for an "intermediate thickness" target was used. For calculation of B, the target is "thick", and the equation of Winsberg[42] was used. Only the 1.52 MeV CM Be^7 energy group is considered.

$F_{calc.} = 0.83$ $\qquad$ $B_{calc.} = 0.00006$

$F_{obs.} = 0.81 \pm 0.08$ $\qquad$ $B_{obs.} = 0.019 \pm 0.002$

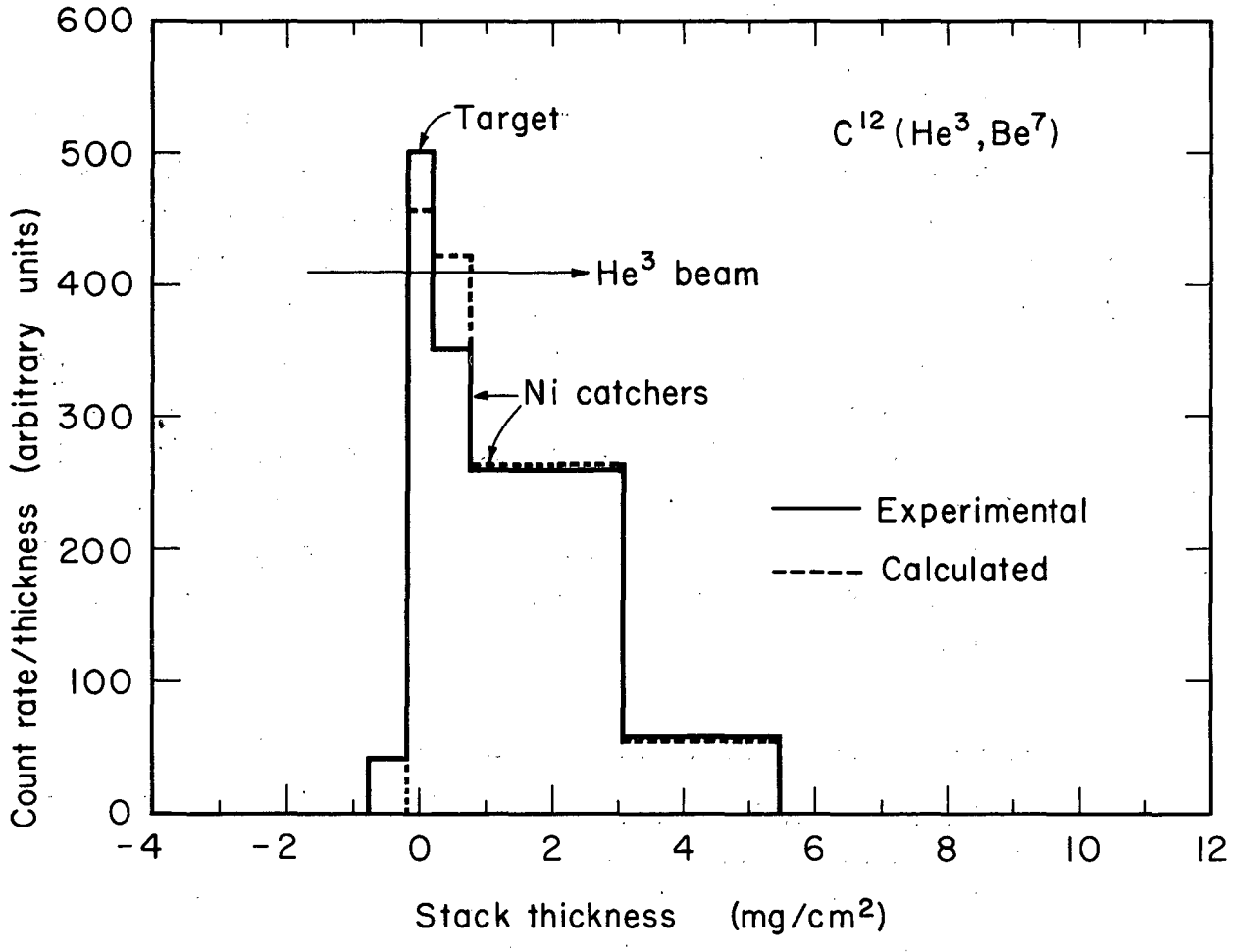

MUB-3178

Fig. 40. Comparison of the calculated Be^7 activity profile with experimental data for $C^{12}(He^3,Be^7)$ reaction. The He^3 bombarding energy was 15.2 MeV.

b. Target of 417 micrograms C per cm^2 ($\langle E^{lab}_{He^3} \rangle$ = 15.0 MeV). The data are given in Table VIII. Calculations are the same as in Part a above.

$F_{calc.} = 0.78$ $\qquad$ $B_{calc.} = 0.00006$

$F_{obs.} = 0.72 \pm 0.04$ $\qquad$ $B_{obs.} = 0.008 \pm 0.001$

c. Target of 2.48 milligrams C per cm^2 ($\langle E^{lab}_{He^3} \rangle$ = 14.6 MeV). The data are presented in Table IV and in Fig. 16. The target is "thick" for F and B calculations and the equations of Winsberg[42] were used. The energy of Be^7 in the CM system was taken to be 1.50 MeV.

$F_{calc.} = 0.28$ $\qquad$ $B_{calc.} = 0.00002$

$F_{obs.} = 0.21 \pm 0.02$ $\qquad$ $B_{obs.} = 0.0014 \pm 0.0001$

D. Analysis of the $C^{12}(He^3,Be^7)$ Reaction at an Average He^3 Bombarding Energy of 10.3 MeV

The data are given in Table V and Fig. 17. Calculations for F and B use the equations of Winsberg[42] for "thick" targets. The $E^{CM}_{Be^7}$ was arbitrarily assumed to be 1.0 MeV. The results of the calculations and the comparison with the data are as follows:

$F_{calc.} = 0.22$ $\qquad$ $B_{calc.} = 0.000002$

$F_{obs.} = 0.078 \pm 0.005$ $\qquad$ $B_{obs.} = 0.004 \pm 0.004$

E. Analysis of the $Al^{27}(He^3,Be^7)$ Reaction

Several thick target recoil experiments were performed in order to study the $Al^{27}(He^3,Be^7)$ reaction mechanisms. In these runs, the thick targets were sandwiched between thick catcher foils. Additional foils were included in the stack to serve as blanks to determine the small Be^7 activation in the catcher foils. The Be^7 activation in the thick catcher foils on either side of the target was taken to be the same as that in neighboring blank foils. The data are presented in Table I. The $Al^{27}(He^3,Be^7)$ excitation function is shown in Fig. 3.

A distinction is made between the mechanism by which Be^7 is evaporated from the compound nucleus of P^{30} and direct interaction processes. The two types of mechanisms are expected to have different recoil properties and, with some assumptions, the thick target experiments will discriminate between the two types of processes. The existence of a compound nucleus mechanism is inferred from the presence of backward Be^7 and from the large fraction of Be^7 produced which remains in the target. The direct interaction part will be apparent from the deviation of the calculated compound nucleus recoil properties from the experimental recoil properties.

For the compound nucleus mechanism, it is assumed that all the Be^7 produced has a center-of-mass kinetic energy equal to its Coulomb barrier energy (8.9 MeV). In the absence of further information, center-of-mass isotropy is also assumed for the Be^7, as is the relationship $R_{Be^7} = k(\text{vel})^2_{Be^7}$. The justification for the use of this range-energy relationship is given in Appendix I. With the range-energy curve for Be^7 in aluminum, which was calculated from the experimental curve for Be^9 in aluminum[39] and the factor 7/9, and the equations of Winsberg,[42] it is possible to calculate F, B, and T for these thick target recoil experiments.

In order to have a model for the direct interaction processes, it is assumed that the incident He^3 picks up an alpha particle and the resulting Be^7 and Na^{23} are formed in their ground states. It is also assumed that all of the Be^7 thus formed goes directly forward.

As an example, the first set of data given in Table I is examined. For this run, the target thickness was 7.34 mg Al per cm^2 and $\langle E_{He^3} \rangle$ = 24.6 MeV. On the basis of the compound nucleus model,

$$B_{calc.} = 0.053 \qquad T_{calc.} = 0.74 \qquad F_{calc.} = 0.21.$$

On the basis of the direct interaction model, 98 percent of the Be^7 escapes the target (in this case). Presence of direct interaction Be^7 then will not be apparent in the experimental (T/B) ratio, but will affect ratios in which F appears. Experimentally this is observed to be the case.

$$(T/B)_{calc.} = 14.0 \qquad (T/B)_{obs.} = 14.0 \pm 1.2$$

$$(F/T)_{calc.} = 0.28 \qquad (F/T)_{obs.} = 0.42 \pm 0.04.$$

The assumption of 9 percent direct interaction and 91 percent compound nucleus mechanism will account for the observed recoil properties.

It is possible to take into account a linear variation of cross section across the target in calculating F, B, and T,[3] but the results do not change much for most target thicknesses. For the two thickest targets used (Table I), the variation of cross section with target thickness was taken into account.

Calculations similar to the one just outlined were performed for the other recoil data. The calculated percentages of the two mechanisms listed in Table XIV are consistent with the data.

Table XIV. Results of thick target recoil experiments on the $Al^{27}(He^3,Be^7)$ reaction mechanisms.

$\langle E_{He^3} \rangle$	σ	% CN	% DI	σ_{CN}	σ_{DI}
24.6 MeV	410 μb	91	9	373 μb	37 μb
24.6	410	92	8	377	33
26.6	545	91	9	496	49
26.9	565	90	10	508	57
30.7	900	83	17	747	153
30.7	900	87	13	783	117

V. DISCUSSION

A. General

Although a limited amount of data has been obtained for He^3 and He^4 excitation functions with various targets, the main emphasis in this work has been the study of the $C^{12}(He^3,Be^7)$ and $Al^{27}(He^3,Be^7)$ reaction mechanisms. First, consider the $C^{12}(He^3,Be^7)$ system.

It has been seen that the experimental recoil data on the $C^{12}(He^3,Be^7)$ reaction have been fit over a range of He^3 ion energies up to 31.2 MeV. The model chosen has used isotropic Be^7 energy groups in the O^{15} center-of-mass system. Since most of the data are not sensitive to the small fraction of the total Be^7 contained in the forward peaks (Figs. 29-30), the peaks have not been included in the model.

In no case was the calculated value for F larger than the experimental value. The calculations depend directly upon the range-energy curve for Be^7 in carbon, and there is evidence that the curve used overestimates the Be^7 range for a given energy (see Appendix VI). Adjusting the range-energy curve in the direction indicated by the available range-energy data has the effect of bringing the calculated values of F toward the experimental values.

The calculations of B are not expected to be very accurate because they depend on the relationship $R_{Be^7} = k(vel)^2_{Be^7}$ in a region where it may not be applicable. For B calculations the true range of Be^7 is probably larger than that estimated with the formula above. (See Appendix I, Fig. 45.) The effect causes calculated values of B to be smaller than the experimental. This is observed in all cases except B calculated for a thick target at $\langle E^{lab}_{He^3}\rangle = 10.3$ MeV (Sec. IV.-D), and this involved other approximations.

For the proposed direct interaction (DI) (see Sec. V.-E), the Be^7 is very energetic and F_{DI} is much larger than $F_{compound\ nucleus}$. From the calculation in Appendix V, it is seen that at He^3 bombarding energy of 30 MeV, the DI Be^7 product has a maximum forward laboratory energy of 23 MeV. There is assumed to be no backward Be^7 product. If the DI Be^7 goes directly forward, F = 1 for many target thicknesses, and

for all the data taken at $E^{lab}_{He^3} = 30$ MeV. Hence an appreciable fraction of DI, if present in the reaction mechanism, would raise the experimental values of F well above the calculated values. This was never the case up to the maximum He^3 bombarding energy of 31.2 MeV.

Consideration of Q-values and classical Coulomb barriers (Appendix VII) for many reactions leading to the formation of Be^7 indicate that Be^7 can most likely be formed from the $He^3 + C^{12}$ system in four ways:

1. $_2He^3 + {}_6C^{12} = [_8O^{15}]^* = {}_4Be^7 + {}_4Be^8$

2. $_2He^3 + {}_6C^{12} = [_8O^{15}]^* = \alpha_1 + [_6C^{11}]^*$
   $\hookrightarrow \alpha_2 + {}_4Be^7$

3. $_2He^3 + {}_6C^{12} = {}_2He^4 + [_6C^{11}]^*$
   $\hookrightarrow \alpha + {}_4Be^7$

4. $_2He^3 + {}_6C^{12} = {}_4Be^7 + {}_4Be^8$ (DI) .

These will be discussed in turn. The $Al^{27}(He^3,Be^7)$ reaction is discussed in Sec. V.-G.

B. The $_2He^3 + {}_6C^{12} = [_8O^{15}]^* = {}_4Be^7 + {}_4Be^8$ Mechanism

Formation of Be^7 by this mechanism occurs by the break-up of the complete-fusion compound system. At the excitation energies encountered in these experiments, this "evaporation" mechanism would necessarily proceed through a limited number of states. These are listed in Table XV.

Table XV. Possible states through which the $O^{15} = Be^{7} + Be^{8}$ step may proceed at a He^{3} bombarding energy of 30 MeV. The excess excitation energy of the compound nucleus is 18.30 MeV. The Coulomb barrier will suppress those channels where the total product kinetic energy is less than approximately 4 MeV. The level schemes for Be^{7} and Be^{8} were taken from Ref. 43.

Excitation energy of Be^{7} (MeV)	Excitation energy of Be^{8} (MeV)	Total kinetic energy of products (MeV, CM)
0	0	18.30
0	2.90	15.40
0	11.40	6.90
0	16.08	2.22
0	16.63	1.67
0	16.94	1.36
0	17.64	0.66
0	18.15	0.15
0.43	0	17.87
0.43	2.90	14.97
0.43	11.40	6.47
0.43	16.08	1.79
0.43	16.63	1.24
0.43	16.94	0.93
0.43	17.64	0.23

The $Al^{27}(p,Be^7)Ne^{21}$ reaction has been studied by Lindsay and Neuzil.[44] The proton bombarding energy varied from 27 to 31.5 MeV. The steps in the reaction are as follows:

$$p + {}_{13}Al^{27} = {}_{14}Si^{28} \qquad Q = +11.6 \text{ MeV}$$

$${}_{14}Si^{28} = {}_{4}Be^{7} + {}_{10}Ne^{21} \qquad Q = -31.5 \text{ MeV}$$

At $E_p^{lab} = 30$ MeV, the excitation of the Si^{28} compound nucleus is 40.6 MeV. At this bombarding energy, the cross section for Be^7 formed by evaporation from the compound nucleus is approximately 100 microbarns and rising rapidly. Magnesium was also used as a target by Lindsay and Neuzil and the compound nucleus cross section is comparable to their results for aluminum.

The $Al^{27}(He^4,Be^7)Na^{24}$ reaction has been studied by Porile[3] at a bombarding energy of 40 MeV. The steps in this reaction are

$${}_{2}He^{4} + {}_{13}Al^{27} = {}_{15}P^{31} \qquad Q = +9.7 \text{ MeV}$$

$${}_{15}P^{31} = {}_{4}Be^{7} + {}_{11}Na^{24} \qquad Q = -31.8 \text{ MeV}$$

At an alpha energy of 40 MeV, the excitation energy of the P^{31} compound nucleus is 44.5 MeV. At this bombarding energy, the compound nucleus cross section is approximately 40 microbarns and is rising rapidly.

By way of comparison, the $C^{12}(He^3,Be^7)Be^8$ steps are given here.

$${}_{2}He^{3} + {}_{6}C^{12} = {}_{8}O^{15} \qquad Q = +12.1 \text{ MeV}$$

$${}_{8}O^{15} = {}_{4}Be^{7} + {}_{4}Be^{8} \qquad Q = -17.8 \text{ MeV}$$

At He^3 ion energy of 30 MeV, the excitation energy of the compound nucleus of O^{15} is 36.1 MeV.

It is not known how the "evaporation" of Be^7 changes in going from the compound nucleus of Si^{28} or P^{31} to that of the low mass O^{15}. Formation of Be^7 (and of Be^8, leaving a Be^7 residue) may occur, or occurs,

but arguments will be presented in Sec. V.-F to show that the O^{15} = $Be^7 + Be^8$ cross section is not a major fraction of the 57 mb $C^{12}(He^3,Be^7)$ cross section at a bombarding energy of 30 MeV.

C. The $_2He^3 + {}_6C^{12} = [{}_8O^{15}]^* = \alpha_1 + [{}_6C^{11}]^*$
$\hookrightarrow \alpha_2 + {}_4Be^7$ Mechanism

In this process the compound nucleus of excited O^{15} evaporates two alpha particles and leaves a residue of Be^7. The Q-values for the steps are

$$_2He^3 + {}_6C^{12} = {}_8O^{15} \qquad Q = +12.1 \text{ MeV}$$

$$_8O^{15} = {}_2He^4 + {}_6C^{11} \qquad Q = -10.2 \text{ MeV}$$

$$_6C^{11} = {}_2He^4 + {}_4Be^7 \qquad Q = -7.5 \text{ MeV}$$

This should be a favorable process because alpha emission competes favorably with nucleon emission from highly excited systems.[45] This is especially true because the Q-values for proton emission and alpha emission from both O^{15} and C^{11} are comparable. (See Appendix VII.)

It is possible to calculate an energy distribution of the Be^7 residue in the O^{15} center-of-mass system. In the calculation it is assumed that alpha emission carries off the entire excess compound nucleus excitation energy, and that the alphas come out isotropically from their respective parent nuclei. The qualitative reasoning of the calculation is this: The emission of the first alpha will take place at low energy, near its Coulomb barrier, with the highest probability. This leaves the second alpha to be emitted with a relatively high energy from the excited C^{11}, giving an energetic Be^7 residue. The calculation is performed in detail in Appendix III.

D. The $_2He^3 + {}_6C^{12} = {}_2He^4 + [{}_6C^{11}]^* \rightarrow \alpha + {}_4Be^7$ Mechanism

According to this mechanism, the He^3 extracts a neutron from C^{12}, leaving an excited C^{11}. The C^{11} then emits an alpha particle and leaves a Be^7 residue.

Neutron transfer reactions have a relatively high cross section. (See, for example, Kaufmann and Wolfgang[46] or Catala, et al.[47]) However, since heavy ion reactions are very predominantly surface reactions, nucleon transfer to the He^3 from the C^{12} surface would not leave the C^{12} in a state of excitation high enough to cause subsequent alpha evaporation. (The binding energy of an alpha particle in C^{11} is 7.5 MeV.) The neutron transfer would be tantamount to removing the top-most neutron from a shell model C^{12}, and leaving the remaining C^{11} configuration undisturbed, to a first approximation. Removal of an inner nucleon would leave the C^{11} in a high state of excitation because an s nucleon in C^{11} is approximately 16 MeV more tightly bound than a p nucleon,[48] but a surface reaction would not remove an inner nucleon. Attempts by He^3 to remove an inner C^{12} neutron would most likely lead to complete fusion of the target and projectile.

It is possible that in the neutron transfer from C^{12}, the C^{11} core becomes excited enough to allow ejection of an alpha. However, the cross section for this high excitation is probably low.[47]

There are other reasons that the Be^7 cross section for this mechanism would be low. If alpha emission did occur from the highly excited C^{11} nucleus, the Be^7 residue in most cases would necessarily retain sufficient excitation energy to cause its subsequent break-up. Furthermore, if the highly excited C^{11} were formed, the alpha evaporation process leading to Be^7 would have competition from proton emission. This is the case because the Q-values plus barrier heights for emission of alphas and protons are within a few percent of each other. It is also possible that since C^{11} is not a particularly good "alpha particle nucleus", proton emission would be favored.

To a first approximation, it would be expected that after a neutron transfer, the C^{11} "spectator" nucleus would remain at rest in

the laboratory frame of reference. Ejection of a given energy alpha from a stationary nucleus will then give a square Be^7 activity distribution as the activity profile in the catcher foils of the sandwiched target recoil experiments.[49] (See Appendix IV.) Not even an approximately square laboratory distribution was seen in any of these experiments.

It is assumed that Be^7 production by means of this mechanism is relatively low.

E. The ${}_2He^3 + {}_6C^{12} = {}_4Be^7 + {}_4Be^8$ Direct Interaction Mechanism

In the direct interaction (DI) process envisioned here, the He^3 plucks a preformed alpha cluster from the C^{12} nucleus, forming an energetic Be^7 product and a Be^8 residue. The Be^7 would be peaked in the forward direction,[50] and the peak would be broadened by the momentum distribution of the alpha particle within the C^{12} nucleus. Another characteristic of the DI cross section is likely to be an increase in magnitude with bombarding energy.

There are experiments which indicate that alpha clusters do have a real existence in nuclei.[51,52] One estimate of the mean life of an alpha in nuclear matter is 4×10^{-23} sec.[53] In view of this work, it is not unreasonable that the $C^{12}(He^3,Be^7)$ "alpha pick-up" reaction would be enhanced over a reaction in which any four nucleons are transferred to the projectile.

It can be calculated (Appendix V) on the basis of this DI model what the maximum expected Be^7 center-of-mass energy would be. The calculated value of 10.4 MeV is in good agreement with the experimental value.

An interpretation for the energetic and forward-peaked Be^7 (Figs. 29 and 30) is that such Be^7 is formed by a direct interaction process. If this is the case for the "10 MeV CM group" the Be^7 formed would be in either its ground state or its only bound excited state at 0.431 MeV,[54] and the Be^8 in its ground state. The first excited state of Be^8 is at 2.9 MeV.[55]

This model assumes that Be^8 remains as a spectator nucleus after the quasi-alpha is plucked out of the C^{12}. The half-life of Be^8 is on the order of 10^{-16} sec., so it is possible to consider the Be^8 as a true spectator in the much faster DI process.

If one looks only at the most energetic DI Be^7 product, then the reaction is as follows:

$$\underset{1/2\,+\,(g.s.)}{{}_2He^3} + \underset{0\,+\,(g.s.)}{{}_6C^{12}} = \underset{3/2\,-\,(g.s.)}{{}_4Be^7} + \underset{0\,+\,(g.s.)}{{}_4Be^8}$$

(or 1/2 - at 0.431 MeV)

The following treatment is similar to that given by Butler and Hittmair.[56] Let

J_{He^3} = spin of He^3

J_{Be^7} = spin of Be^7

L_α = orbital angular momentum with which the alpha particle is received by He^3

S_α = spin of the captured alpha

Then,

$$\vec{J}_{Be^7} = \vec{J}_{He^3} + \vec{L}_\alpha + \vec{S}_\alpha$$

$$(J_{He^3} + J_{Be^7}) \geqslant L_\alpha \geqslant |J_{He^3} - J_{Be^7}|$$

$$(1/2 + 3/2) \geqslant L_\alpha \geqslant |1/2 - 3/2| \; ; \qquad L_\alpha = 2,1$$

Or for the excited state of Be^7,

$$(1/2 + 1/2) \geqslant L_\alpha \geqslant |1/2 - 1/2| ; \qquad L_\alpha = 1,0$$

By conservation of parity, $L_\alpha = 1$, and Be^7 is regarded as

$$\underset{S = 1/2}{{}_2He^3} + \underset{S = 0}{{}_2He^4} \equiv {}_4Be^7 .$$

$$\underbrace{\qquad\qquad}_{L = 1}$$

$J = 3/2$ -

$J = 1/2$ - in the excited state)

Let the momentum of the incident He^3 be $\hbar \vec{k}_{He^3}$ and the momentum of the outgoing Be^7 be $\hbar \vec{k}_{Be^7}$. The magnitude of the momentum of the outgoing particle is given by energy conservation and the scattering angle θ. By momentum conservation, for a particular $\vec{k}_{Be^7}$, the captured particle will take into the nucleus a momentum $\hbar \vec{Q}$ where

$$\vec{Q} = \vec{k}_{He^3} - \frac{(m_{He^3})}{(m_{Be^7})} \vec{k}_{Be^7}.$$

$\vec{Q}$ is a function of the scattering angle θ and is smallest at $\theta = 0$ deg.

Classically the orbital angular momentum carried into the initial nucleus (He^3) by the captured particle (alpha) will be given by $\hbar \vec{Q} r_0$ where r_0 is an impact parameter. For the reaction to conserve angular momentum and to proceed at all

$$Qr_0 \geqslant L_\alpha .$$

Consider the data of Fig. 30. The incident laboratory He^3 energy is 31.2 MeV. Incident $E^{CM}_{He^3}$ is then 20.0 MeV. The observed $E^{CM}_{Be^7} = 10$ MeV at zero degrees.

$$p^{CM}_{He^3} = \hbar \vec{k}_{He^3} = 17.86 \times 10^{-15} \text{ (g-erg)}^{1/2}$$

$$p^{CM}_{Be^7} = \hbar \vec{k}_{Be^7} = 19.29 \times 10^{-15} \text{ (g-erg)}^{1/2}.$$

Therefore,

$$Q = \frac{9.59 \times 10^{-15}}{1.05 \times 10^{-27}} = 9.13 \times 10^{+12} \text{ cm}^{-1}$$

Take for a "reasonable" interaction radius (impact parameter) the following value (refer to Fig. 41):

$$r_0 = AB = (1.5 \times 10^{-13})(1.59 + 1.59) = 4.77 \times 10^{-13}\text{cm}$$

$$r_0 = (AB)(\sin 60^\circ)(2/3)$$

$$r_0 = 2.75 \times 10^{-13}\text{cm}$$

$$Qr_0 = (9.13 \times 10^{+12})(2.75 \times 10^{-13}) = 2.51.$$

This assumed interaction radius and the experimental value of $\vec{Q}$ indicate that with respect to conservation of linear and angular momentum, the angular distribution can peak at 0 deg. because

$$Qr_0 = 2.51 \gtrsim 1.$$

In fact, much smaller interaction radii can still meet the condition that $Qr_0 \gtrsim 1$.

The peak width of the energetic direct interaction peak may be estimated on the basis of a classical model.

The kinetic energy of an alpha cluster will be smallest on the surface of the nucleus where the direct alpha pick-up reaction is most likely to occur. On the basis of an alpha particle model of C^{12}, the following conservation of energy equation may be written:

$$M_{C12} = 3M_\alpha + 3V_\alpha + 3T_\alpha$$

$$V_\alpha + T_\alpha = \text{Constant} = -2.43 \text{ MeV}$$

V = potential energy
T = kinetic energy

As the alpha moves toward the edge of the nucleus, V_α is less negative and T_α becomes less positive. It has also been calculated that the probability of the existence of alpha clusters inside the nucleus is a

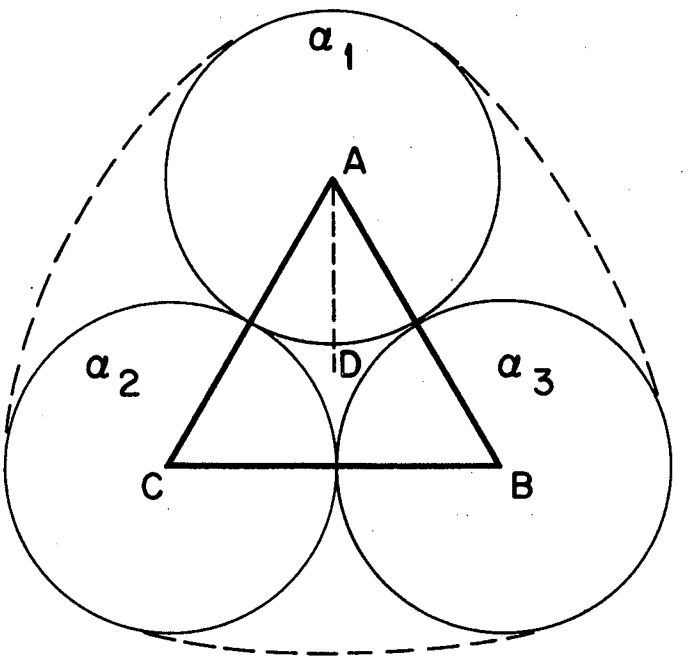

MU-34522

Fig. 41. Alpha cluster model of C^{12} for determining a "reasonable" impact parameter for the $He^3 + He^4$(cluster) = Be^7 direct interaction mechanism.

decreasing function of the energy of alpha particle motion inside the nucleus,[57] so that an alpha cluster exists with highest probability in the nuclear surface.

The kinetic energy of a surface alpha cluster can be estimated from data reproduced in Fig. 42. The formula $(3M_\alpha - M_{C12})/3 = 2.4$ MeV also yields a similar estimate. Kinetic energy calculated on the basis of the Uncertainty Principle is higher.

We assume then that the picked-up alpha cluster has a kinetic energy of approximately 2 MeV inside the C^{12} nucleus. The velocity component of the alpha perpendicular to the beam axis is then

$$V_\alpha = \sqrt{\frac{(2)(E_\alpha)}{(4)}}$$

where E_α is 4/3 MeV and $E_\alpha + E_{Be^8} = 2$ MeV. The velocity vector diagram shown in Fig. 43 can then be set up, and the approximate width of the most energetic Be^7 can be calculated.

$$\sin\theta = 0.817/1.69 = 0.483$$

$$\theta \cong 29^\circ$$

$$\cos\theta = 0.87.$$

The width of the experimental peak (Fig. 30) is approximately 29 deg.

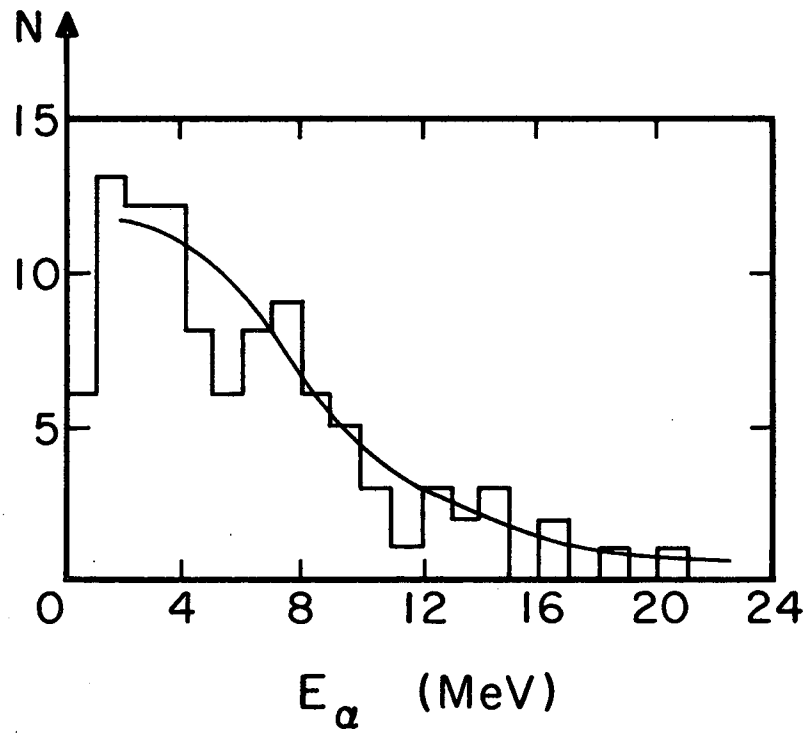

MU-34523

Fig. 42. Experimental energy distribution of alphas inside the C^{12} nucleus. Reproduced from Samman and Cüer.[58]

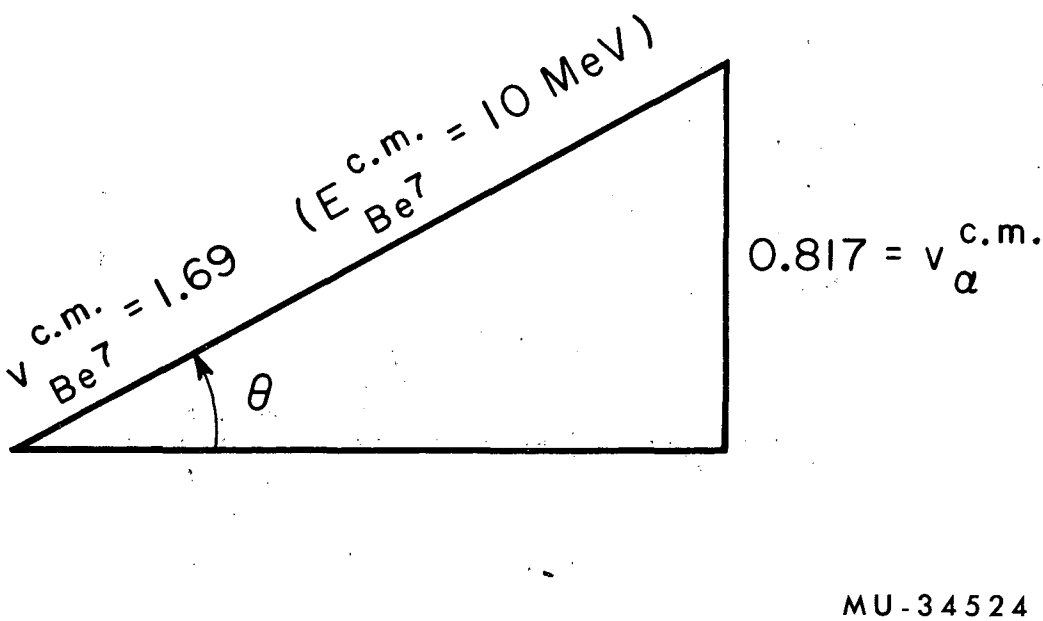

Fig. 43. Velocity vector diagram used to calculate the approximate width of the $C^{12}(He^3,Be^7)$ direct interaction peak.

F. Separation of the Compound Nucleus Type Processes in the $C^{12}(He^3,Be^7)$ Reaction at $E^{lab}_{He^3} = 31.2$ MeV

At this point in the discussion, there are two compound nucleus mechanisms which have not been eliminated as being major contributors to the $C^{12}(He^3,Be^7)$ cross section at 31 MeV bombarding energy. They are: 1) the break-up of O^{15} into Be^7 and Be^8 and 2) the evaporation of two alpha particles from O^{15} to leave a Be^7 residue. These two mechanisms will be discussed in turn.

1. The $O^{15} = Be^7 + Be^8$ break-up

The O^{15} compound nucleus will have a maximum angular momentum of approximately $11\hbar$. The average angular momentum will be approximately $7\hbar$.

In the two-body break-up of O^{15} into Be^7 and Be^8, the maximum spin angular momentum of the products in any of the open decay channels (Table XV and Ref. 43) is $(3/2 + 4) = 11/2$. This is for decay to the ground state of Be^7 and the 11.4 MeV state of Be^8. Any other combination of levels to which O^{15} decays into Be^7 and Be^8 will have a lower value for the sum of the Be^7 and Be^8 spins.

Since the average angular momentum of the O^{15} compound nucleus is greater than the maximum value possible for the Be^7 and Be^8 spins in the decay, the two products must have angular momentum in their relative motion, if angular momentum is to be conserved. This may lead to forward-backward peaking of Be^7 in the CM system.[59]

The forward peaks in the angular distributions in the double differential cross section experiment (Figs. 29 and 30) for the higher energy CM groups are predicted either for the $O^{15} = Be^7 + Be^8$ mechanism discussed in this section or for the proposed DI mechanism which was discussed in Sec. V.-E. The double differential cross section experiment therefore does not yield unambiguous information concerning the $O^{15} = Be^7 + Be^8$ break-up.

The result of the differential cross section experiment (Fig. 21) shows no evidence of backward peaking. Since, by conservation of parity,

compound nucleus products must be symmetrical about 90 deg. in the CM, the absence of a backward peak eliminates the compound nucleus forward peak. The small forward peaks (Figs. 29-30) in the double differential cross section are then attributed to the DI mechanism.

It was stated that the $O^{15} = Be^7 + Be^8$ break-up may lead to forward-backward peaking of the Be^7.[59] Absence of forward-backward peaking, however, does not completely eliminate this mechanism. It can be argued that only low partial waves contribute to the Be^7 production and that they contribute in such a manner that the Be^7 distribution will be isotropic. The energetics of the $O^{15} = Be^7 + Be^8$ break-up is investigated next.

The shoulder in the calculated angular distribution at $\cos\theta_L = 0.6$ (Fig. 37) is prominent because the 2 MeV CM Be^7 energy group was weighted so highly. For this CM energy, the Be^7 is confined to a cone in the forward direction, in the laboratory system. The laboratory cut-off angle is $\cos^{-1} 0.6$. If, for example, a 1 MeV (CM) Be^7 group is considered, its laboratory cut-off (and shoulder) will appear at $\cos\theta_L = 0.8$. Taking many discrete Be^7 CM energy groups will smooth out the calculated curve and bring the calculated curve into better agreement with the experimental curve. (The DI Be^7 is not included in Fig. 37. The laboratory cut-off for the DI Be^7 is approximately $\cos^{-1} 0.96$.)

In order to bring the calculated laboratory Be^7 angular distribution into agreement with the experimental angular distribution, Be^7 CM energies below the $Be^7 + Be^8$ Coulomb barrier (Be^7 CM energy of approximately 2 MeV) must be assumed. Because the probability for Be^7 tunneling through the barrier of the compound nucleus is expected to be very small, Be^7 at CM energies below approximately 2 MeV is not predicted for the $O^{15} = Be^7 + Be^8$ break-up. The presence of substantial amounts of Be^7 below 2 MeV (CM) is an argument against the $O^{15} = Be^7 + Be^8$ break-up mechanism.

The energy spectrum of Be^7 from the $O^{15} = Be^7 + Be^8$ break-up is now examined. It is seen in Table XV that the energy of the Be^7 formed in the O^{15} two-body break-up can vary widely. When the Be^7 energies are

calculated from the information contained in Table XV, it is seen that Be^7 cannot be formed with a CM kinetic energy between 5 and 7 MeV. The experimental CM energy distribution shows the presence of substantial Be^7 in this energy range. (See Table IX.)

It may be possible that the $O^{15} = Be^7 + Be^8$ break-up accounts for all the Be^7 energy spectrum except that at 5-7 MeV. The only other likely compound nucleus mechanism for producing Be^7, the $C^{12}(He^3;\alpha_1\alpha_2)Be^7$ mechanism, would have to fill out the 5-7 MeV cross section. On the basis of one model, however, the $C^{12}(He^3;\alpha_1\alpha_2)Be^7$ mechanism does contribute at 5-7 MeV and also contributes substantially at other CM energies. (See next section.) Therefore, if Be^7 from the $C^{12}(He^3;\alpha_1\alpha_2)Be^7$ mechanism fills out the 5-7 MeV range, this two-alpha evaporation mechanism must account for a large fraction of the total Be^7 formed.

On the basis of the discussion in this section, it is estimated that the $O^{15} = Be^7 + Be^8$ compound nucleus break-up does not account for the bulk of the Be^7 formation cross section at a He^3 bombarding energy of 31 MeV.

2. The $O^{15} = \alpha_1 + \alpha_2 + Be^7$ mechanism

The model chosen for this mechanism assumes that alpha particles are evaporated isotropically from the parent nuclei and that all the products (α_1,α_2,Be^7) are formed in their ground states.

On the basis of this model a square CM energy distribution is predicted (Appendix III) for the Be^7 when each alpha decay occurs at a fixed energy. For the model where the first alpha is ejected with a Maxwellian energy spectrum, several square distributions are combined so that the Be^7 CM energy spectrum peaks at a Be^7 energy of approximately 5 MeV. (See Appendix III for the detailed calculation.)

If there are no preferred directions of emission for either of the two alpha particles when they are emitted from the compound nucleus, the angular distribution of Be^7 will be isotropic in the O^{15} rest system.

The experimental Be^7 energy distribution from 4 MeV to the maximum Be^7 energy (Fig. 38) can be fitted approximately by using the

calculated energy distribution shown in Appendix III, Fig. 50. The 1/4 of the Be^7 cross section which is not fitted by the calculated curve appears at Be^7 energies below 4 MeV. The presence of substantial amounts of low energy Be^7 can be explained if both alpha particles are emitted in opposite directions from the compound nucleus. The 180 deg. angle of emission between the two alphas (because of lower Coulomb energy) would be expected if the alphas were emitted "simultaneously" from the O^{15}.

The Be^7 energy spectrum and isotropic Be^7 angular distribution predicted on the basis of the $C^{12}(He^3;\alpha_1\alpha_2)Be^7$ mechanism are consistent with the experimental data. Since all of the other simple compound nucleus mechanisms for producing Be^7 have been eliminated, it is concluded that Be^7 from the $C^{12}(He^3,Be^7)$ reaction at a bombarding energy of 31 MeV is formed mainly through the $C^{12}(He^3;\alpha_1\alpha_2)Be^7$ mechanism.

G. The $Al^{27}(He^3,Be^7)$ Results

A study similar to the one performed on the $Al^{27}(He^3,Be^7)$ reaction has been made by Porile[3] on the $Al^{27}(He^4,Be^7)$ system. His results show that at 40 MeV bombarding energy, the reaction proceeds by approximately equal parts evaporation and direct interaction. The direct interaction cross section is then about 40 microbarns at E_α^{lab} = 40 MeV. The direct interaction cross section for the $Al^{27}(He^3,Be^7)$ reaction, while not the major fraction of the Be^7 production cross section at the bombarding energies studied, is still approximately 100 microbarns at $E_{He^3}^{lab}$ = 30 MeV.

In thick target recoil experiments as were performed by Porile and in this work, the nature of the direct interaction remains obscure. One idea is that the incident projectile captures a preformed cluster from the target and forms Be^7 directly. If this is the case, the direct interaction cross section for (He^3,Be^7) and (He^4,Be^7) reactions, at equivalent bombarding energies, will be a measure of the amount of He^4 and He^3 clustering in the target's nuclear surface. The results of this work and that of Porile on aluminum nuclei are consistent with the idea that alpha clustering is favored over He^3 clustering in the nuclear surface.

VI. SUMMARY AND CONCLUSIONS

Following a survey of some (He^3,Be^7) and (He^4,Be^7) nuclear reaction cross sections, a more extensive study was made of the $C^{12}(He^3,Be^7)$ and $Al^{27}(He^3,Be^7)$ reactions in order to elucidate their mechanisms. In particular, it was sought to discover the importance of the direct interaction process by which Be^7 is formed when an incident He^3 projectile picks up a preformed alpha cluster from the C^{12} or Al^{27} target. The $He^3 + He^4(\text{cluster}) = Be^7$ reaction could then be used as a tool to study alpha clustering in any nuclear surface.

For the $C^{12}(He^3,Be^7)$ reaction, the direct interaction process was determined to be about 2 percent, or 1 millibarn, of the total Be^7 formation cross section at a He^3 bombarding energy of 31.2 MeV. The total Be^7 production cross section at this energy is 57 millibarns.

Three compound nucleus type processes may be important in the formation of Be^7 from C^{12} at a He^3 bombarding energy of 30 MeV. They are:

A. $${}_2He^3 + {}_6C^{12} = {}_2He^4 + [{}_6C^{11}]^* \hookrightarrow \alpha + {}_4Be^7$$

B. $${}_2He^3 + {}_6C^{12} = [{}_8O^{15}]^* = {}_4Be^7 + {}_4Be^8$$

C. $${}_2He^3 + {}_6C^{12} = [{}_8O^{15}]^* = \alpha_1 + [{}_6C^{11}]^* \hookrightarrow \alpha_2 + {}_4Be^7$$

Experimental data on the $C^{12}(He^3,\alpha)C^{11}$ reaction to specific states of C^{11} indicate that the cross section for Process (A) is relatively small. Because the angular and energy distributions of Be^7 predicted for Process (B) are not in agreement with the experimental data, the cross section for Process (B) is also estimated to be relatively small. Elimination of Processes (A) and (B) leaves Process (C) as the most likely mechanism for producing Be^7. Since angular and energy distributions predicted on the basis of a simple model of Process (C) are consistent with the data, it is concluded that Be^7 from the $C^{12}(He^3,Be^7)$ reaction is

formed mainly by the $C^{12}(He^3;\alpha_1\alpha_2)Be^7$ mechanism at a He^3 laboratory energy of 30 MeV. At He^3 energies below 30 MeV, it was never necessary to invoke any large fraction of the direct interaction alpha pick-up process to fit the recoil data.

The results of the $Al^{27}(He^3,Be^7)$ thick target recoil experiments indicate that at He^3 bombarding energies up to 30 MeV, Be^7 evaporation accounts for approximately 90 percent of the Be^7 production cross section. The other 10 percent is attributed to direct interaction processes. The magnitudes of the direct interaction cross sections for (He^3,Be^7) and (He^4,Be^7) reactions on aluminum are consistent with the idea that alpha clustering is favored over He^3 clustering in the nuclear surface.

ACKNOWLEDGMENTS

This research would not have been possible without the assistance and cooperation of many people.

It is a pleasure to acknowledge the interest and encouragement of my research director Dr. S. S. Markowitz.

I am also indebted to David Anderson for an almost continual discussion of matters, mostly scientific, and for the use of many reference materials.

Many critical and often spontaneous discussions with Paul Croft and Lawrence Altman are acknowledged as is one with Dr. Jacob Gilat.

I am grateful to Lawrence Altman for the use of several Be^7 range-energy curves which he willingly supplied.

I wish also to acknowledge the numerous spectral analyses performed by George Shalimoff during the course of this work.

Others deserving of mention for discussions and their interest are Lee Hyder, Paul Reeder, Prof. Joseph Cerny, Victor Viola, Bruce Wilkins, Richard Pehl, Ernest Rivet, John Alexander, John Mahony, Charles Smith, and John Nash.

Others deserving mention for special services performed are:

The operators of the cyclotrons and of the Hilac;

Roberta Garrett who took care of the scheduling of the numerous Hilac runs;

Ruth Mary Larimer who was most helpful with problems arising at the 88-in. cyclotron;

Daniel O'Connell who fabricated many pure carbon targets from filter paper;

Harold Rothacker and Kenneth Pettit who handled storeroom needs and orders most efficiently;

Bert Watkins and Hagop Hagopian who build and modified some experimental apparatus;

The Health Chemistry Group which handled the targets and was always available when needed;

The administration and the secretaries of the Nuclear Chemistry Division who performed unheralded services throughout the work.

This work was performed under the auspices of the U. S. Atomic Energy Commission.

APPENDIX I

This appendix deals with the calculation of activity profiles for sandwiched thin target recoil experiments. Calculation of the profiles shown in Figs. 31-35 follow this (non-relativistic) treatment.

Let $\vec{u}$ = velocity of the center-of-mass in the laboratory system,
$\vec{v}$ = velocity of the emitted product (Be^7) in the CM system,
$\vec{w}$ = resultant velocity of the emitted product in the laboratory system.

From Fig. 44 it is seen that the projection of w on the beam direction is given by,

$$w_x \equiv (\vec{w}\cdot\vec{u})/|u| = (u^2 + \vec{u}\cdot\vec{v})/|u| = u + (v)(\cos\theta_{CM}).$$

The component of w perpendicular to the beam axis is

$$w_y \equiv (v)(\sin\theta_{CM}) = (w)(\sin\theta_L)$$

$$(w)^2 = (w_y)^2 + (w_x)^2$$

$$= (v)^2(\sin\theta_{CM})^2 + (u)^2 + (2uv)(\cos\theta_{CM}) + (v)^2(\cos\theta_{CM})^2$$

$$w^2 = u^2 + v^2 + (2uv)(\cos\theta_{CM}).$$

The relationship

$$R = kw^2$$

is now assumed for the range-energy relationship of the Be^7 product.

Let t be the projection of the range R along the beam axis.

$$R_x \equiv t = (k)(w)^2(\cos\theta_L)$$

$$t = (k)(u^2 + v^2 + 2uv\cos\theta_{CM})(\cos\theta_L)$$

$$\cos\theta_L = (u + v\cos\theta_{CM})/(u^2 + v^2 + 2uv\cos\theta_{CM})^{1/2}$$

$$\therefore t = (k)(u^2 + v^2 + 2uv\cos\theta_{CM})^{1/2}(u + v\cos\theta_{CM})$$

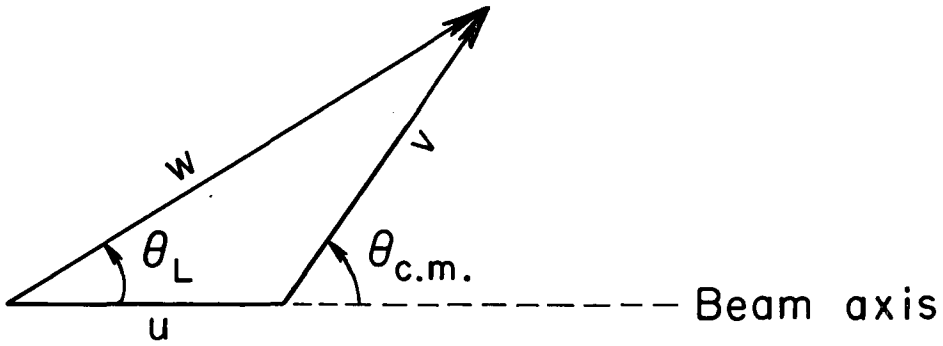

MU-34525

Fig. 44. Velocity vector diagram used to calculate activity profiles for the sandwiched thin target recoil experiments.

For isotropic center-of-mass product emission,

$$(dN/d\Omega)_{CM} = \text{const.} = dN/d\cos\theta_{CM} = dN/(-\sin\theta_{CM} d\theta_{CM})$$

$$dN/d\theta_{CM} = -(\text{const.})(\sin\theta_{CM})$$

$$dN/dt = (dN/d\theta_{CM})(d\theta_{CM}/dt) = -(\text{const.})(\sin\theta_{CM})(d\theta_{CM}/dt)$$

$$= (\text{const.})(d\cos\theta_{CM}/dt)$$

where N is the number of product nuclei and (const.) is a normalizing factor.

$$\int (dN/dt)dt = (\text{const.}) \int (d\cos\theta_{CM}/dt)dt$$

$$(N_2 - N_1) = (\text{const.}) [\cos\theta_{CM}(t_2) - \cos\theta_{CM}(t_1)]$$

The last equation gives the relative count rates in the individual catcher foils sandwiching the thin target. The $(d\cos\theta_{CM}/dt)$ part could be obtained analytically from the expression for t above, but in practice it was easier to make a plot of $\cos\theta_{CM}$ vs. t and take the values of $\cos\theta_{CM}$ corresponding to certain stack thicknesses from the graph. For plotting purposes, the calculated count rate per catcher foil is divided by the thickness of that particular catcher foil.

The assumption has been made that the range of the Be^7 product is proportional to its energy over the entire range of Be^7 laboratory energies up to, and above, 20 MeV. This approximation has also been used by Porile.[3] That this relationship is approximately valid over a large energy range is shown in Figs. 45 and 46. On these graphs are plotted k $(= R/w^2)$ against E_{Be^7}. The range-energy curve used for Fig. 45 is that of Altman.[60] That used in Fig. 46 was calculated from the Be^9 range-energy data of Hower and Fairhall.[39] Straight horizontal plots would indicate that the relationship $R = kw^2$ holds true.

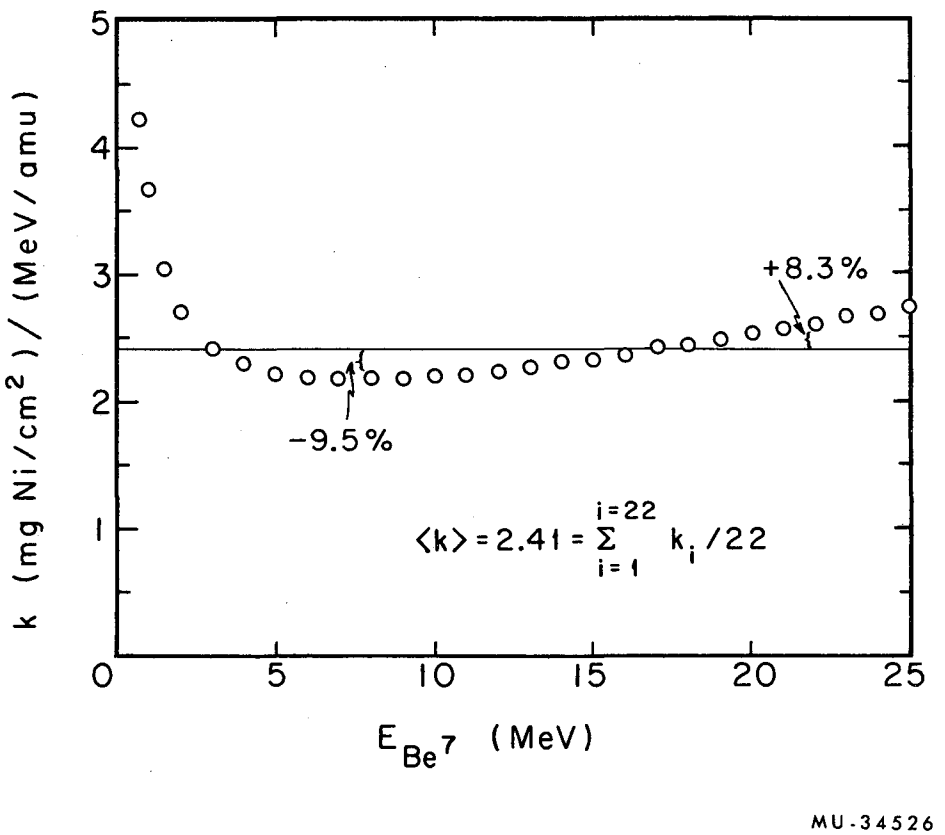

Fig. 45. Plot showing the approximate constancy of the "constant" k in the relationship $R = kw^2$. The range-energy curve used was that for Be^7 in nickel.[60]

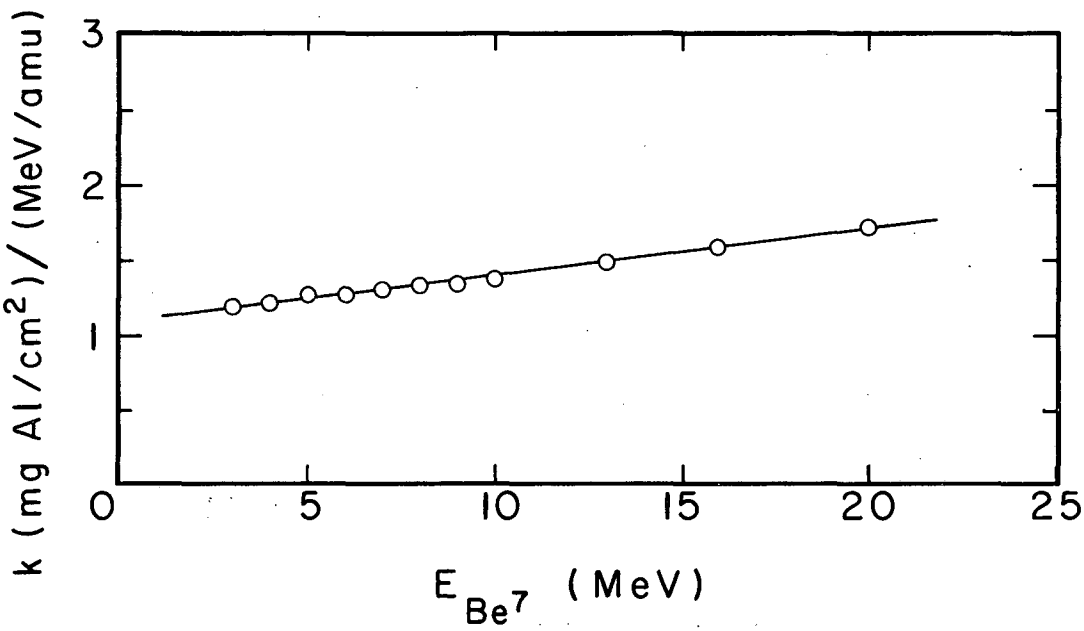

MU-34527

Fig. 46. Plot showing the approximate constancy of the "constant" k in the relationship $R = kw^2$. The range-energy curve used was that for Be^7 in aluminum.[39]

APPENDIX II

This appendix deals with the treatment of recoil data from "thick" and "intermediate thickness" targets.

It is difficult to calculate the activity profiles for up- and downstream catcher foils when the sandwiched target is not infinitely thin, unless the range-energy curve for the product of interest is the same for both the target and the catcher foils. However, expressions for the fractions of the total activity recoiling forward and backward from "thick" and "intermediate thickness" targets are readily derived. The approach here is to derive exact expressions instead of the series expansions of Winsberg.[42] This is necessary in some cases because the expansions do not always give rapidly converging values for F and B. The method used in the derivation is that of Winsberg.

A "thick" target is one whose thickness is greater than the maximum range of the product of interest. An "intermediate thickness" target is one that is not infinitely thin and also is not thicker than the range of the maximum energy recoil of the product of interest.

This treatment is directed in part at the calculation of F for the data shown in Fig. 14. In this experiment the target was 2.48 mg C per cm^2. The target then is not as thick as the maximum forward range of the Be^7 product, and hence the target is of "intermediate thickness" for forward laboratory products.

The vector diagram used in this discussion is shown in Fig. 47. If all the quantities in the diagram are multiplied by the velocity of the Be^7 product in the CM system, the more familiar velocity vector diagram results.

$$\eta = \frac{\text{velocity of CM in laboratory system}}{\text{velocity of } Be^7 \text{ in CM system}} = v/V,$$

t = projection of the laboratory range of the Be^7 along the beam axis,

F = fraction of the total activity formed which recoils out of the target in the forward direction,

W = target thickness,

R = range of Be^7 having energy the same as its CM energy.

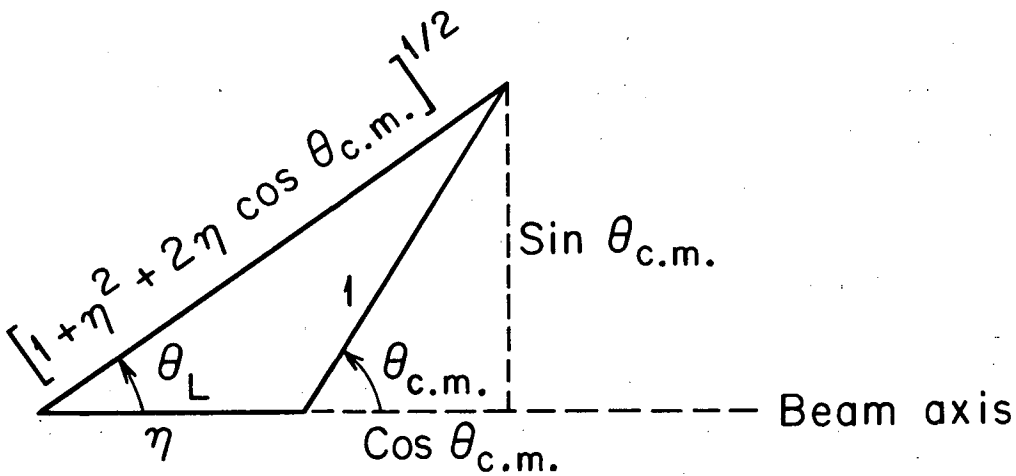

MU-34528

Fig. 47. Vector diagram used in the derivation of the expression for F in the case of an "intermediate thickness" target.

If the range-energy relationship $R = k(w)^2_{Be^7}$ is assumed, then

$$t = (R)(\eta + \cos\theta_{CM})(1 + \eta^2 + 2\eta\cos\theta_{CM})^{1/2}$$

The expression for F for a target of "intermediate thickness" is

$$F = \frac{1}{2W}\int_0^W dt \int_0^{\theta_{CM}} \sin\theta_{CM} d\theta_{CM}$$

$$F = \frac{1}{2W}\int dt[1 - \cos\theta_{CM}]$$

where dt is obtained from the expression for t above. After substituting for dt and integrating, the exact result is obtained,

$$\frac{-2WF}{R} = \sqrt{1 + \eta^2 + 2\eta\cos\theta_{CM}}\left[\frac{(2\eta^2 + 1 - 3\eta)(\eta\cos\theta_{CM} - \eta^2 - 1)}{3\eta^2}\right.$$

$$\left. - \frac{(2\eta^2+1)}{\eta} + \frac{(3)[(2)(1+\eta^2)^2 - (1+\eta^2)(2\eta)(\cos\theta_{CM}) + 3\eta^2\cos^2\theta_{CM}]}{15\eta^2}\right]_{\cos\theta_1(t=0)}^{\cos\theta_2(t=W)}$$

$$F = \frac{-R}{2W}(1+\eta^2+2\eta\cos\theta_{CM})^{1/2}\left[\frac{4\eta^3\cos\theta_{CM} - \eta\cos\theta_{CM} - 15\eta^2\cos\theta_{CM}}{15\eta^2}\right.$$

$$\left.\frac{+9\eta^2\cos^2\theta_{CM} - 4\eta^4 - 3\eta^2 + 1 - 15\eta^3}{}\right]_{\cos\theta_1(t=0)}^{\cos\theta_2(t=W)}$$

Using the expression for t, t in mg C cm^2 vs. $\cos\theta_{CM}$ was plotted and the values of $\cos\theta_2(t=W)$ and $\cos\theta_1(t=0)$ were taken from the graph.

For the calculation of B for the 2.48 mg C per cm^2 target, the target is many times thicker than the range of the most energetic backward Be^7 recoil in the laboratory system. The exact expressions for F and B, assuming range is proportional to energy, for "thick" targets are derived by Winsberg.[42]

This model for calculating F and B assumes a constant production cross section for Be^7 across the target thickness. Expressions have been derived by Porile for cases where the cross section varies linearly across the target.[3] Calculations of F and B for both treatments were performed for the recoil studies on aluminum, but the differences between F's and B's calculated by the two methods differed very little except for very thick targets. In view of the uncertainties in the range-energy curves used for Be^7, and the assumption about isotropic CM emission of Be^7, the simpler constant cross section formulas have been used in the treatment of all the $C^{12}(He^3,Be^7)$ data.

APPENDIX III

The Be^7 center-of-mass energy distribution based on a simple model of double alpha evaporation from an O^{15} compound nucleus is calculated in this appendix. The velocity vector diagram is shown in Fig. 48.

$$p_{C^{11}} = p_{\alpha_1}$$

where $p \equiv$ momentum and $T \equiv$ kinetic energy

$$p_{C^{11}} = \sqrt{(2)(4)(T_{\alpha_1})}$$

$$v_{C^{11}}^{\text{CM of } O^{15}} = \frac{\sqrt{(2)(4)(T_{\alpha_1})}}{(11)} .$$

In the C^{11} rest system,

$$p_{Be^7} = p_{\alpha_2}$$

$$v_{Be^7}^{\text{CM of } C^{11}} = \frac{\sqrt{(2)(4)(T_{\alpha_2})}}{(7)}$$

$$\vec{v}_{Be^7}^{\text{CM of } O^{15}} = \vec{v}_{Be^7}^{\text{CM of } C^{11}} + \vec{v}_{C^{11}}^{\text{CM of } O^{15}}$$

$$\left[v_{Be^7}^{\text{CM of } O^{15}}\right]^2 = \left[v_{Be^7}^{\text{CM of } C^{11}}\right]^2 + \left[v_{C^{11}}^{\text{CM of } O^{15}}\right]^2$$

$$+ (2) \left[v_{Be^7}^{\text{CM of } C^{11}}\right] \left[v_{C^{11}}^{\text{CM of } O^{15}}\right] \cos\theta .$$

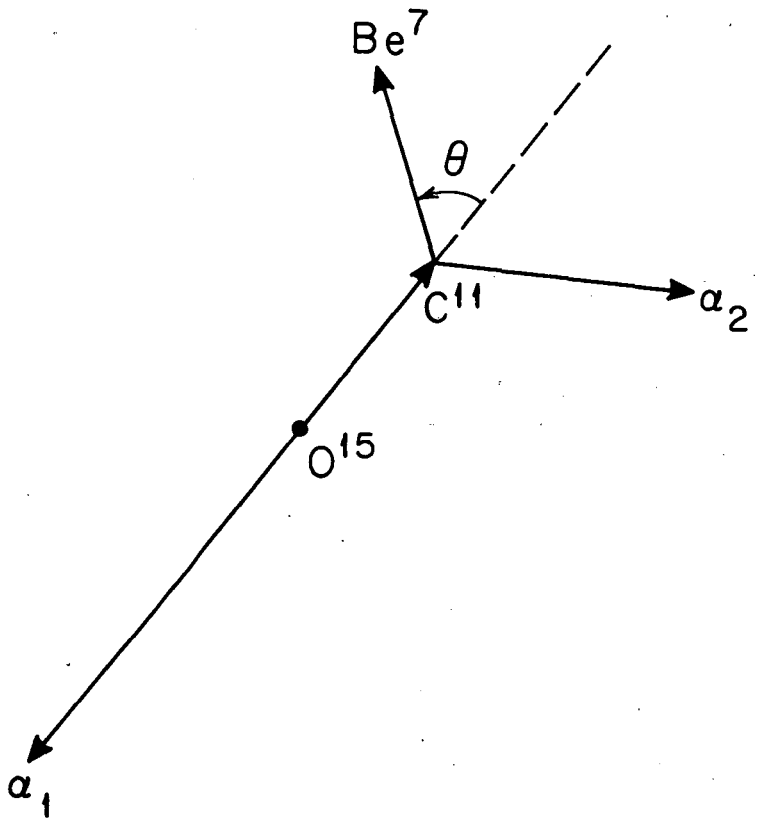

MU-34529

Fig. 48. Velocity vector diagram used to calculate the energy distribution of Be^7 in the O^{15} CM system, using the $C^{12}(He^3;\alpha_1\alpha_2)Be^7$ model.

Multiply the last equation by $(1/2)m_{Be^7}$ to get

$$\overset{\text{CM of } O^{15}}{T_{Be^7}} = \overset{\text{CM of } C^{11}}{T_{Be^7}} + \left(\frac{7}{11}\right) \overset{\text{CM of } O^{15}}{T_{C^{11}}} + (7) \left[\overset{\text{CM of } C^{11}}{v_{Be^7}}\right] \left[\overset{\text{CM of } O^{15}}{v_{C^{11}}}\right] \cos\theta \ .$$

If α_1 and α_2 come off at fixed energies, then $\overset{\text{CM of } C^{11}}{v_{Be^7}}$ and $\overset{\text{CM of } O^{15}}{v_{C^{11}}}$ are constants and

$$\frac{d \overset{\text{CM of } O^{15}}{T_{Be^7}}}{d \cos\theta} = (7) \left[\overset{\text{CM of } C^{11}}{v_{Be^7}}\right] \left[\overset{\text{CM of } O^{15}}{v_{C^{11}}}\right] .$$

$$\frac{dN}{d \overset{\text{CM of } O^{15}}{T_{Be^7}}} = \left[\frac{dN}{d \cos\theta}\right] \left[\frac{d \cos\theta}{d \overset{\text{CM of } O^{15}}{T_{Be^7}}}\right]$$

Assuming $dN/d \cos\theta$ is equal to one (i.e., Be^7 is formed isotropically in the C^{11} system) then

$$\frac{dN}{d \overset{\text{CM of } O^{15}}{T_{Be^7}}} = \frac{1}{(7) \left[\overset{\text{CM of } C^{11}}{v_{Be^7}}\right] \left[\overset{\text{CM of } O^{15}}{v_{C^{11}}}\right]}$$

The energy distribution in the O^{15} center-of-mass system is now estimated assuming that all the excess energy of the compound nucleus is dissipated as kinetic energy. For the $C^{12} + He^3 = O^{15}$ reaction, the excitation of the O^{15} compound nucleus is 36.1 MeV when the He^3 bombarding energy is 30 MeV. To form $Be^7 + 2\alpha$, 17.8 MeV must be supplied, leaving the excess excitation of (36.1 - 17.8) = 18.3 MeV to be taken off by the products. By analogy to other systems studied,[61,62] the assumption that all the excess energy is carried off by alpha emission may not be too bad. Emission of other light particles will not likely

lead to an eventual Be^7 product because of energy limitations (Appendix VII). Both alphas must come off in their ground states because they have no excited levels below 20 MeV. Likewise, the residual Be^7 has to be in, or near, its ground state. Its only bound excited level is at 0.431 MeV.[54]

The energy distribution of the first emitted alpha is taken to be that shown in Fig. 49. This figure was drawn by analogy to a curve shown in Ref. 63. Numbers derived from Fig. 49 which are necessary for this calculation are given in Table XVI.

$$\int dN = \frac{1}{(7)\left[{}^{\text{CM of } C^{11}}_{v_{Be^7}}\right]\left[{}^{\text{CM of } O^{15}}_{v_{C^{11}}}\right]} \int d\, {}^{\text{CM of } O^{15}}_{T_{Be^7}}$$

$$\left(N_2 - N_1\right)^{\text{CM of } O^{15}} = \frac{1}{(7)\left[{}^{\text{CM of } C^{11}}_{v_{Be^7}}\right]\left[{}^{\text{CM of } O^{15}}_{v_{C^{11}}}\right]} \left[T_2 - T_1\right]^{\text{CM of } O^{15}}_{Be^7}$$

The equation states that a constant Be^7 activity is found per unit energy interval in the O^{15} CM. This square distribution will be bounded by the maximum and minimum Be^7 energies available (Table XVI). The final results of this calculation are shown in Fig. 50. The heavy line is drawn to represent the calculated histogram.

Table XVI. Numbers derived from Fig. 49 which are used to calculate the energy distribution of Be^7 produced in double alpha evaporation from O^{15}.

E_{α_1}	$\sigma_{\alpha_1}(E)$[a]	CM of O^{15} [b] $v_{C^{11}}$	CM of C^{11} [b] v_{Be^7}	CM of O^{15} [c] Max. E_{Be^7}	CM of O^{15} [d] Min. E_{Be^7}
3 MeV	34	0.445	1.21	9.5 MeV	2.1 MeV
6	17	0.630	1.02	9.5	0.5
9	8	0.772	0.79	8.5	0.0
12	5	0.890	0.44	7.2	0.7

[a] Arbitrary units.

[b] The velocity units are $(\text{MeV/amu})^{1/2}$.

[c] Calculated with the formula $(1/2)(7)\left[\text{CM of } O^{15}\ v_{C^{11}} + \text{CM of } C^{11}\ v_{Be^7}\right]^2$

[d] Calculated with the formula in Note c, but using a minus sign.

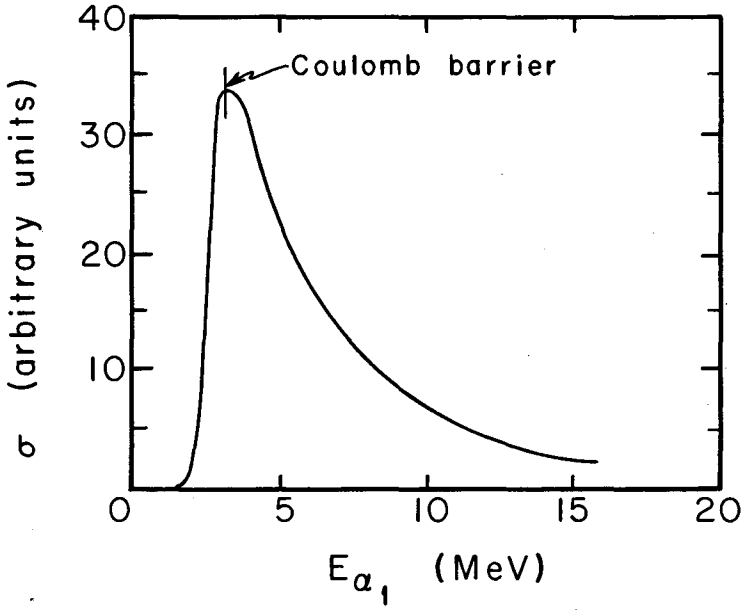

MU-34530

Fig. 49. Assumed energy spectrum of first evaporated alpha particle from the O^{15} compound nucleus.

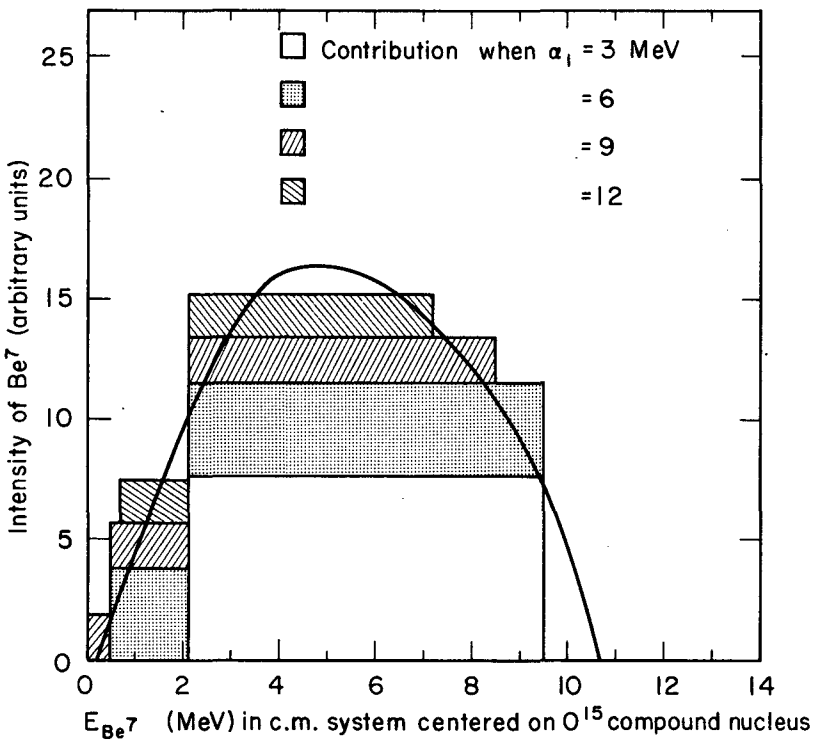

Fig. 50. Calculated energy spectrum of Be^7 formed by the evaporation of two alpha particles from O^{15}.

APPENDIX IV

In this appendix it is shown that a stationary nucleus emitting a product with a fixed energy will give a square activity distribution in a stack of catcher foils. The diagram used for this calculation is shown in Fig. 51.

Since the product is assumed to have a fixed energy, all of the given products ideally will stop on the surface of a sphere. The problem is then to show that the sphere area intercepted by each unit thickness of catcher foil is constant. In the diagram of Fig. 51, one catcher foil is represented by two vertical lines.

Let S = arc length

A = area on the square

$$\frac{dx}{dS} = \cos(90^\circ - \theta)$$

$$= \sin\theta$$

$$dS = dx/\sin\theta$$

$$dA = (2\pi)(y)(dS)$$

$$dA = (2\pi)(r\sin\theta)\left(\frac{dx}{\sin\theta}\right)$$

$$A = 2\pi r\,[\Delta x]$$

That is, the area of the sphere intercepted by the catcher foil, divided by the catcher foil thickness, is a constant.

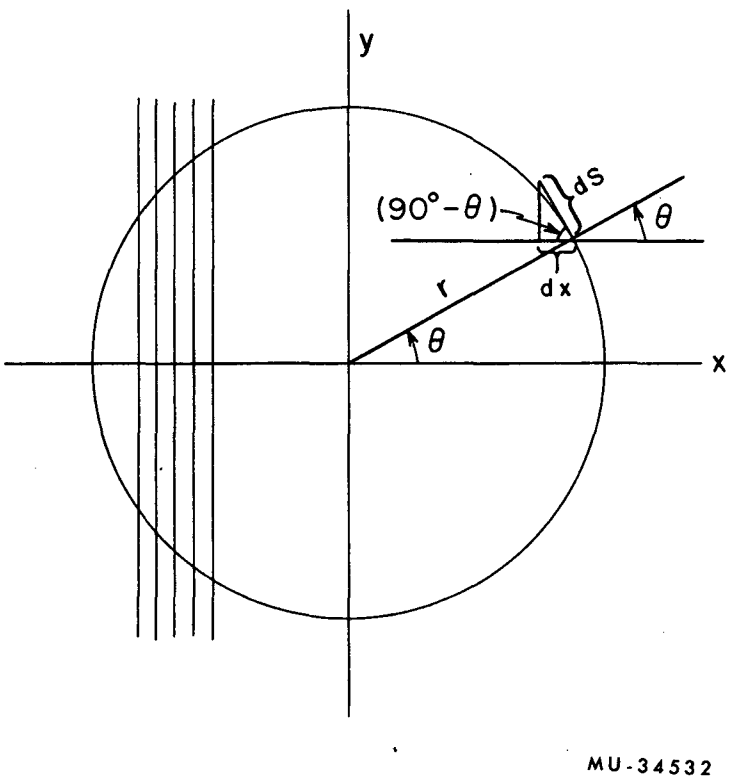

Fig. 51. Diagram used in the calculation of the activity profile for a stationary emitter.

APPENDIX V

The maximum laboratory and CM energies expected for Be^7 from the $C^{12}(He^3,Be^7)$ reaction are calculated in this appendix. The treatment is non-relativistic and assumes that the products are formed in their ground states.

Let T = kinetic energy

p = momentum

M = mass (see mass unit = 1)

E_f = energy of fusion of He^3 and He^4 (1.58 MeV)

E_b = binding energy of alpha in C^{12} (7.37 MeV)

In the laboratory coordinate system,

$$T_{He^3} + E_f = T_{Be^7} + E_b + T_{Be^8}.$$

For maximum Be^7 momentum,

$$p_{Be^7} = p_{He^3} + p_{Be^8}$$

$$T_{He^3} + 1.58 \text{ MeV} = T_{Be^7} + 7.37 \text{ MeV} + \frac{p^2_{Be^7} - 2p_{Be^7}p_{He^3} + p^2_{He^3}}{(2)(8)} \text{ MeV}$$

Also,

$$\frac{p^2_{Be^7}}{(2)(8)} = \frac{(7)}{(8)} T_{Be^7} \quad \text{and} \quad \frac{p^2_{He^3}}{(2)(8)} = \frac{(3)}{(8)} T_{He^3}$$

$$T_{He^3} + 15.8 \text{ MeV} = T_{Be^7} + 7.37 + \frac{7}{8} T_{Be^7} + \frac{3}{8} T_{He^3} - \frac{\sqrt{(2)(3)(T_{He^3})}\sqrt{(2)(7)(T_{Be^7})}}{(8)}$$

$$\left\{ \frac{\sqrt{(6)(T_{He^3})}\ \sqrt{(14)(T_{Be^7})}}{8} = 5.79 \text{ MeV} + \frac{15}{8} T_{Be^7} - \frac{5}{8} T_{He^3} \right\}^2$$

$$\frac{84}{64} T_{He^3} T_{Be^7} = \frac{225}{64} T^2_{Be^7} + \frac{15}{4} (5.79 \text{ MeV} - \frac{5}{8} T_{He^3}) T_{Be^7}$$

$$+ 33.52 \text{ MeV}^2 - 7.24 T_{He^3} \text{ MeV} + \frac{25}{64} T^2_{He^3}$$

Let $T_{He^3} = 31.2$ MeV.

$$(40.95)(T_{Be^7})\text{MeV} = (3.52)(T^2_{Be^7}) - (51.41)(T_{Be^7})\text{MeV} + 33.52 \text{ MeV}^2$$

$$- 225.9 \text{ MeV}^2 + 380.2 \text{ MeV}^2$$

$$0 = 3.52 T^2_{Be^7} - 92.36 T_{Be^7} \text{ MeV} + 187.8 \text{ MeV}^2$$

$$T^{\text{Max., lab}}_{Be^7} = 24.0 \text{ MeV}$$

Now the maximum CM energy of Be^7 is calculated.

$$T^{lab}_{CM} = 6.24 \text{ MeV}$$

$$v^{lab}_{CM} = \sqrt{\frac{(2)(6.24)}{(15)}} = 0.904 \ (\text{MeV/mu})^{1/2}$$

$$v^{\text{Max.,lab}}_{Be^7} = \sqrt{\frac{(2)(24)}{(7)}} = 2.62$$

$$v^{\text{Max.,CM}}_{Be^7} = 2.62 - 0.90 = 1.72$$

$$T^{\text{Max.,CM}}_{Be^7} = (\tfrac{1}{2})(7)(1.72)^2 = 10.35 \text{ MeV}$$

APPENDIX VI

Range-energy curves for He^3 in various materials used in this work have been calculated by Rich and Madey,[29] Bromley and Almqvist,[30] and Demildt.[31] Range-energy curves for He^4 ions were calculated from the corresponding He^3 curves by the formula,

$$\bar{R} = \bar{R}_o(m/m_o)(Z_o/Z)^2$$

for ions of the same velocity and same stopping medium.

Range-energy curves for Be^7 in various stopping media were calculated from a variety of sources using the above formula. Calculations for Be^7 were made from the He^3 curves of Rich and Madey, Bromley and Almqvist, and Demildt, and from curves of heavy ions in different media as presented by Hubbard,[64] Northcliffe,[65] and Roll and Steigert.[66] Since some of the same range-energy curves calculated from different sources differed considerably from one another, it was decided finally to use a set of self-consistent range-energy curves computed for Be^7 in various stopping materials by Altman.[60] When compared to the meager existing experimental data, these curves predict range differences well, and absolute ranges fairly well as is seen in Table XVII. The only experimental data available on range-energy curves for beryllium are those for Be^9 ions in aluminum and gold.[39]

Table XVII. Comparison of experimental range-energy curve for Be^7 in Au with the calculated curve.

E_{Be^7}	R(calculated) mg Au/cm^2	R(experimental) mg Au/cm^2	ΔR(calculated) mg Au/cm^2	ΔR(experimental) mg Au/cm^2
3 MeV	5.3	2.9	1.1	0.9
4	6.4	3.8	1.1	1.1
5	7.5	4.9	1.1	1.1
6	8.6	6.0	1.2	1.2
7	9.8	7.2	1.3	1.2
8	11.1	8.4	1.2	1.2
9	12.3	9.6	1.2	1.2
10	13.5	10.8	7.3	6.5
15	20.8	17.3	8.2	6.8
20	29.0	24.1[a]	9.1	7.4
25	38.1	31.5[a]		

[a]Extrapolated value.

APPENDIX VII

Some Q-values relevant to this work are listed below. The masses used in the computations were obtained from Refs. 67 and 68.

REACTION	Q-VALUE
$He^3 + C^{12} = O^{15}$	+12.1 MeV
$O^{15} = n^1 + O^{14}$	-13.2
$O^{14} = Be^7 + Be^7$	-23.5
$O^{15} = H^1 + N^{14}$	- 7.3
$N^{14} = He^4 + B^{10}$	-11.6
$N^{14} = Be^7 + Li^7$	-27.8
$O^{15} = D^2 + N^{13}$	-15.6
$N^{13} = Be^7 + Li^6$	-24.5
$O^{15} = He^3 + C^{12}$	-12.1
$C^{12} = Be^7 + He^5$	-27.2
$O^{15} = He^4 + C^{11}$	-10.2
$C^{11} = Be^7 + He^4$	- 7.5
$C^{11} = C^{10} + n^1$	-13.1
$C^{11} = H^1 + B^{10}$	- 8.7
$O^{15} = Be^7 + Be^8$	-17.8
$Be^8 = n^1 + Be^7$	-18.9
$Be^8 = H^1 + Li^7$	-17.3
$C^{12} = 3He^4$	- 7.3
$C^{12} = He^3 + Be^9$	-26.3
$C^{12} = Be^8 + He^4$	- 7.4
$C^{12} = C^{11} + n^1$	-18.7
$He^3 + n^1 = He^4$	+20.6

REACTION	Q-VALUE
$He^3 + He^4 = Be^7$	+ 1.6 MeV
$He^3 + C^{12} = He^4 + C^{11}$	+ 1.8
$Be^7 = Li^6 + H^1$	- 5.6

Some calculated Coulomb barriers are (R_o = 1.5f):

$He^4 + He^4$	1.2 MeV
$He^3 + Au^{197}$	20.8
$He^3 + C^{12}$	3.1
$He^3 + Fe^{56}$	9.5
$He^3 + Ag^{107}$	14.6
$He^3 + Al^{27}$	5.7
He^4 out of O^{15}	3.0
H^1 out of O^{15}	2.0
He^4 out of C^{11}	2.2
H^1 out of C^{11}	1.5
Be^7 out of O^{15}	3.9
Be^7 out of P^{30}	8.9

APPENDIX VIII

In this appendix the procedure used to separate Be^7 from aluminum foils is given. Beryllium and aluminum are very similar chemically. There is, however, a large difference in their complexing behavior with EDTA, in that beryllium is complexed weakly and aluminum strongly.[14]

1. Add holdback carriers of Fe^{+++}, Cu^{++}, Co^{++}, and Zn^{++}. Add an accurately known amount of Be^{++}. Dissolve the Al foil in concentrated HCl.

2. Add NaOH (this serves as a carrier also) in large excess. Keep the test tube cool in an ice bath. The beryllium is now in solution since $Be(OH)_2$ is soluble in excess NaOH.

3. Centrifuge and discard the precipitate which consists mostly of $Fe(OH)_3$. Make the solution acidic with concentrated HCl.

4. Add approximately 10 ml. of 10 percent EDTA. Add excess concentrated NH_4OH. EDTA strongly complexes all the carriers except Be. $Be(OH)_2$ is insoluble in excess NH_4OH.

5. Centrifuge and discard the supernatant solution. Dissolve the $Be(OH)_2$ in HCl. Dilute and add more EDTA. Add excess NH_4OH.

6. Precipitate $Be(OH)_2$ four times in the presence of EDTA as in Step 5. Then precipitate $Be(OH)_2$ three times without EDTA to insure that EDTA is completely removed. Wash the $Be(OH)_2$ four times with dilute NH_4OH.

7. The final precipitate is now radiochemically pure and in one analysis contained by weight 100 parts Be and 0.3 parts Al. No other emission lines appeared in the spectral analysis.

Other radiochemical separations from other metal foils are not included here, but they are similar. Always the final $Be(OH)_2$ precipitate was radiochemically pure and spectral analysis showed nothing except Be present (except for the separation from Al foils).

APPENDIX IX

Since in many low cross section experiments, it is desirable to use as high a beam current as possible without damaging the target, the following limited compilation of beam tolerations of various targets is included in the hope that it will save a certain amount of duplicated effort.

Unless otherwise noted in the "Comment" column, the collimation was 1/2 inch or larger, and the target was a stack of foils. Stacked targets were always water cooled with deionized water. Bombardments were long enough so that equilibrium between beam heating and heat dissipation should easily have been established. A provision for randomly directing the Hilac beam over the target surface was usually used in He^3 bombardments. This has the effect of increasing the beam intensity a given target can take without damage.

TARGET	AVERAGE BEAM INTENSITY	COMMENTS
Polyethylene ($2.85\ mg/cm^2$)	30mμa of $He^4(++)$ incident at 48 MeV	Stack fused
Polystyrene ($3.2\ mg/cm^2$) alternated with Al spacers	3mμa $He^4(++)$ incident at 48 MeV	Stack undamaged
C(carbonized filter paper)	150mμa $He^4(++)$ incident at 48 MeV	Stack undamaged
C(carbonized filter paper)	450mμa $He^4(++)$ incident at 85 MeV	Stack undamaged
Al(3 mil)	500mμa $He^4(++)$ incident at 80 MeV	Stack undamaged
Ni(1/2 mil)	500mμa $He^3(+)$ incident at 31.2 MeV	Stack undamaged
Ni(1/2 and 1/10 mil)	320mμa $He^3(+)$ incident at 31.2 MeV	Stack undamaged
Au(1 mil)	820mμa $He^3(+)$ incident at 31.2 MeV	Stack undamaged

TARGET	AVERAGE BEAM INTENSITY	COMMENTS
Ag(1 mil)	1000mμa He^3(+) incident at 31.2 MeV	Stack undamaged
Ag(1/10 mil)	130mμa He^3(+) incident at 31.2 MeV	Stack undamaged
C(carbonized filter paper)	320mμa He^3(+) incident at 31.2 MeV	Stack undamaged
Pb(1 mil)	500mμa He^3(+) incident at 31.2 MeV	Quickly put hole through entire stack
Pb(1 mil)	60mμa He^3(+) incident at 31.2 MeV	Stack undamaged
Polystyrene (2.4 mg/cm^2) alternated with Al spacers	25mμa He^3(+) incident at 31.2 MeV	Stack undamaged
Sn(1 mil)	75mμa He^3(+) incident at 31.2 MeV	Stack undamaged
Fe(1/2 mil)	900 mμa He^3(+) incident at 31.2 MeV	Most of the foils were undamaged, but stack could not have taken more intense beam
Al(1 mil)	500mμa He^3(+) incident at 31.2 MeV	Most of the foils were undamaged, but stack could not have taken more intense beam
Polystyrene (2.3 mg/cm^2)	5mμa He^3(+) incident at 31.2 MeV	Stack fused
Single 780 microgram per cm^2 carbon film	600mμa He^3(+) incident at 31.2 MeV	Uncooled, 1/8-in. collimation, film undamaged

When the total beam flux from a run is read on a beam integrator, the total number of beam particles can be obtained as follows:

$$1\ \mu\text{ampere} = \frac{1\ \text{Coulomb}}{\text{second}} \times 10^{-6} = \frac{\text{Coulomb}}{\text{second}} \times \frac{\text{proton}}{1.6 \times 10^{-19}\ \text{Coulomb}} \times 10^{-6}$$

$$= 0.625 \times 10^{+13}\ \frac{(+)}{\text{sec}}$$

$$1\ \text{m}\mu\text{a-hr} = (0.625 \times 10^{13})(10^{-3})\ \frac{(+)}{\text{sec}} \times \frac{60\ \text{sec}}{\text{min}} \times \frac{60\ \text{min}}{\text{hr}} \times \text{hr}$$

$$= 2.25 \times 10^{13}\ (+)$$

$$1\ \text{m}\mu\text{ah} = 1.125 \times 10^{13}\ (++)\ \text{particles.}$$

REFERENCES

1. Lucretius, The Nature of the Universe, Translated by R. E. Latham (Penguin Books Limited, Harmondsworth, Middlesex, 1951), p. 34.
2. See, for example, R. K. Sheline and K. Wildermuth, Nucl. Phys. 21, 196 (1960). Also T. A. Tombrello and G. C. Phillips, Nucl. Phys. 20, 648 (1960).
3. N. T. Porile, Phys. Rev. 127, 224 (1962).
4. E. L. Hubbard, et al., Rev. Sci. Instr. 32, 627 (1961).
5. H. Grunder (Lawrence Radiation Laboratory, Berkeley), private communication.
6. S. S. Markowitz and J. M. Hall, Bull. Am. Phys. Soc. 4, 8 (1959).
7. V. E. Viola, Angular Distributions from Heavy-Ion-Induced Fission (Ph.D. Thesis), Lawrence Radiation Laboratory Report UCRL-9619, March 1961 (unpublished).
8. V. V. Andreeva, Trudy Inst. Fiz-Khim. Akad. Nauk, SSSR, No. 6, and Novye Metody Fiz-Khim Issledovani, No. 2, 79 (1957).
9. D. Strominger, J. M. Hollander, and G. T. Seaborg, Rev. Mod. Phys. 30, 604 (1958).
10. E. Rivet (Lawrence Radiation Laboratory, Berkeley), private communication.
11. Obtained from Acheson Colloids Co., Port Huron, Michigan.
12. S. S. Markowitz and J. D. Mahony, Anal. Chem. 34, 329 (1962).
13. G. Jura (Department of Chemistry, University of California, Berkeley), private communication.
14. A. W. Fairhall, The Radiochemistry of Beryllium, NAS-NS-3013 (1960), p.6.
15. Obtained from the Millipore Filter Corp., Bedford, Massachusetts.
16. R. L. Heath, Scintillation Spectrometry Gamma-Ray Spectrum Catalogue, AEC Research and Development Report, IDO-16, 408 (1957).
17. Obtained from the specifications accompanying the scintillation crystal.
18. VYNS is a polyvinylchloride-acetate copolymer product of Bakelite Co., New York.

19. B. D. Pate and L. Yaffe, Can. J. Chem. 33, 18 (1955).

20. Ibid., p. 934.

21. Calibrated by H. Marshall Blann.

22. Videne-TC is a product of the Goodyear Tire Company.

23. J. R. Stehn and E. F. Clancy, Nucleonics 13, 27 (1955).

24. J. J. Kraushaar, E. D. Wilson, and K. T. Bainbridge, Phys. Rev. 90, 610 (1953).

25. J. G. V. Taylor and J. S. Merritt, Can. J. Phys. 40, 926 (1962).

26. A. W. Fairhall, The $He^3(He^4,\gamma)Be^7$ Reaction, University of Washington, Department of Physics, Cyclotron Research Progress Report, 24 (1961).

27. C. O. Hower, Jr., The (α,Be^7) Reaction in Light Elements at Energies Below 42 MeV (Ph.D. Thesis), Department of Physics, University of Washington, 1962 (unpublished).

28. L. C. Becker, et al., Nucl. Instr. Meth. 21, 298 (1963).

29. M. Rich and R. Madey, Range-Energy Tables, Lawrence Radiation Laboratory Report UCRL-2301, March 1954 (unpublished).

30. D. A. Bromley and E. Almqvist, He^3-Induced Reactions, Atomic Energy of Canada Limited, C.R.P. 881, 9 (1959).

31. A. C. Demildt, Range-Energy Relations of He^3 Calculated for Several Elements, Lawrence Radiation Laboratory Report UCRL-10647, February 1963 (unpublished).

32. R. D. Evans, The Atomic Nucleus (McGraw-Hill Book Co., Inc., New York, 1955), pp. 757-771.

33. D. R. F. Cochran and J. D. Knight, Phys. Rev. 128, 1281 (1962).

34. G. H. Bouchard and A. W. Fairhall, Phys. Rev. 116, 160 (1959).

35. R. H. Lindsay and R. J. Carr, Phys. Rev. 120, 2168 (1960).

36. Evans, op. cit., pp. 652-3.

37. J. D. Mahony (Lawrence Radiation Laboratory, Berkeley), private communication.

38. C. Hatch (Lawrence Radiation Laboratory, Berkeley), private communication.

39. C. O. Hower and A. W. Fairhall, Phys. Rev. 128, 1163 (1962).

40. Evans, op. cit., pp. 420-1.

41. J. B. Marion, T. I. Arnette, and H. C. Owens, Tables for the Transformation Between the Laboratory and Center-of-Mass Coordinate Systems and the Calculation of Energies of Reaction Products, Oak Ridge National Laboratory Report ORNL-2574, April 1959 (unpublished).

42. L. Winsberg, The Mathematical Treatment of Data from Recoil Experiments, Lawrence Radiation Laboratory Report UCRL-8618, p. 44, January 1959 (unpublished).

43. F. Ajzenberg-Selove and T. Lauritsen (edited by K. H. Hellwege), Landolt-Börnstein—Numerical Data and Functional Relationships in Science and Technology (Springer-Verlag, Berlin, 1961), pp. I-14, I-16.

44. R. H. Lindsay and E. F. Neuzil, Phys. Rev. 127, 1269 (1962).

45. A. Zucker, Proceedings of the Conference on Reactions Between Complex Nuclei, Oak Ridge National Laboratory Report ORNL-2606, p. 132, October 1958 (unpublished).

46. R. Kaufmann and R. Wolfgang, Phys. Rev. 121, 206 (1961).

47. J. Catala, A. Garcia, and G. Pardo, Anales de Fisica y Quimica LVIII-A, 267 (1962).

48. H. Tyren, P. Hillman, and T. A. J. Maris, Nucl. Phys. 7, 10 (1958).

49. This fact was kindly pointed out by Prof. J. O. Rasmussen during a student seminar.

50. Although direct reaction products do not always peak at zero degrees, the alpha pick-up reaction $F^{19}(d,Li^{6})N^{15}$ is strongly forward peaked at a laboratory deuteron energy of 15 MeV. See R. M. Drisko, G. R. Satchler, and R. H. Bassel, Proceedings of Conference on Reactions Between Complex Nuclei, edited by A. Ghiorso, R. M. Diamond, and H. E. Conzett (University of California Press, Berkeley, 1963), p. 85.

51. G. Igo, L. F. Hansen, and T. J. Gooding, Phys. Rev. 131, 337 (1963).

52. A. N. James and H. G. Pugh, Nucl. Phys. 42, 441 (1963).

53. Y. I. Serebrennikov, Izv. Vysshikh Uchebn. Zavedenii, Fiz., No. 4, 151-3 (1962). (Nuclear Science Abstracts).

54. F. Ajzenberg-Selove and T. Lauritsen, Nucl. Phys. 11, 37 (1959).

55. Ibid., p. 45.

56. S. T. Butler and O. H. Hittmair, Nuclear Stripping Reactions (John Wiley and Sons, Inc., New York, 1957), Chap. I.

57. N. A. Perfilov, Fragmentation Induced by High Energy Particles, 1963 International Conference on High Energy Physics and Nuclear Structure, Session VI, CERN, Geneva, February-March 1963 (preprint).

58. A. Samman and P. Cüer, J. Phys. rad. 19, 13 (1958).

59. Evans. op. cit., pp. 244-249.

60. L. Altman (Lawrence Radiation Laboratory, Berkeley), private communication.

61. J. F. Mollenauer, Effects of Angular Momentum on Gamma-Ray Production in Compound Nucleus Reactions (Ph.D. Thesis), Lawrence Radiation Laboratory Report UCRL-9724, June 1960 (unpublished).

62. G. N. Simonoff and J. M. Alexander, Phys. Rev. 133, B104 (1964).

63. W. J. Knox, Proceedings of Conference on Reactions Between Complex Nuclei, edited by A. Zucker, F. T. Howard, and E. C. Halbert (John Wiley and Sons, New York, 1960), p. 264.

64. E. L. Hubbard, Range-Energy Relation for Heavy Ions in Metals, Lawrence Radiation Laboratory Report UCRL-9053, January 1960 (unpublished).

65. L. C. Northcliffe, Phys. Rev. 120, 1744 (1960).

66. P. G. Roll and F. E. Steigert, Nucl. Phys. 17, 54 (1960).

67. B. G. Harvey, Introduction to Nuclear Physics and Chemistry (Prentice-Hall, Inc., Englewood Cliffs, New Jersey, 1962), Appendix II.

68. G. Friedlander and J. W. Kennedy, Nuclear and Radiochemistry (John Wiley and Sons, Inc., New York, 1957), Appendix G.

This report was prepared as an account of Government sponsored work. Neither the United States, nor the Commission, nor any person acting on behalf of the Commission:

A. Makes any warranty or representation, expressed or implied, with respect to the accuracy, completeness, or usefulness of the information contained in this report, or that the use of any information, apparatus, method, or process disclosed in this report may not infringe privately owned rights; or

B. Assumes any liabilities with respect to the use of, or for damages resulting from the use of any information, apparatus, method, or process disclosed in this report.

As used in the above, "person acting on behalf of the Commission" includes any employee or contractor of the Commission, or employee of such contractor, to the extent that such employee or contractor of the Commission, or employee of such contractor prepares, disseminates, or provides access to, any information pursuant to his employment or contract with the Commission, or his employment with such contractor.